Experimental investigation of the Al-Mn-Zn system through diffusion couples and key samples coupled with thermodynamic modeling

Tian Wang

A Thesis

in

The Department

of

Mechanical and Industrial Engineering

Presented in Partial Fulfillment of the Requirements

for the Degree of Master of Applied Science (Mechanical Engineering) at

Concordia University Montreal, Quebec, Canada

February 2013

CONCORDIA UNIVERSITY

SCHOOL OF GRADUATE STUDIES

This is to certify that the Thesis prepared,

By: **Tian Wang**

Entitled: **"Experimental Investigation of the Al-Mn-Zn System through Diffusion Couples and Key Samples Coupled with Thermodynamic Modeling"**

and submitted in partial fulfillment of the requirements for the Degree of

Master of Applied Science (Mechanical Engineering)

Complies with the regulations of this University and meets the accepted standards with respect to originality and quality.

Signed by the Final Examining Committee:

Chair

Dr. M. Paraschivoiu

Examiner

Dr. M. Hojjati

Examiner
External

Dr. M. Harsh
Centre for Engineering in Society

Supervisor

Dr. M. Medraj

Approved by:

Dr. S. Narayanswamy, MASc Program Director

Department of Mechanical and Industrial Engineering

Dean Robin Drew

Faculty of Engineering & Computer Science

Date: _____

Abstract

Experimental investigation of the Al-Mn-Zn system through diffusion couples and key samples coupled with thermodynamic modeling

Tian Wang

Al-Mn-Zn ternary system is experimentally investigated at 400℃ via diffusion couples and key samples experiments. Three new ternary compounds have been found in the current study. Phase relations and homogeneity ranges are determined for binary and ternary phases through EPMA, SEM/EDS and XRD. Compositions of the ternary intermetallic compounds τ_1, τ_2 and τ_3 have been found as $Al_{62}Mn_{16}Zn_{22}$, $Al_{76}Mn_{13}Zn_{11}$, and $Al_xMn_yZn_z$ (x=9.5-12.7 at%; y=11-15 at%; z=74.6-77.2 at%). Al_4Mn is found to form quasicrystal or stable equilibrium phase in the presence of Zn and depending on the solidification conditions. Binary compounds Al_4Mn, $Al_{11}Mn_4$, Al_8Mn_5 and β-Mn exhibit limited ternary solid solubility. Experimental data on this system from the literature is spare, isothermal section of the Al-Mn-Zn phase diagram at 400℃ is constructed based on the current phase analysis results and experimental data.

DSC analysis approach is also used to investigate this ternary system. Partial vertical sections at 13, 14 and 15 at% Mn have been experimentally investigated and compared with preliminary thermodynamic calculations. Discrepancy is observed due to the absence of the ternary phases in the thermodynamic database. Thus, this ternary system has to be remodeled in the future.

Acknowledgements

I would like to express my sincere gratitude and appreciation to my thesis supervisor Dr. Mamoun Medraj for his constant advice, support and encouragement during my study in Concordia University. Without his cooperation and continuous inspiration, it would not be possible to carry out this work.

I also like to thank research associate Dr. Dmytro Kevorkov, for his support and valuable suggestions throughout my experimental work and writing this thesis.

I would like to thank all the TMG members of Dr. Medraj's research group, particularly Mezbahul Islam, Yinan Zhang and Ahmad Mostafa for their constant help and suggestion during my research. In addition, financial support from General Motors Canada Ltd and NSERC through the CRD grant program is gratefully acknowledged.

Finally, I like to extend my warm and sincere thanks to my parents. I would never have been able to stand at this point of my life without their unconditional love and support.

Table of Contents

List of Figures

List of Tables

Lists of Abbreviations

OM	Optical Microscopy
SEM	Scanning Electron Microscopy
EDS	Energy Dispersive X-ray Spectroscopy
EPMA	Electron Probe Microanalysis
WDS	Wavelength Dispersive X-ray Spectroscopy
XRD	X-ray Diffraction
DSC	Differential Scanning Calorimetry
DTA	Differential Thermal Analysis

CHAPTER 1

Introduction

Aluminum is the most abundant metal elements in earth's crust. It has unique properties like the light weight, high strength and corrosion resistance which make it an ideal material for use in conventional and novel applications. The automotive market represents one of the most promising opportunities for aluminum. The desire for lighter, more efficient vehicles has enabled automakers to look to aluminum for reducing the weight of cars and trucks without compromising performance and safety. Aluminum alloys have also been widely used in aerospace and space technology, and they have also found increasing use in other fields [1-2]. A basic understanding of phase relationships and solidification behavior of this system is essential for developing new materials as well as for improving the performance of existing materials.

Many different elements which include Mg, Cu, Zn, Mn, Si, etc. are alloyed with Al to improve its properties for specific applications. The Al-Mn-Zn system is an important ternary system for the development of Al based alloys, which used intensively by automotive and aerospace industries. The Al-Zn based alloys have high strength and hardness, improved creep, wear resistance and lower density. It is well known that a small amount of Mn added to aluminum alloys plays a positive role in fracture toughness, recrystallization, grain refinement and in increasing the resistance to stress corrosion

fatigue [1-3]. Al-Mn-Zn system is also an essential sub-system for AZ, AM-series magnesium alloys, high strength steels, galvanizing-related alloy system.

However, up to date little effort has been made to construct the phase relationships of the Al-Mn-Zn ternary system. The limited publications on this system are only focused on the structure of the ternary compounds in the system. The experimental phase equilibrium information and published thermodynamic data are insufficient for the accurate description of this system.

In the present work, experimental investigations on the Al-Mn-Zn ternary system are specifically performed to provide experimental data to enable thermodynamic modeling of this system.

Phase diagram plays an important role in basic aspects of materials research such as phase transformation, solidification, solid-state reaction etc. It also serves as a guideline for material design and processing variables to achieve the desired microstructures and mechanical properties [4, 5]. The properties of a material depend first on the phases and microstructural constituents that are presented. The alloy systems containing several elements have complex phase relations. Thus, phase diagram is essential for better understanding and investigating these complex phase relationships.

The CALPHAD (Calculation of Phase Diagrams) approach is based on the fact that a phase diagram is a representation of the thermodynamic properties of a system [6]. Thus, if the thermodynamic properties are known, it would be possible to calculate the multi-component phase diagram [7]. The Gibbs energy of a phase is described by a representative model that contains some experimental information such as melting, transformation temperatures, solubility, as well as thermodynamic properties.

Experimental investigation of a multi-component phase diagram such as the Al-Mn-Zn ternary system can be time-consuming and expensive. Therefore, CALPHAD method offers a versatile alternative and reliable means to generate phase diagrams, and requires key experiments that are identified using preliminary calculations to validate the thermodynamic models and to check inconsistencies in the reported experimental data. This combined approach of thermodynamic modeling and the experimental investigation is used in this research to provide consistent description of the phase equilibria in the Al-Mn-Zn system at 400℃.

A preliminary thermodynamic modeling of the Al-Mn-Zn system is performed through combining the thermodynamic descriptions of the constituent binaries using FactSage program [8]. The three binary thermodynamic models were reported by Asgar-Khan [24] and Wasiur-Rahman [48]. Calculated liquidus surface and isothermal section of the Al-Mn-Zn system at 400℃ are illustrated in Figures 1.1 and 1.2.

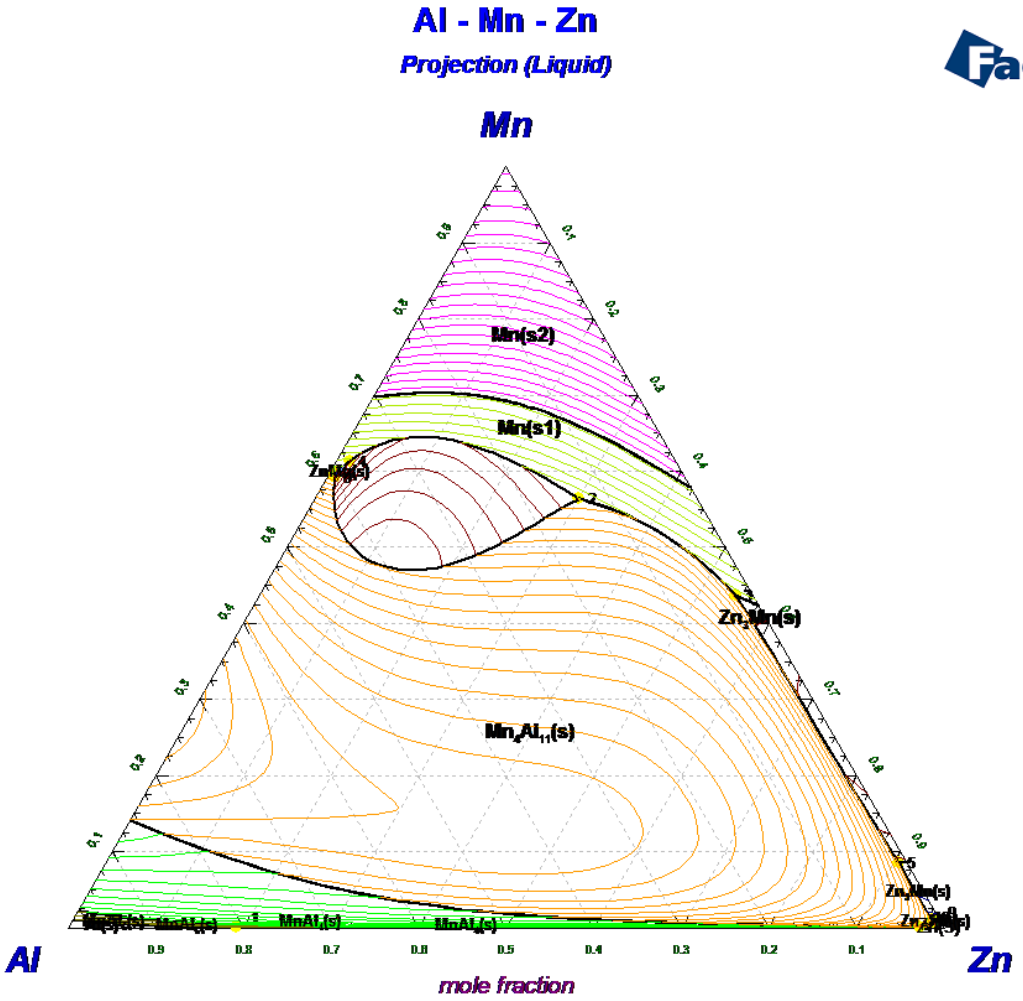

Figure 1.1: Preliminary calculation of the liquidus projection of the Al-Mn-Zn ternary system.

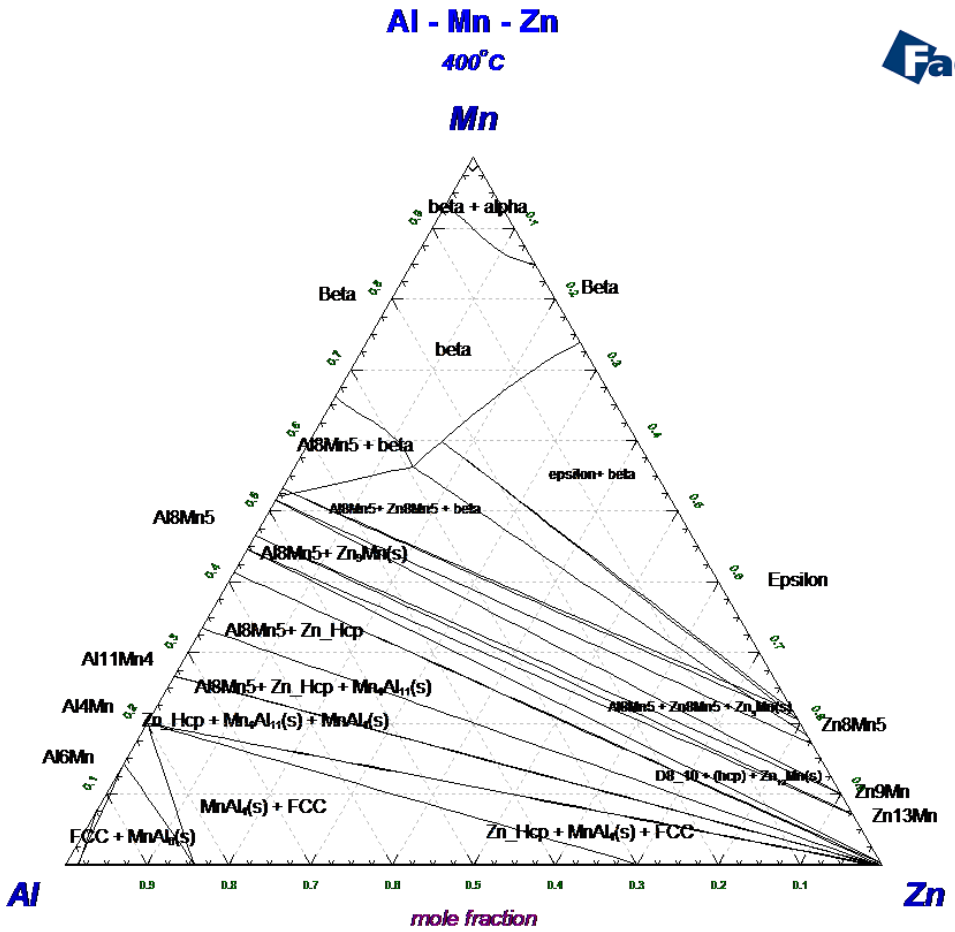

Figure 1.2: Preliminary calculation of the 400℃ isothermal section of the Al-Mn-Zn ternary system.

The objectives of this study

Since the experimental phase equilibrium information and published thermodynamic data on the Al-Mn-Zn ternary system are limited, it is necessary to investigate this system experimentally. The objective of this study is to carry out the experimental investigation on the Al-Mn-Zn ternary system using X-Ray Diffraction (XRD), Electron Probe Micro-Analysis (EMPA), Scanning Electron Microscopy/Energy Dispersive X-Ray Spectrometry (SEM/EDS) and Differential Scanning Calorimetry (DSC). Experimental results will be compared with the thermodynamic calculations. Specific objectives include:

1. Build up a preliminary thermodynamic model by combining thermodynamic description of three constituent binaries.
2. Establish the phase relationships among the various phases in the system.
3. Determine the ternary solubility of binary compounds.
4. Identify the ternary phases and determine their compositions by XRD, EPMA.
5. Construct the isothermal section of the Al-Mn-Zn system at 400℃.
6. Establish the vertical section of the Al-Mn-Zn system at around 14 at% Mn experimentally.

CHAPTER 2

Literature Review

2.1 Al-Mn binary system

Al-Mn binary phase diagram is characterized by a large number of stable phases. Numerous experimental investigations have been done on this system. The general form of Al-Mn binary phase diagram was established in the 1940s using DTA techniques [5]. Taylor [10] and Godecke [11] studied the Al-rich region. Taylor [10] characterized the structure of Al_4Mn. Two forms of structure μ and λ were defined for Al_4Mn. Taylor [10] also demonstrated that φ ($Al_{10}Mn_3$) was a metastable phase which formed from the liquid during cooling and probably also during decomposition of supersaturated Al-fcc solid solution. According to the observation of Godecke [11], the phases labeled φ and μ by Taylor [10] did not belong to the equilibrium diagram; therefore neither do peritectic reaction at 880 nor 820℃. Godecke [71] defined φ phase as the metastable phase that participated in two peritectic reactions: $L+Al_{11}Mn_4$ (HT) ↔ φ and L+ φ↔Al_4Mn through thermal analysis study.

There were some disagreements regarding the Al-rich region of the phase diagram. Taylor [10] proposed no Al_4Mn phase found above 810℃ using XRD technique while Godecke [11] presented that Al_4Mn can be stable up to 923℃ based on thermal analysis.

There were also conflicts about the peritectic temperature at which Al_6Mn formed. Raynor [9] found that Al_6Mn was firmly established as a stable equilibrium phase. Reaction have been reported by [10] and [11] at 670 to 690℃ (on cooling) and at about 710℃ (on heating). Both authors placed the equilibrium peritectic isotherm between 700 and 710℃. But, Phillips [12] observed thermal signals at 690℃ on heating and cooling, none at 710℃. When the λ phase was incorporated into the diagram, it was plausible to suppose that Al_6Mn may be formed from either L+ μ or L+ λ and that two reactions could occur near 700℃. Murrary [13] confirmed the eutectoid reaction at 957℃: $\gamma_1 \leftrightarrow Al_{11}Mn_4 + \gamma_2$; and the $\gamma_1 + \gamma_1 \leftrightarrow \gamma_2$ peritectoid reaction at 900℃ reported by Godecke [11] via DTA, XRD and TEM methods. Murrary [13] presented evidence from melting studies that λ was a stable equilibrium phase, formed from the peritectoid reaction Al_6Mn+ μ↔ λ at 693℃ ±2℃. The stable equilibrium peritectic reaction L+ μ↔Al_6Mn occurred at 706±3℃. The eutectic reaction L↔Al + Al_6Mn occurred at 658±1℃ and the eutectic composition was 1.0±0.1 at% Mn [14].

The ε-phase was first found by Kono [15], who also identified two eutectoid reactions: ε↔ γ_2+β-Mn at 870℃ and γ↔ γ_2+ β-Mn reaction at 840℃ by specific heat measurements. The eutectoid compositions were estimated as 50 and 55 at% Mn. Kuznestsov et al. [16] measured the solubility of Mn in Al in a wide temperature range of 250-600℃ by means of XRD, OM, electrical resistance measurement (ER), and hardness measurement (HM). The results from different methods were consistent with each other. Sigli [17] reported the solubility of Mn in Al from 550-650℃. Matuo et al. [18] determined the solid solubility curve of Mn in Al based on the phenol filtrate analysis method.

McAlister and Murray [19] critically reviewed the experimental information on the Al-Mn system and provided their assessment of the system which is shown in Figure 2.1. They found that $Al_{12}Mn$ phase was observed in the sample which formed in the solid state after prolonged annealing. Ellner [20] reported that the transition from γ to γ_2 was sufficiently rapid that γ-phase cannot be obtained by quenching. He has found the γ-phase was isotypic with tungsten and had lattice parameter a=0.3063 nm which was determined by high temperature X-ray diffraction. Janson [21] simplified the phase relationships of the Al-Mn system as compared to the assessed phase diagram of [19] and presented a thermodynamic description of the system for the first time. Their optimized Al-Mn phase diagram is shown in Figure 2.2. Liu et al. [22] investigated the Al-Mn system between 800 to 1200℃ using diffusion couples technique. They reported that ε/δ-Mn phase boundary was located at approximately 72 at% Mn. The ε-phase region was wider and extended to higher Mn content than that reported before [19, 21]; and the eutectoid reaction (δ-Mn → ε+β-Mn) occurred at approximately 1040℃. The ε-phase with more than 58 at% Mn content transforms to β-Mn, while the same phase with less than 58 at% Mn retained the high temperature HCP phase structure on quenching. Based on their experimental results, Liu et al. [23] re-molded the Al-Mn system and their phase diagram is shown in Figure 2.3. Recently, Asgar-Khan [24] has re-evaluated the system which was in good agreement with most of the experimental results [27-32] as shown in Figure 2.4 and 2.5. From his work [24], thermodynamic calculation almost reproduced the EPMA results of Minamino et al. [25]. Also, his calculation was consistent with the observation of Okamoto [26] who suggested a smooth continuous liquidus curve between the terminal δ-phase (BCC) throughout the ε-phase (HCP) as mentioned in [10].

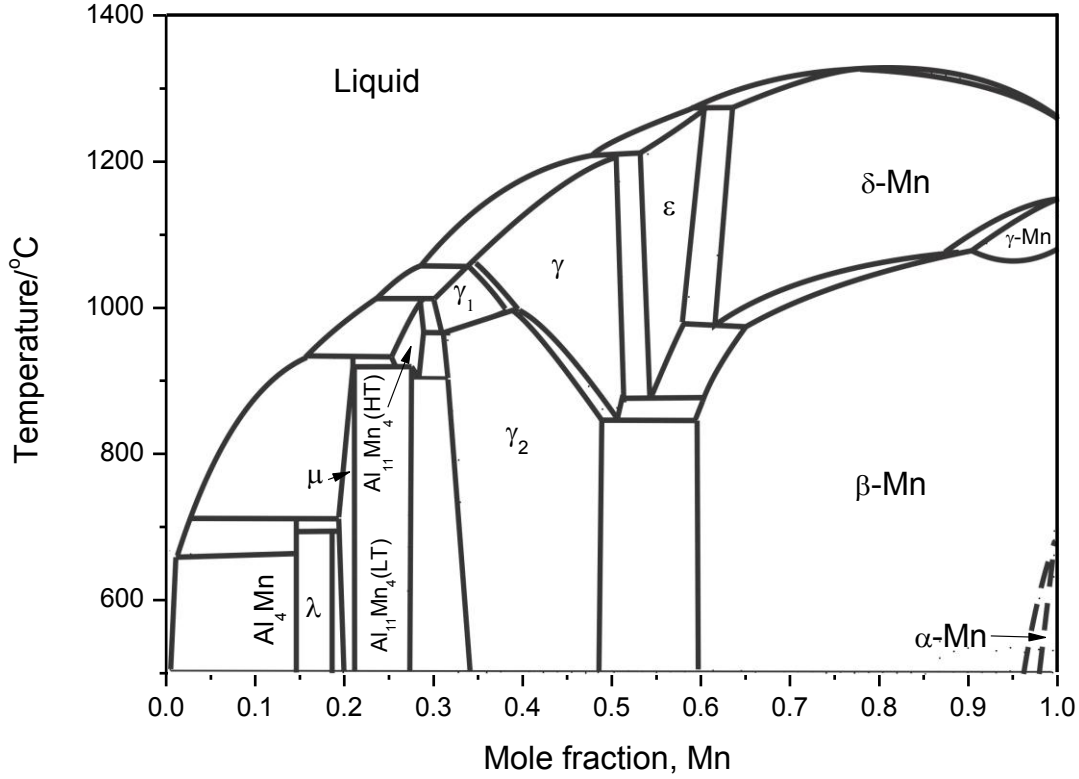

Figure 2.1: Al-Mn phase diagram, 30-70 at% Mn [19].

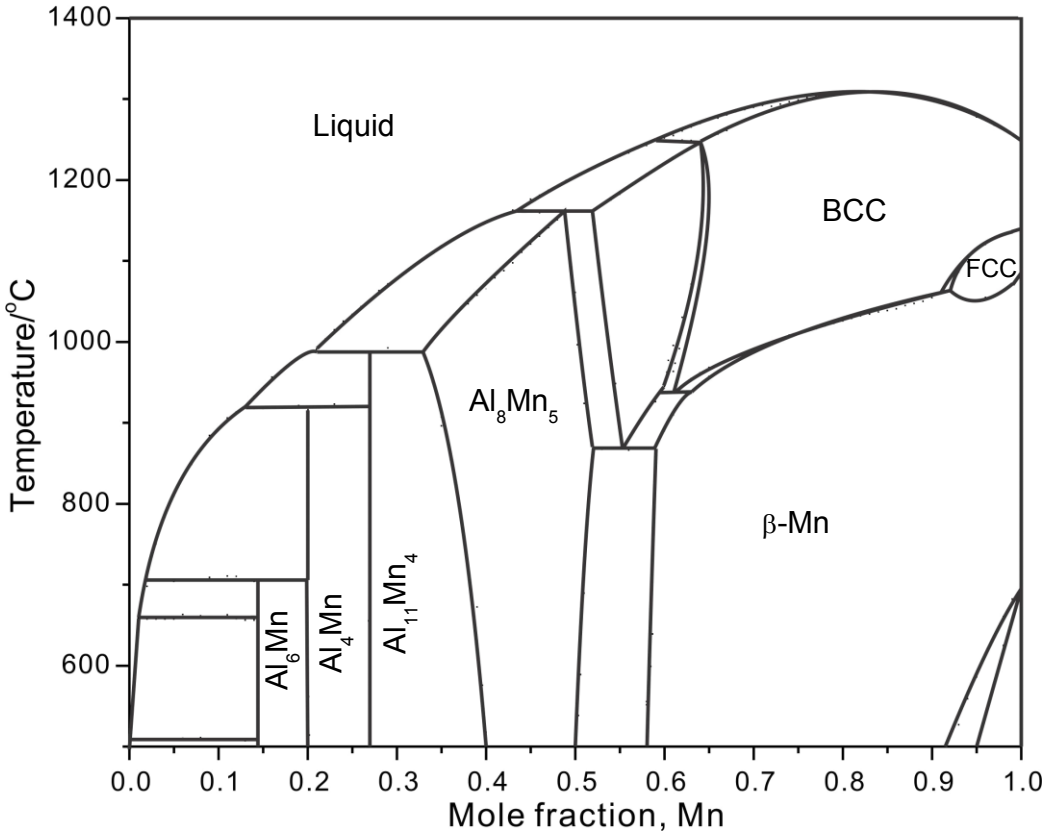

Figure 2.2: Al-Mn phase diagram optimized by [22].

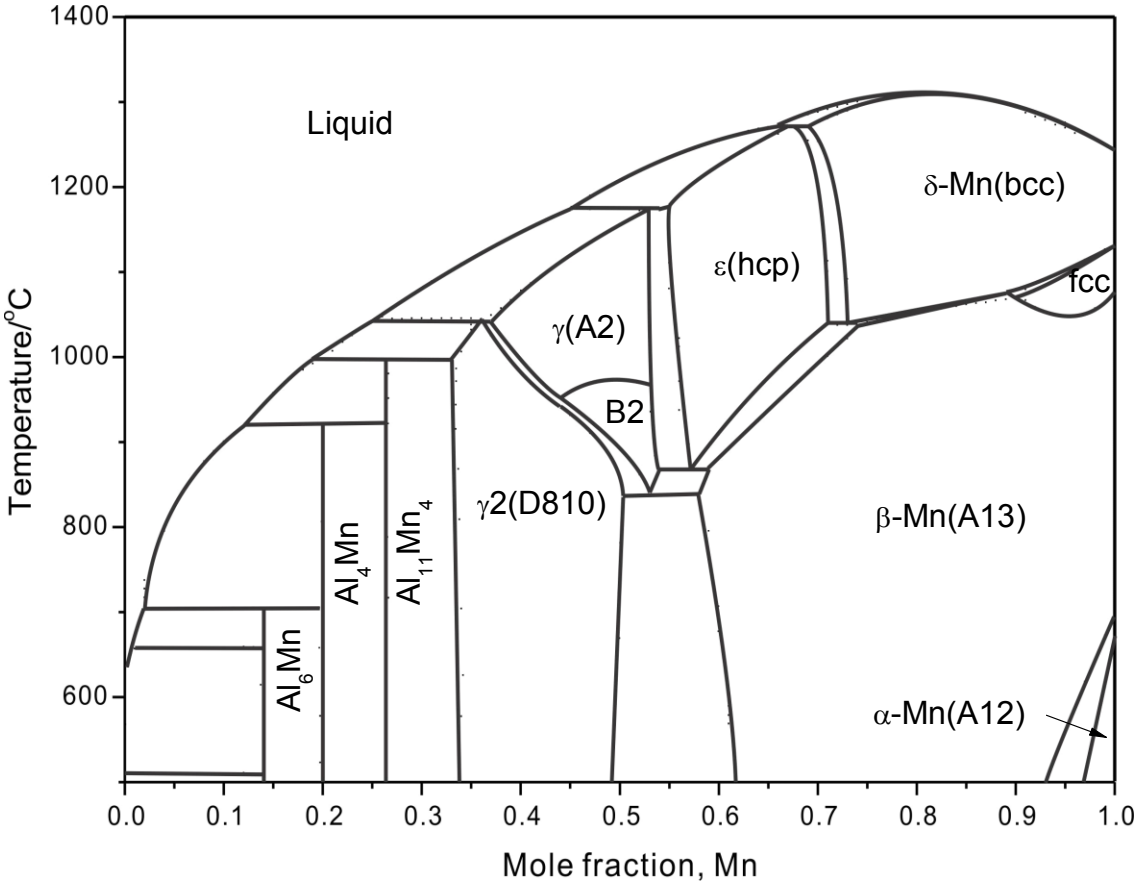

Figure 2.3: Al-Mn phase diagram optimized by [23].

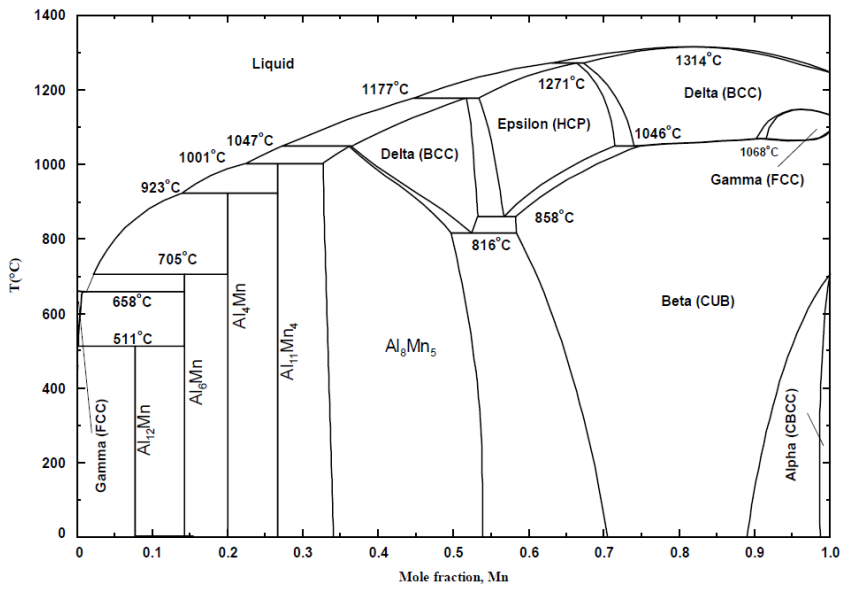

Figure 2.4: Al-Mn phase diagram optimized by [24].

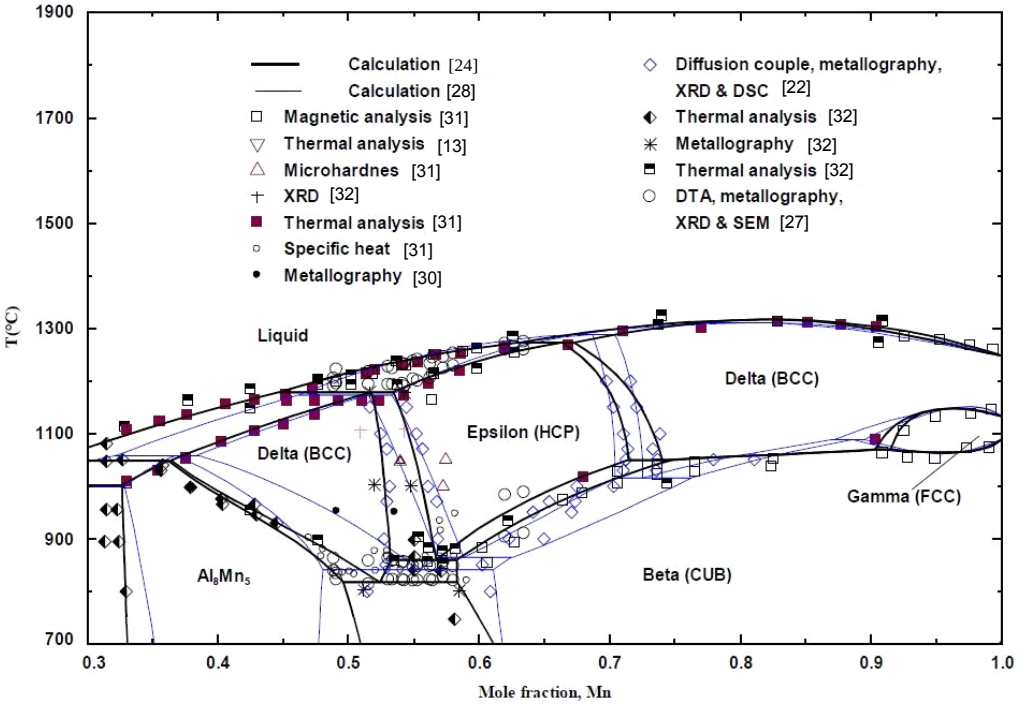

Figure 2.5: Portion of Al-Mn phase diagram optimized by [24] compared with accepted experimental results [27-32].

2.2 Al-Zn binary system

Al-Zn binary system has been studies by several researchers. Heycock and Neville [33] first reported eutectic point in the Zn-rich corner at 380.5℃ with 89.5 at% Zn by using thermal analysis method. Later, Isihara [34] determined the eutectic point at 380℃ and 88.7 at% Zn by electric resistivity method. Similar value was obtained by Tanabe [35] who reported the eutectic point at 380^{o}C with 88.7 at% Zn by electric resistivity and thermal analysis methods. He [35] also measured the liquidus and Al-solidus curve by means of thermal analysis, metallographic analysis and electric-resistance methods. Isihara [34] critically reviewed the results obtained by [35]. He measured the system

using the same methods supplemented by the diatometric method and X-ray diffraction analysis. Isihara [34] mentioned that there was considerable amount of discrepancy between the values of heating and cooling. Both [34] and [35] found a series of thermal arrests between 440℃ and 447℃, and they associated them to the peritectic reaction: L + (Al) ↔ solid solution (β). The liquidus and the Al-solidus curve of the Al-Zn system were also determined by Gayler et al. [36] from 20 to 100 at% Zn using thermal and microscopic analysis. They [36] reported that both the heating and cooling curves for the liquidus were higher than other measurements from the literature. The eutectic temperature was reported as 381℃ by [36]. Pelzel and Schneider [37] studied the system from 30 to 100 at% Zn using specific volume method and their data agreed fairly with the data of [36]. The eutectic point was determined by [37] to be at 380℃ with 88.7 at% Zn. However, Morinaga [38] reported a eutectic point at 382℃ with 90 at% Zn by thermal analysis which was a bit higher than the other researchers [36, 37]. Recently, Peng et al. [39] used the acoustic emission method to do their experimental investigation. They found different acoustic emission signals during solidification. They reported higher liquidus temperatures than other researchers and concluded that the eutectic reaction occurs at 382℃ with 88.7 at% Zn. They also argued that their method was more precise than the conventional thermal analysis because of the absence of the heat hysteresis phenomenon.

Another feature of the Al-Zn binary system is the fcc miscibility gap which has also been studied by many groups of researchers [40-44]. Fink and Willey [40] found two aluminum solid solutions in equilibrium at a temperature above 275℃ by electric resistivity method and reported the critical temperature was 353℃ occurring at 38.5 at%

Zn. This temperature was also confirmed by Simerska and Bartuska [41]. They [41] measured the Al-solvus line boundary of the miscibility gap up to 30.0 at% Zn by X-ray diffraction and transmission electron microscopy. Their results were in good agreement with the previous experimental observations. Borelius and Larsson [42] reported the eutectoid decomposition at 277℃ with an uncertainty of about ± 0.5℃. Münster and Sagel [43] reported the critical temperature and its composition as 341.5 ± 0.4℃ and 39.5 ± 0.002 at% Zn. Terauchi et al. [44] found that the critical temperature should be 351℃ with 39.16 at% Zn and the eutectoid temperature as 275℃ by the means of small-angle X-ray scattering method and cooling curve technique.

The phase equilibrium data were critically assessed by Murray [45]. However, the calculated phase diagram was not in good agreement with the former experimental data. Later, Mey [46] Chen and Chang [47] optimized the Al-Zn system. Both assessments achieved reasonable consistency with the available experimental data. The Al-Zn phase diagram was calculated by [47] and shown in Figure 2.6. However, they did not consider the short range ordering neither for the liquid nor for the Al-fcc solid solution in their calculations. Recently, Wasiur-Rahman [48] has reviewed the previous experimental results and thermodynamic calculation and re-optimized the system and obtained good agreement with most of the experimental results as demonstrated in Figure 2.7.

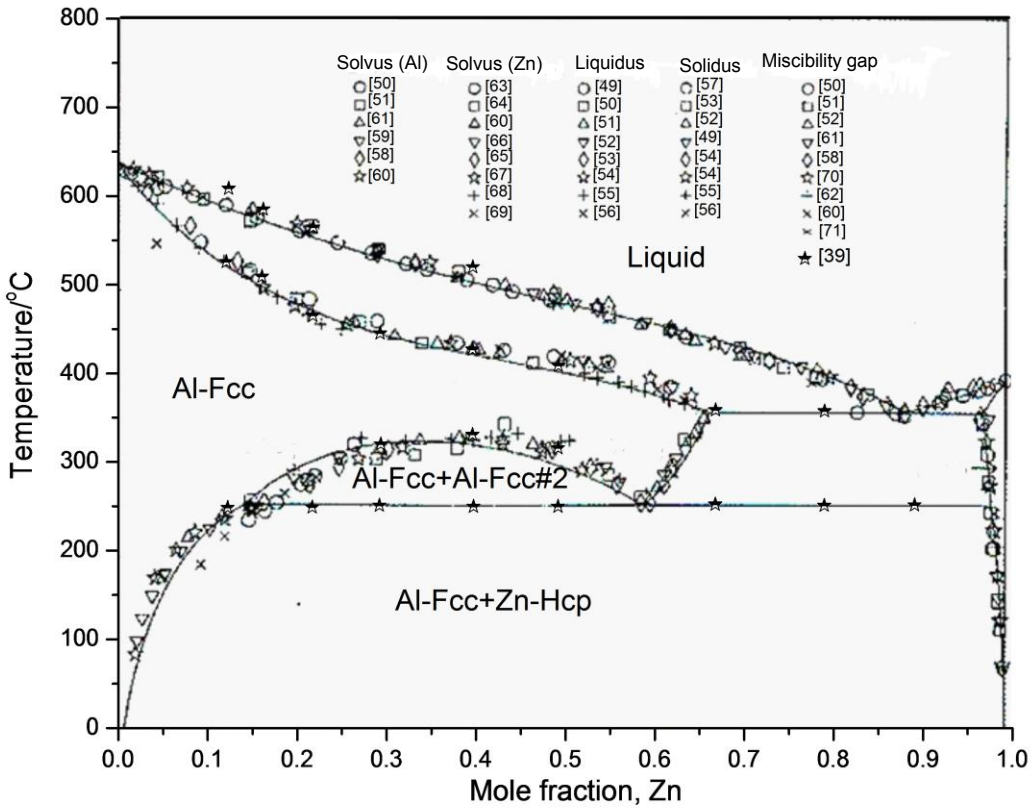

Figure 2.6: Calculated Al-Zn phase diagram [47] (the reference numbers are changed to be consistent with the references of this thesis).

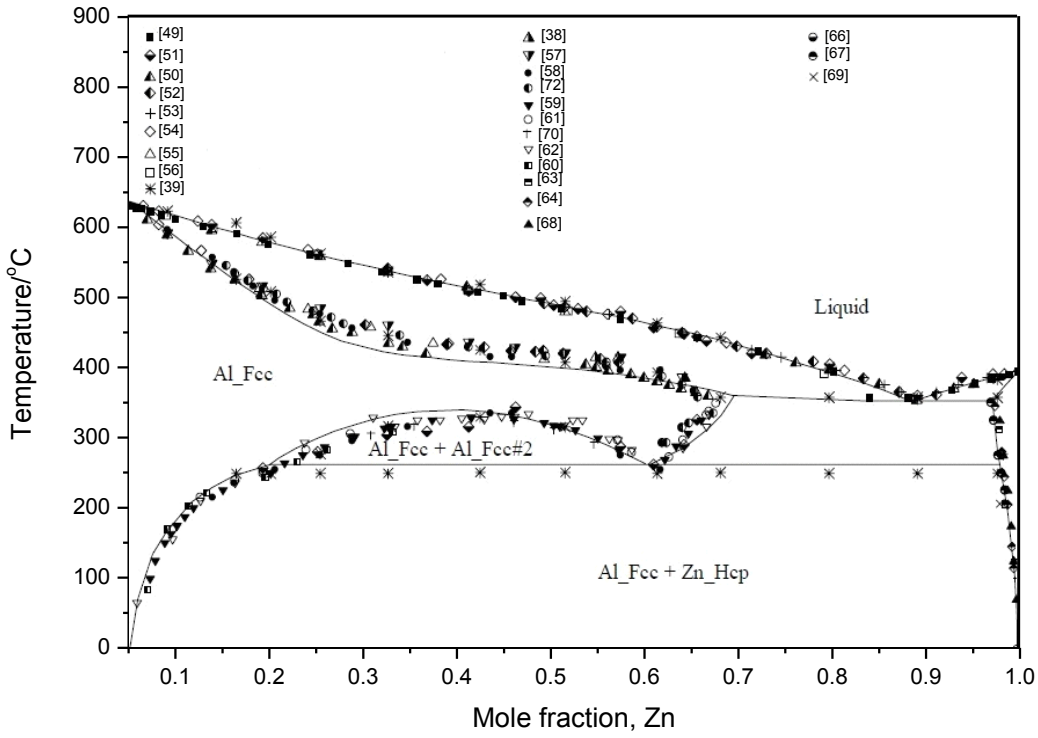

Figure 2.7: Calculated Al-Zn phase diagram [48] (the reference numbers are changed to be consistent with the references of this thesis).

2.3 Mn-Zn binary system

Mn-Zn binary system has been experimentally investigated by numerous researchers in order to establish the phase equilibria and thermodynamic aspects of the system. Experimental results obtained from the prior researches contradicted with each other. Controversy on whether the hexagonal ε-phase has three different forms (ε, ε_1 and ε_2) is still unresolved. Wachetel and Tsiuplak [75] performed magnetic susceptibility measurements on Zn-rich Mn-Zn alloys. Their results indicated that hexagonal ε-phase can be subdivided into a region consisting of three phases: ε, ε_1 and ε_2. However, the investigations performed by Romer [76] and Nakagawa [77] did not show the separation of ε-phase. Xu [79] only confirmed the existence of ε_1 phase by diffusion couple method

at 600℃. He assumed that another controversial subdivision ε_2 could also exist due to the difference in the observed mechanical properties of the Mn-Zn binary alloys. Liang [80] analyzed the Mn-Sn-Zn at 500℃ through XRD and SEM/EDS. $MnZn_3$ region consisted of two subdivisions (ε and ε_1) achieved by Xu [79] also confirmed in Liang's work. Liang [80] also investigated the Mn-Zn system at 400℃. However, only single $MnZn_3$ region was observed at this temperature.

Hansen [73] early summarized the work on the Mn-Zn binary system. Later, Okamoto and Tanner [74] critically reviewed and reported an assessed Mn-Zn phase diagram based on the previously published literature as shown in Figure 2.8. They proposed that the ε phase ($MnZn_3$) could be divided into three regions (ε, ε_1 and ε_2). This conclusion mainly based on the work of Wachtel [75], Romer [76] and Nakagawa [77]. Miettinen [78] re-optimized the Mn-Zn binary system as shown in Figure 2.9 using the experimental results recommend by Okamoto and Tanner [74]. Recently, Asgar-Khan [24] re-investigated the Mn-Zn system and improved the Miettinen's work. The optimized phase diagram is shown in Figure 2.10 together with the experimental data of [75, 76]. His [24] work provided better agreement with the representative experimental data and included some of the low temperature phases which were excluded in Miettinen's [78] work.

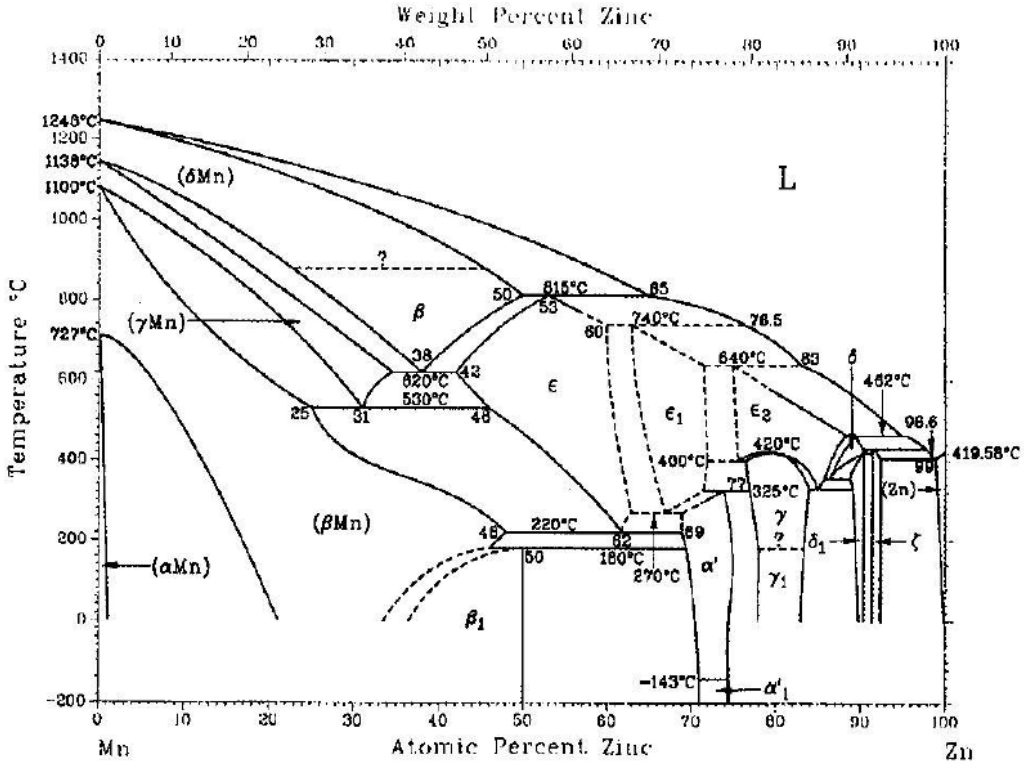

Figure 2.8: Mn-Zn phase diagram assessed by [74].

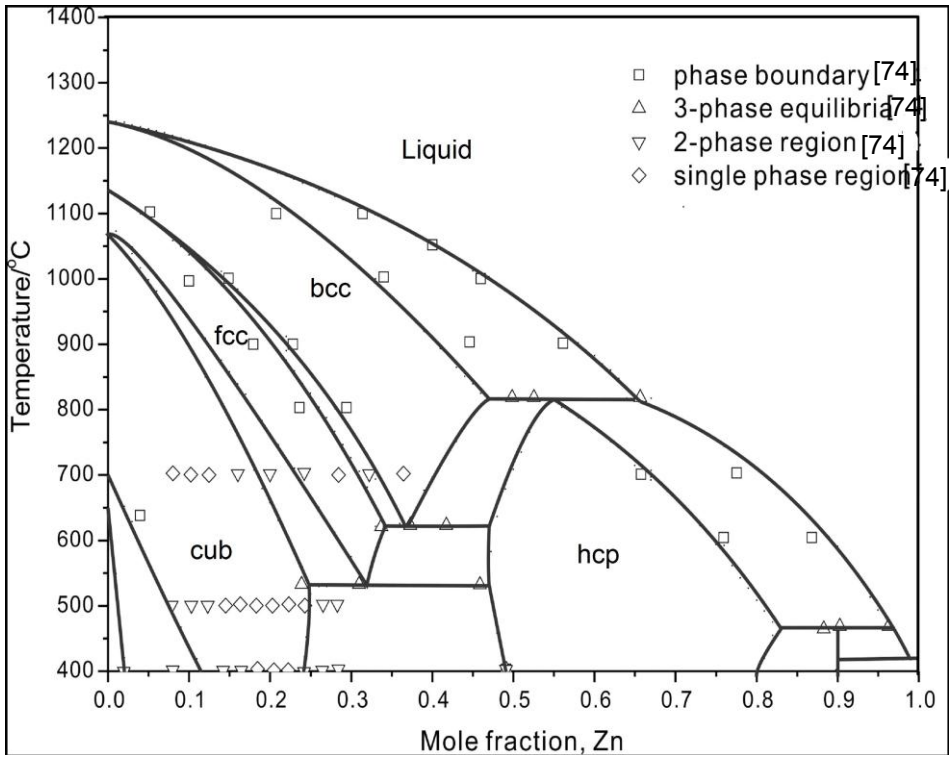

Figure 2.9: Mn-Zn binary system optimized by [78].

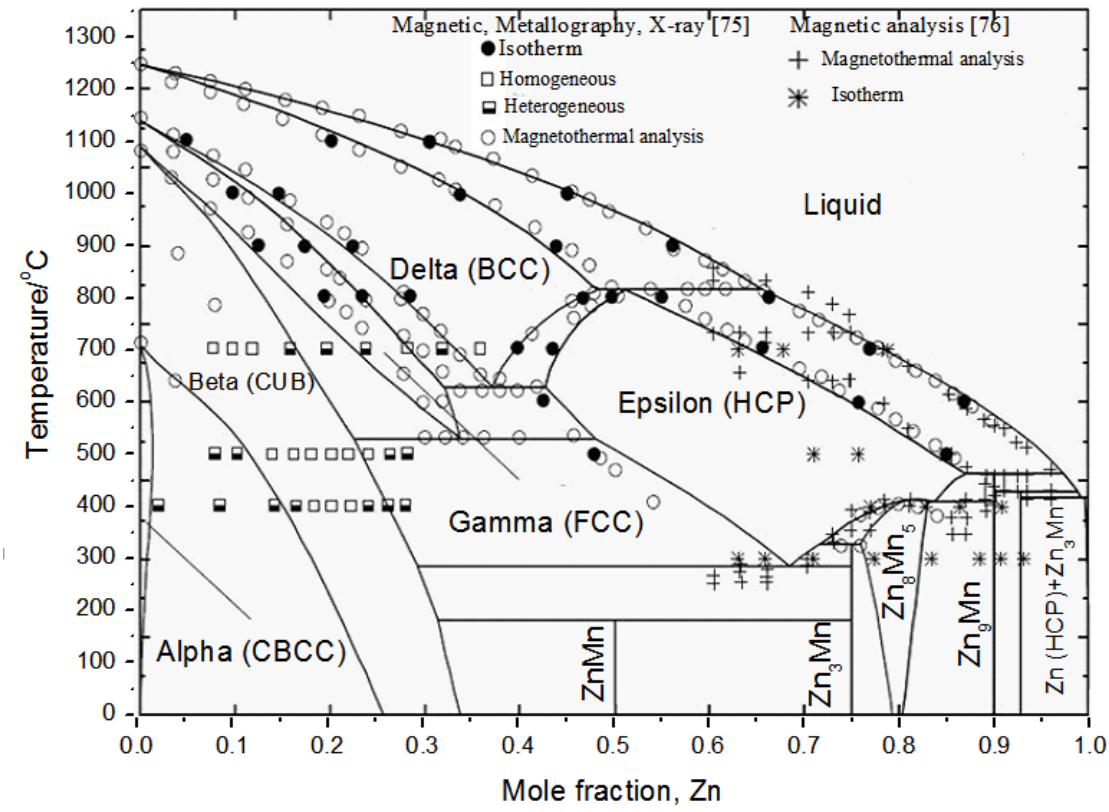

Figure 2.10: Mn-Zn phase diagram optimized by [24].

2.4 Al-Mn-Zn ternary system

The Al-Mn-Zn system was first examined by Gebhardt [81] as summarized in Figures 2.11 and 2.12 which shown projections of the surfaces of primary separation and partial equilibrium relations in solid state at 350℃. Also, Gebhardt found at 412.5℃, the liquid and binary Zn-Mn ζ-phase reacted together to form the Zn-rich solid solution and a phase named V. Later, Raynor and Wakeman [82] optimized the system and specified that the V compound was $MnAl_3$, as shown in Figure 2.13. The equilibrium relations in ternary eutectic region were complex. And with a small increase in manganese content above that of the ternary eutectic, MnAl may separate as primary crystal. The intersections of the boundaries with the eutectic valley are plotted in Figure 2.14. Raynor and Wakeman [82]

used electrolytic deposition methods to obtain three compounds and indicated that the consequence of phases deposited on passing along the eutectic valley towards the ternary eutectic was $MnAl_6 \rightarrow T1 \rightarrow MnAl_4 \rightarrow T2 \rightarrow T3 \rightarrow MnAl_3$ (T1, T2, T3 were from [82] and different from τ_1, τ_2, τ_3 which were reported in this thesis). The formulae of T1, T2 and T3 were reported as $Al_{24}Mn_5Zn$, Al_9Mn_2Zn, $Al_{11}Mn_{2.8}Zn_{2.2}$, respectively. They pointed out that $MnAl_4$ can dissolve up to approximately 5.2 wt% Zn and $MnAl_6$ can take up a small quantity of Zn, at least 0.78 wt%; Zn probably substitute for Mn in the compound. Raynor and Wakeman [82] observed that two factors affected the formation of Al-rich ternary compounds: 1. the ratios of four aluminum atoms in one atom of combined solutes; 2. the electron per atom ratio is approximately 1.85. They [82] observed similar ratios for Ni and Cu atoms in in Al-Mn-Ni and Al-Mn-Cu systems and the comparison demonstrated in Figure 2.15.

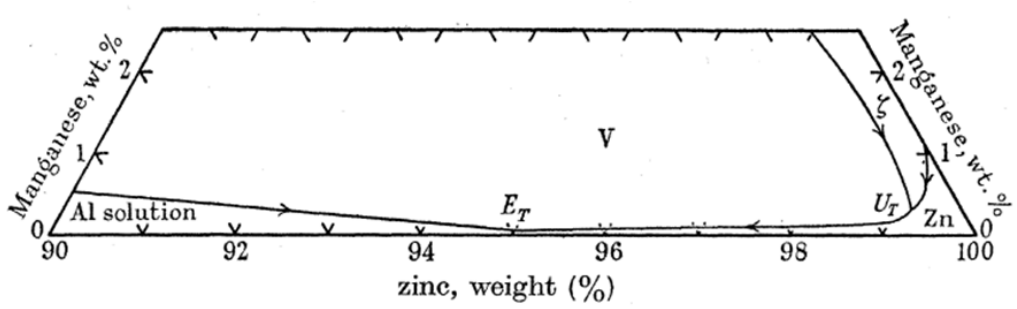

Figure 2.11: Partial liquidus projection obtained by [81].

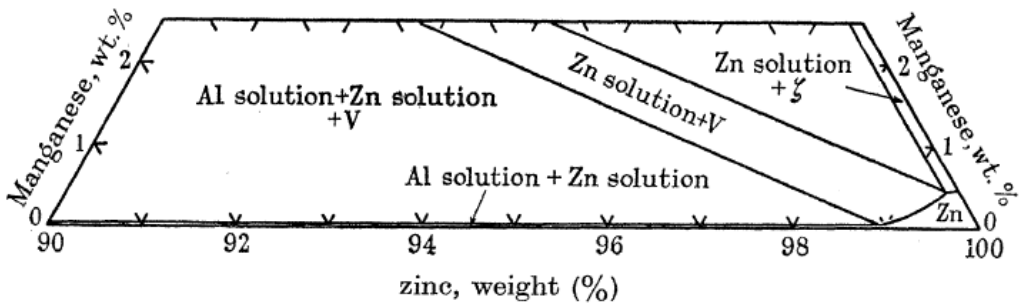

Figure 2.12: partial isothermal section at 350℃ obtained by [81].

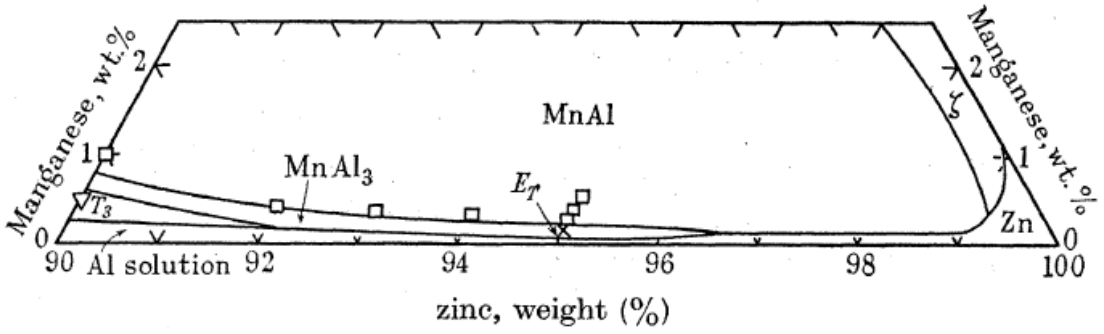

Figure 2.13: The optimized surface of primary separation by [82].

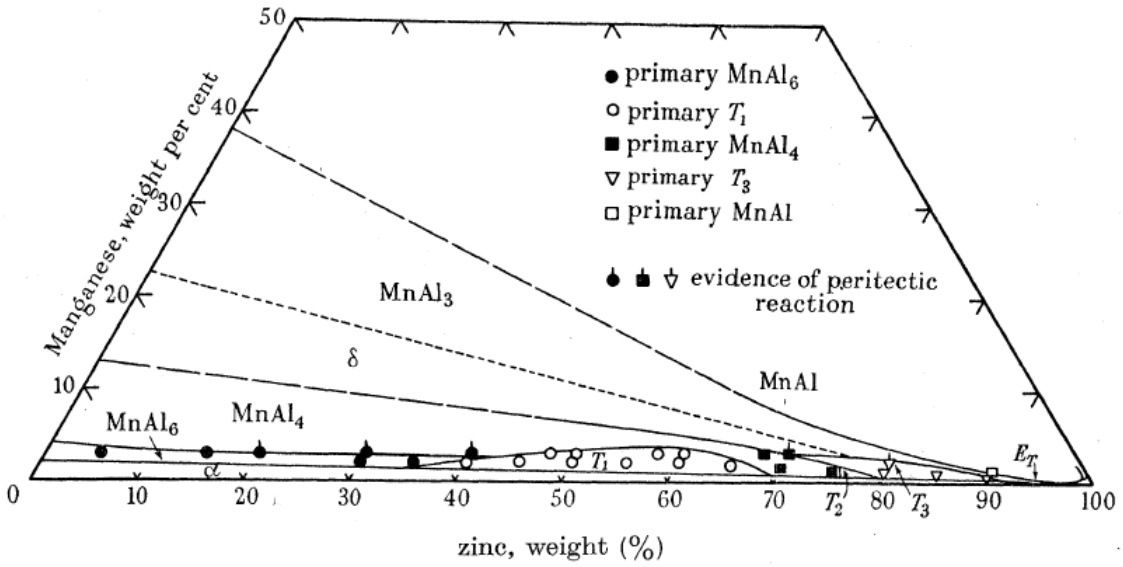

Figure 2.14: The optimized surface of primary separation by [82].

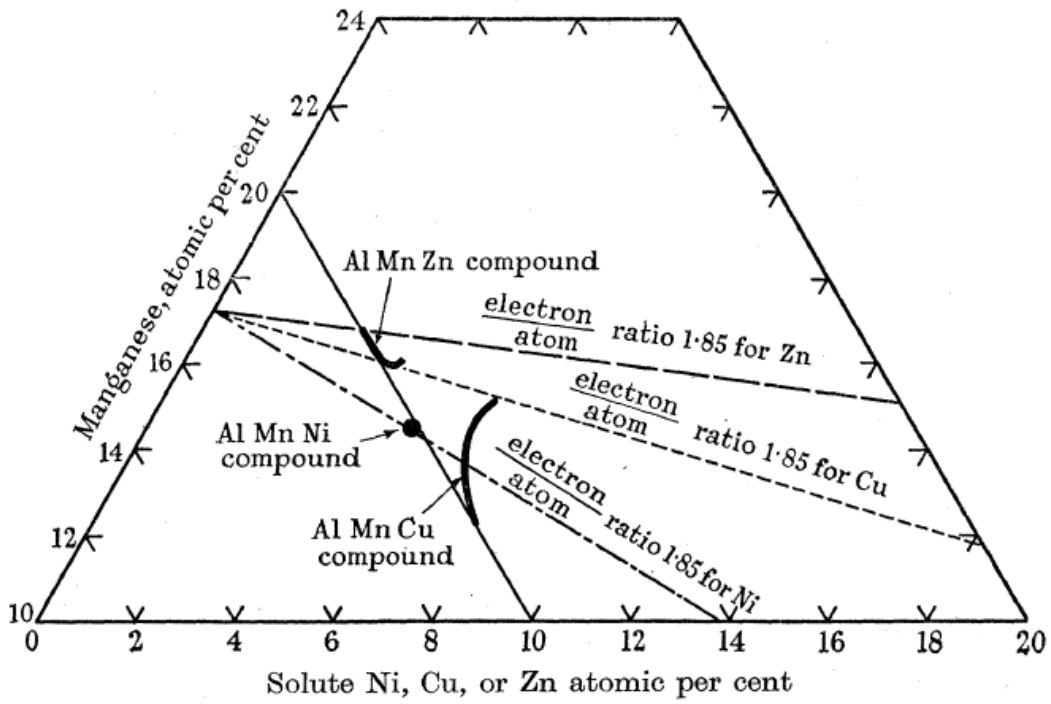

Figure 2.15: Comparison of different system presented by [82].

In the recent years, the research only focused on the structure of the ternary compounds in the Al-Mn-Zn system. Robinson [83] reported that $Al_{24}Mn_5Zn$ phase was centered orthorhombic crystals in the Al-Mn-Zn system with lattice parameters a=2.48, b=2.52 and c=3.03nm. Damjanovic [84] found that $Al_{11}Mn_{2.8}Zn_{2.2}$ was the same structure with lattice parameters a=0.778, b=2.88 and c=1.26nm. Schaefer and Bendersky [85] showed that an addition of Zn to Al-Mn alloys promoted the formation of decagonal phase. Singh and Bendersky [86] used TEM to examine the formation of quasicrystal and the approximant structures to the quasicrystals of $Al_{24}Mn_5Zn$ and $Al_{12}Mn_{2.9}Zn$ (close to T3 phase) in melt-spun condition. They observed that the quasicrystals transformed during annealing at 500 and 600℃.

CHAPTER 3

Experimental Procedures

7 diffusion couples and 35 key alloys have been prepared to investigate the whole composition range of the Al-Mn-Zn ternary system at 400℃ based on the preliminary thermodynamic model. The reasons to choose 400℃ as the annealing temperature are: 1. Annealing temperature should be high enough for faster interdiffusioin and reaction among elements in the alloys; 2. Annealing temperature should be lower than minimum liquidus temperature to avoid melting the alloys.

The starting materials are Al ingots with purity 99.7%, Zn rods with purity 99.99% and Mn pieces with purity 99% all supplied by Alfa Aesar. The key alloys were all prepared by induction melting furnace with Ta crucible under argon protective atmosphere. Samples are re-melted three times to ensure the homogeneity.

3.1 Diffusion couples technique

Diffusion couple technique is employed in the current study. Diffusion couple approach is a valuable experimental method which is widely used to investigate the phase diagram of ternary systems [87-89]. In the diffusion couples or diffusion multiples, there are no problems associated with melting or powder contamination since all the phases form by diffusion reactions of bulk constituents at the interested temperature [90]. Equilibrium

phases form grains or layers and local equilibrium occurs at the phase interface. However, the diffusion couples approach is not omnipotent [90]. It is normal that some phases are missing when the diffusion couple technique is used to determine the phase diagram [87]. This is because the growth rate of some phases is too slow resulting in thin diffusion layer which is hard to detect by EPMA or SEM/EDS as observed in the current work. This issue resulted in difficulties in determining the tie-line composition for some phases. In order to solve this issue and ensure the accuracy of analysis, other diffusion couples with different terminal compositions and key alloys are used to compare and determine the phase equilibria. In the present study, a combination of diffusion couples approach with an investigation of selected equilibrated key alloys is followed, especially for the regions where the exact phase boundaries are questionable.

To prepare solid-solid diffusion couples, the contacting surfaces are grinded down to 1200 grit SiC paper and polished using 1μm water-based diamond suspension and 99% pure ethanol as lubricant. The two end members are carefully pressed and clamped using a steel ring, placed in a Ta container, and sealed in a quartz tube filled with argon. The encapsulated samples are then annealed at 400℃ for 4 weeks. Terminal compositions of diffusion couples have been listed in Table 3.1. Diffusion couples 1, 3, 6 and 7 are crossing many phase regions which could show the phase information along the diffusion path. Diffusion couples 2, 4 and 5 are prepared to investigate the phase relations in Al-rich corner.

Table 3.1: Terminal compositions of diffusion couples.

Diffusion couple number	End members
1	Al-$Mn_{16}Zn_{84}$
2	Al_4Mn-$Al_{85}Zn_{15}$
3	Al-$Mn_{13}Zn_{87}$
4	Mn-$Al_{94}Zn_6$
5	Mn-$Al_{65}Mn_{30}Zn_5$
6	Al-$Mn_{32}Zn_{68}$
7	Al-$Mn_{30}Zn_{70}$

3.2 Key alloys preparation

35 samples have been chosen based on the preliminary thermodynamic calculations to study phase fields and confirm the phase equilibrium relations in certain areas. Special attention is focused on Al-rich corner because of the importance for the Al alloys.

The key alloys are prepared using induction furnace under protective Ar atmosphere in order to protect the melt from oxidation. Then, they are encapsulated in tantalum foil, sealed in evacuated quartz tube annealed at 400℃ for 4 weeks. The actual compositions of these key alloys are determined by Inductively Coupled Plasma/Optical Emission Spectrometry (ICP/OES).

3.3 Characterization of samples

The microstructure and phase composition of critical samples are all analyzed by quantitative EPMA (JOEL-JXA-8900) with a 2μm probe diameter, 15kV acceleration voltage, 20nA probe current. Homogeneity range of certain phases and diffusion layers are studied by EPMA as well. Phi-Rho-Z (PRZ) matrix corrections (modified ZAF) are applied during the analysis. Some samples are analyzed by SEM/EDS (HITACHI S-3400N). The difference between WDS and EDS is less than 2 at%. This value has been checked and compared by several samples. The equilibrium compositions of each phase are obtained by extrapolating the composition-distance curves for each element to the phase boundaries [89, 92].

X-ray diffraction is used for phase analysis and determination of the solubility limits in key alloys. The XRD patterns are obtained using PANanalytical Xpert Pro powder X-ray diffractometer with a CuKα radiation at 45kV and 40mA. The XRD spectrum is acquired from 20 to 120º 2θ with a 0.02º step size. X-ray diffraction study of the samples is carried out using X'Pert HighScore Plus Rietveld analysis software. Pearson's crystal database [93] is used to export the crystallographic entry to check the known phases in the Al-Mn-Zn system. The Crystallographic information of the phases is listed in Table 3.2.

Table 3.2: Crystallographic information of the phases in the Al-Mn-Zn system [93].

Phase	Pearson symbol	Space group	Lattice parameter /nm		
			a	b	c
Al-FCC	cF4	*Fm-3m(225)*	0.40458	0.40458	0.40458
Zn-HCP	hP2	*$P6_3/mmc$(194)*	0.2652	0.2652	0.5025
Beta-Mn	cP20	*$P4_132$(213)*	0.6313	0.6313	0.6313
$Al_{12}Mn$	cI26	*Im*-3 (204)	0.747	0.747	0.747
Al_6Mn	oS28	*Cmcm* (63)	0.75551(4)	0.64994(3)	0.88724(17)
$Mn_{0.55}Al_{0.45}(Al_8Mn_5)$	cI2	*Im*-3*m* (229)	0.3063(3)	0.3063(3)	0.3063(3)
Al_4Mn(μ-Al_4Mn)	hP574	*$P6_3/mmc$(194)*	1.998(1)	1.998(1)	2.4673(4)
$Al_{11}Mn_4$	aP15	*P-1(2)*	0.5062(3)	1.7098(10)	0.5047(3)
Al_3Mn	oP156	*Pnma(62)*	1.4883(3)	1.2447(4)	1.256(3)
$Mn_5Zn_8(Mn_3Zn_7)$	hP2	*$P6_3/mmc$(194)*	0.27584	0.27584	0.44456
$MnZn_{13}$	mS28	*C12/m1(12)*	1.3483(5)	0.76626(1)	0.5134(3)
Mn_3Zn_7	hP2	*$P6_3/mmc$(194)*	0.27584	0.27584	0.44456
$Al_{24}Mn_5Zn$			2.51	2.48	3.03
$Al_{25.80}Mn_{6.40}Zn_{5.80}$	oS152	*Cmcm (63)*	0.778(4)	2.38(1)	1.26(1)

3.4 Thermal Analysis using DSC

Differential scanning calorimeter (DSC) is introduced to perform thermal investigation of the Al-Mn-Zn system using Setaram Setsys DSC-2400. Temperature calibration of the DSC equipment is done using 4 standard pure metals (Al, Ag, Au and Zn), and temperature range is from 420℃ to 1400℃. The samples are cut and mechanically grinded to remove any possible oxidation surface layers. Then, samples are cleaned with ethanol and placed in alumina crucible with a lid cover to prevent Zn evaporation and

protect the apparatus. To avoid the oxidation during the analysis process, multiple evacuations followed by purging with argon were done. The DSC measurements are carried out under flowing argon atmosphere. The experimental conditions used for analysis are listed in Table 3.3. Selection of crucibles, heating and cooling rate and dimensions of the samples are three main factors in thermal analysis by DSC. Zn has high vapor pressure. Thus, In order to minimize the evaporation, fast heating/cooling rates are used. Based on the experimental results, melting range started from around 600℃ accompanied with a mass loss. Therefore, it is better to reduce the holding time during the DSC measurement to minimize the evaporation and the resulting experimental errors. Because of the Zn evaporation, the actual composition could be shifted. Thus, only second cycle of DSC curves is taken into consideration. The details of DSC results are discussed in section 4.4.

Table 3.3: Experimental conditions of DSC analysis.

Item	Conditions
Atmosphere	Argon
Cooling rate	15℃/min
Heating rate	15℃/min
Temperature range	30 -1000℃
Weight of samples	40-50mg

A typical DSC curve for pure Al is presented in Figure 3.1. The sharp peak melting at 650 ℃ corresponds to the melting temperature of Al at 650℃. In the samples that show melting range, onset temperature for the melting is obtained from the points of intersection of the extrapolated baseline and the line of maximum slope. It is common practice to select the onset cooling temperature or peak temperature of the last thermal

event on heating as the liquidus temperature. The sharp and narrow peak demonstrated the isothermal reaction when the heat capacity approaches infinity indicating invariant reaction. Lower and broader peak represents the univariant transition. A single endothermic peak without any tail indicates the characteristics of a congruently melting phase [94]. In order to facilitate the calculation of overlap peaks, the means of subtracting baseline is being used for the horizontal plotting. The baseline is obtained using empty crucibles in sample and reference pan. Onset heating temperature is used for invariant reactions while peak maximum is used for phase field boundaries. During the cooling process, onset temperature is used for both invariant reactions and the phase field boundaries.

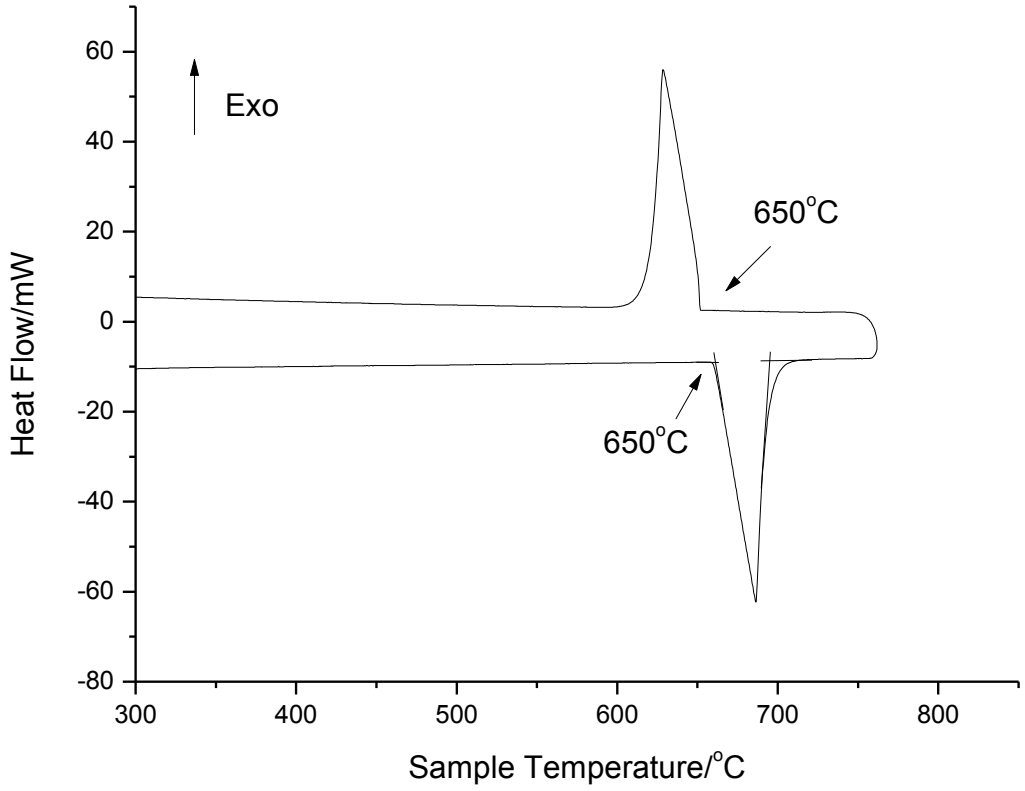

Figure 3.1: DSC curve of Al.

CHAPTER 4

Results and Discussions

4.1 Experimental investigation through diffusion couples

4.1.1 Diffusion couple Al/$Mn_{16}Zn_{84}$, $Al_4Mn/Al_{85}Zn_{15}$ and Al/$Mn_{13}Zn_{87}$

Backscattered electron image of solid-solid diffusion couple Al/$Mn_{16}Zn_{84}$ is presented in Figure 4.1 (a). During heat-treatment, interdiffusion phenomenon happens between the two end members which could allow various equilibrium phases to form. New ternary intermetallic compound τ_1 has been found in this diffusion couple. EPMA line scan is used to measure the elemental gradients along a linear direction which can map the interdiffusion and determine the solubility ranges of each phase. EPMA point analysis has been carried out for the composition identification on the selected layers or phases. Based on compositional information obtained by EPMA analysis, ternary and binary intermetallic compounds and the solid solubility of the binary compounds extending in the ternary system have been identified at 400℃. It is clear to see that there are three diffusion layers. Using local equilibrium principal, the sequence of phases along the diffusion path has been obtained: $Mn_{16}Zn_{84} \rightarrow Al_8Mn_5 \rightarrow Al_{11}Mn_4 \rightarrow \tau_1 \rightarrow$ Al-fcc. The composition profile of EPMA line scan is illustrated in Figure 4.1 (b). τ_1 has been determined as a stoichiometric compound with the composition of 62 at% Al, 16 at% Mn and 22 at% Zn. Al_8Mn_5 phase has ternary solid solubility up to 7.2 at% Zn. In contrast,

$Al_{11}Mn_4$ phase doesn't have significant ternary solid solubility. The equilibrium content of Zn in $Al_{11}Mn_4$ phase is 2.1 at%.

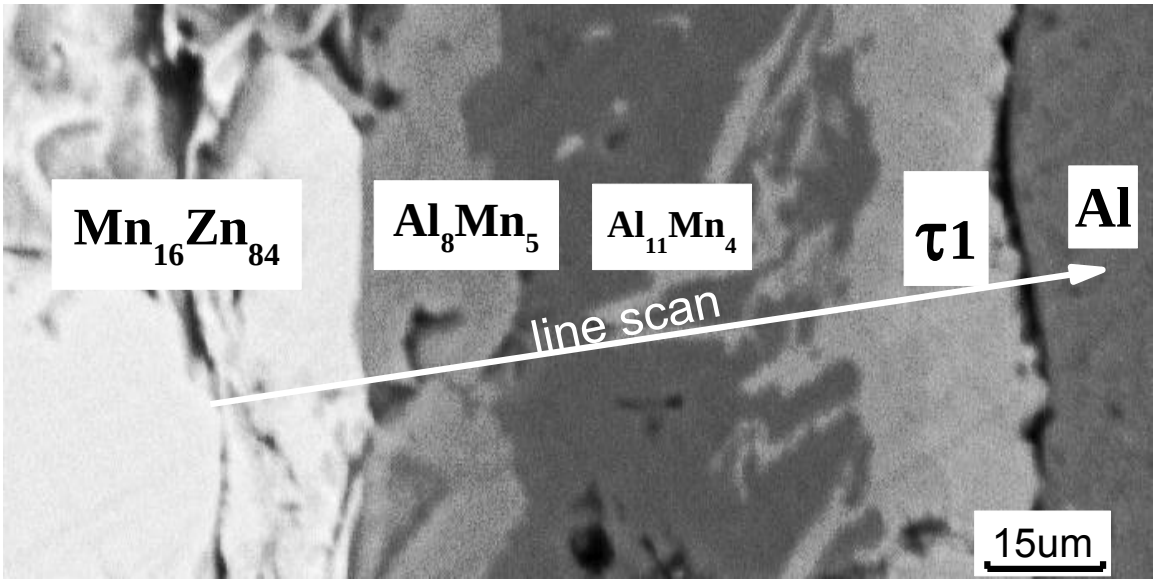

(a)

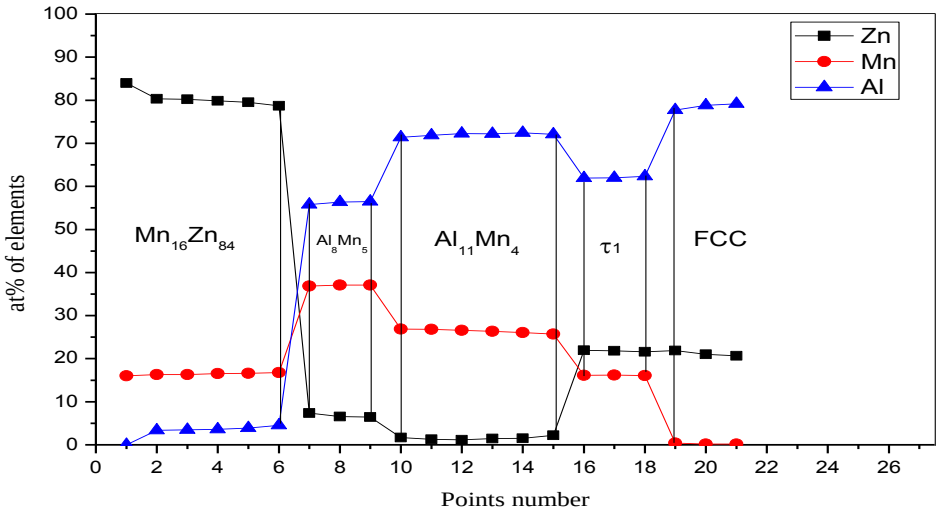

(b)

Figure 4.1: (a) Backscattered electron image of solid-solid diffusion couple Al/$Mn_{16}Zn_{84}$; (b) composition profile of line scan in diffusion couple Al/$Mn_{16}Zn_{84}$.

Backscattered electron image of solid-solid diffusion couple $Al_4Mn/Al_{85}Zn_{15}$ is illustrated in Figure 4.2 (a). The sequence of the phases along the diffusion path is: $Al_4Mn \rightarrow \tau_2 \rightarrow$ Al-fcc. Composition profile of EPMA line scan is shown in Figure 4.2 (b). Ternary intermetallic compound τ_2 has been observed in this diffusion couple. The composition of this ternary intermetallic compound has been determined by EPMA point analysis as 77 at% Al, 12 at% Mn and 11 at% Zn. The experimental results show that Al_4Mn phase has ternary solid solubility about 3.5 at% Zn. Al-fcc phase has binary solid solubility around 11at% Zn.

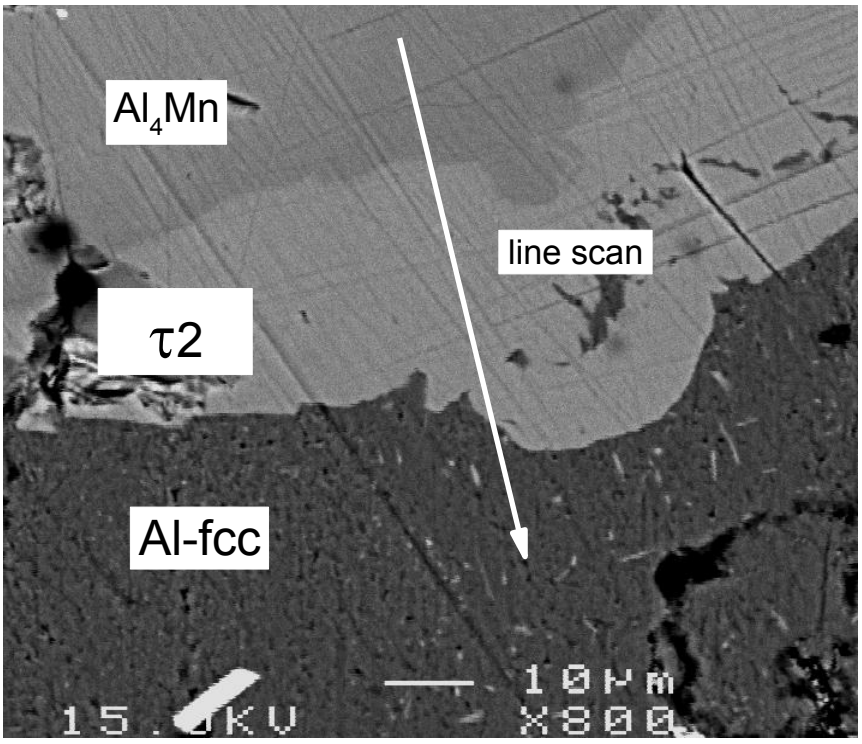

(a)

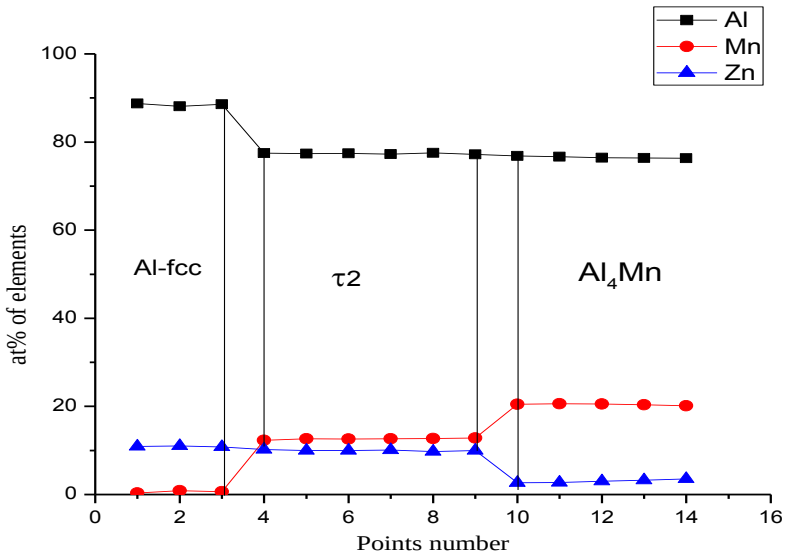

(b)

Figure 4.2: (a) Backscattered electron image of solid-solid diffusion couple $Al_4Mn/Al_{85}Zn_{15}$; (b) composition profile of line scan in diffusion couple $Al_4Mn/Al_{85}Zn_{15}$.

Magnified microstructure of solid-solid diffusion couple $Al/Mn_{13}Zn_{87}$ is presented in Figure 4.3 (a). The results of the EPMA line scan of this diffusion couple are shown in Figure 4.3 (b). Four phases have been identified through EPMA line scan: τ_3, Al_8Mn_5, $Al_{11}Mn_4$ and Al-fcc. The line scan indicates that the ternary intermetallic compound τ_3 has the composition of 10 at% Al, 15 at% Mn and 75 at% Zn. Al_8Mn_5 phase has maximum ternary solid solubility of 7.7 at% Zn. The equilibrium Zn content in $Al_{11}Mn_4$ phase is about 4.2 at%. The binary solid solubility of Al-fcc phase is 23 at% Zn.

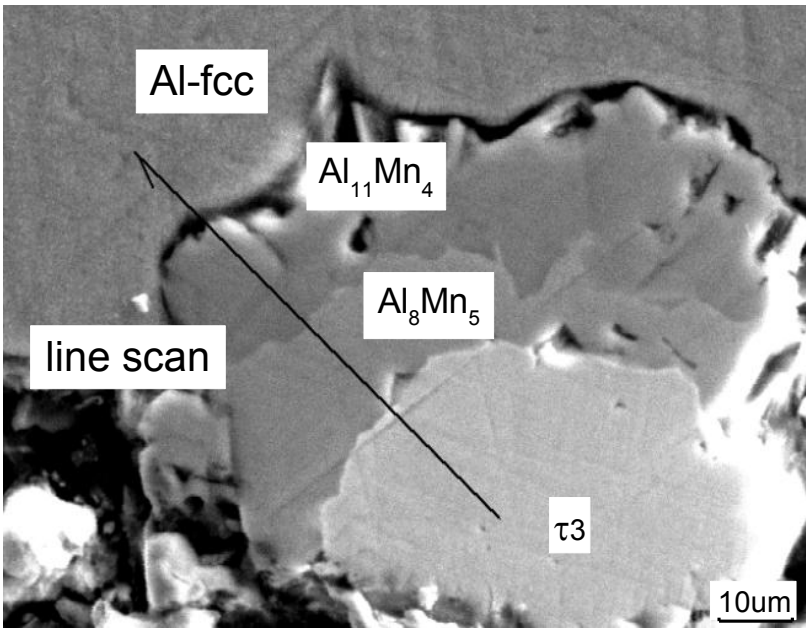

(a)

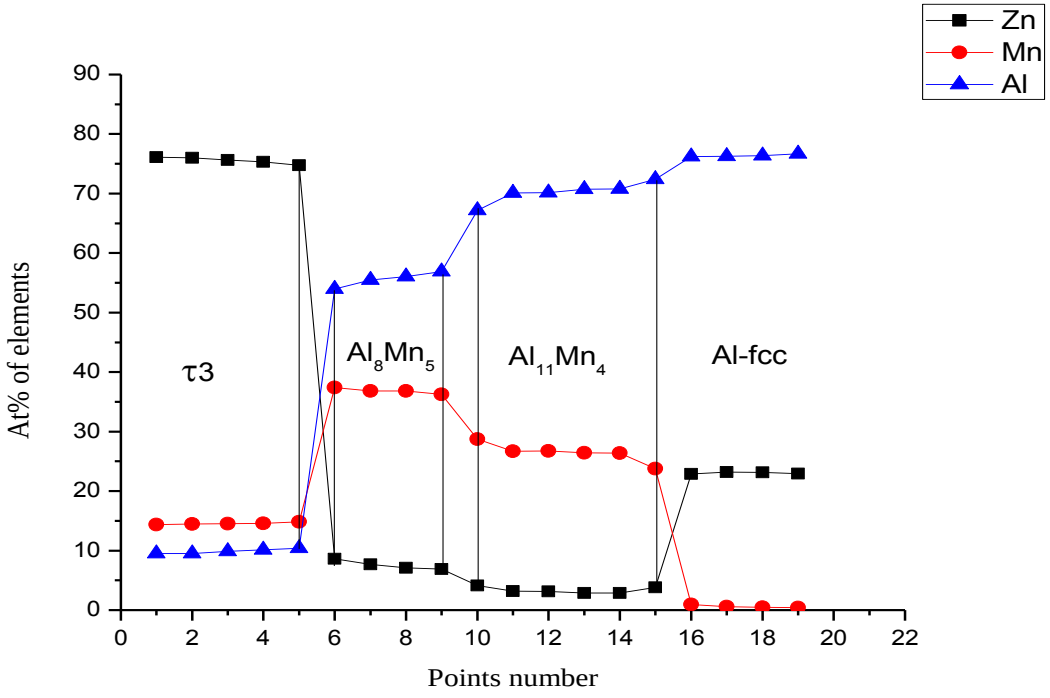

(b)

Figure 4.3: (a) Magnified microstructure of diffusion couple Al/$Mn_{13}Zn_{87}$; (b) composition profile of line scan in Al/$Mn_{13}Zn_{87}$ diffusion couple.

4.1.2 Diffusion couples $Mn/Al_{94}Zn_6$ and $Mn/Al_{65}Mn_{30}Zn_5$

Backscattered electron images of diffusion couple $Mn/Al_{94}Zn_6$ along with magnified microstructure of the area of interest are demonstrated in Figure 4.4. The sequence of the phases along the diffusion path is: Mn → beta-Mn (with ternary solid solubility of 1 at% Al) → beta-Mn (with ternary solid solubility of 2 at% Zn) → $Al_{11}Mn_4$ → $Al_{94}Zn_6$. Beta-Mn and $Al_{11}Mn_4$ phases are dominated in the diffusion layers. Comparing EPMA results with the calculated binary Al-Mn phase diagram, Al_8Mn_5 phase is missing in the $Mn/Al_{94}Zn_6$ diffusion couple. By magnifying BSE image which is shown in Figure 4.4 (b), there are three small layers embedded in between these two phases. With EPMA point analysis, thicker beta-Mn layer in Figure 4.4 (b) has ternary solid solubility of 1 at% Al. The next small layer adjacent to it has been examined as another beta-Mn layer with ternary solid solubility of 2 at% Zn. The missing Al_8Mn_5 layer may belong to the other thin layers. However, point analysis in EPMA process could not be used to analyze the next two continuous small layers, because the thicknesses of them are less than 2 μm. Formation of those thin layers could be due to the different growth rates of the phases. $Al_{11}Mn_4$ layer grows faster than the other stable phases like Al_4Mn and Al_6Mn, which could build up a barrier to stop the subsitutional atoms exchange. Thus, Al_8Mn_5 layer grows slowly and forms much thinner layer.

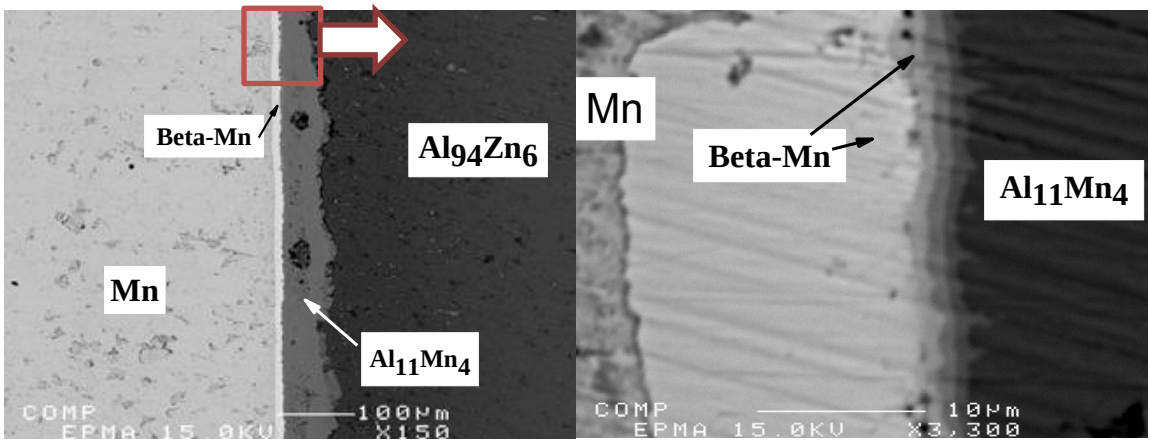

(a) (b)

Figure 4.4: (a) BSE imagine of diffusion couple Mn/$Al_{94}Zn_6$; (b) magnified structure of the area of interest.

In order to determine the homogeneity range of Al_8Mn_5 and investigate the phase relations among beta-Mn, $Al_{11}Mn_4$ and Al_8Mn_5 phases, another diffusion couple Mn/$Al_{65}Mn_{30}Zn_5$ is prepared. Because $Al_{11}Mn_4$ phase has higher growth rate, one end member of this diffusion couple has been selected near the Al_8Mn_5 region. In this diffusion couple Mn/$Al_{65}Mn_{30}Zn_5$, three phases are observed by SEM/EDS: β-Mn, $Al_{11}Mn_4$ and Al_8Mn_5 solid solution. The sequence of phases along the diffusion path is Mn→ β-Mn → Al_8Mn_5 → $Al_{11}Mn_4$ + Al_8Mn_5. BSE image of this diffusion couple along with diffusion path is illustrated in Figure 4.5 (a). The diffusion path starts at pure Mn. Among the interaction with Al, Mn and Zn, β-Mn phase forms with limited ternary solid solubility of 4.8 at% Zn. Al_8Mn_5 phase forms thick layer and the color changes along with decreasing Mn content which suggests the presence of a homogeneity range. Line scan is made to determine the homogeneity range of Al_8Mn_5 phase. Composition profile of the line scan is shown in Figure 4.5 (b). Tie line relations between Al_8Mn_5 and $Al_{11}Mn_4$ have been constructed. From SEM/EDS analysis results, Al_8Mn_5 has ternary

solid solubility of 9 at% Zn and $Al_{11}Mn_4$ has maximum ternary solid solubility around 5.1 at% Zn.

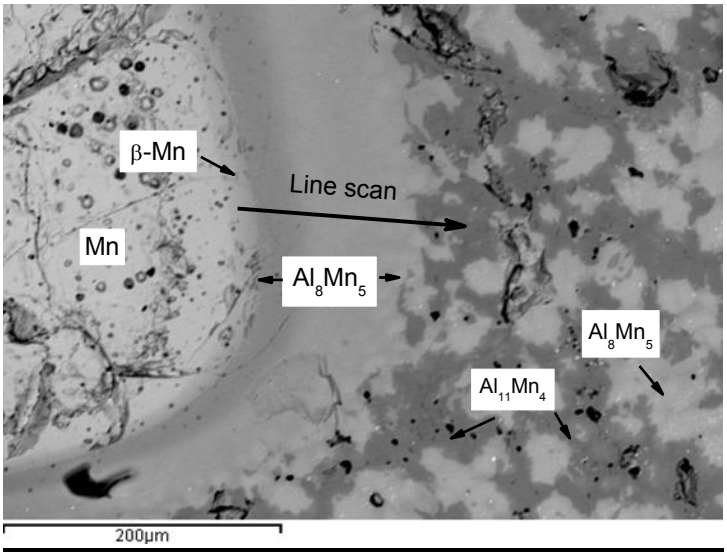

(a)

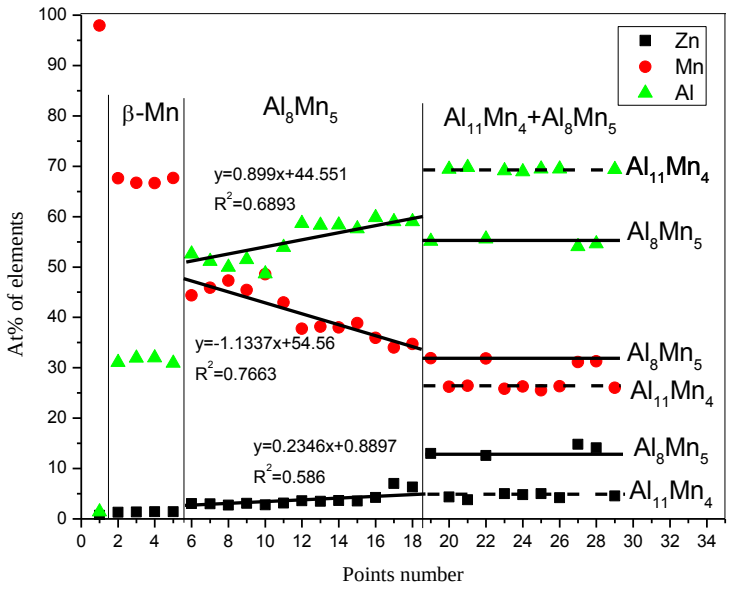

(b)

Figure 4.5: (a) BSE image of diffusion couple Mn/$Al_{65}Mn_{30}Zn_5$; (b) composition profile of line scan in diffusion couple Mn/$Al_{65}Mn_{30}Zn_5$.

4.1.3 Diffusion couples $Al/Mn_{32}Zn_{68}$ and $Al/Mn_{30}Zn_{70}$

Backscattered electron images of diffusion couple $Al/Mn_{32}Zn_{68}$ and $Al/Mn_{30}Zn_{70}$ which are annealed at 400℃ for one month are presented in Figure 4.6 (a) and (b). Both end members $Mn_{32}Zn_{68}$ and $Mn_{30}Zn_{70}$ are in the same ε-phase region. Four phases are identified in these two diffusion couples by EPMA point analysis: ε, Beta-Mn, $Al_{11}Mn_4$ and Al-fcc. Maximum ternary solid solubility of beta-Mn phase has been measured as 5.88 at% Zn by EPMA point analysis. EPMA line scan is used to determine the ternary solubility of binary phases, such as $Al_{11}Mn_4$, Al_6Mn and Al-fcc in the $Al/Mn_{30}Zn_{70}$ diffusion couple. The composition profile of EPMA line scan is presented in Figure 4.6 (c). The results of line scan illustrate that $Al_{11}Mn_4$ phase has limited ternary solubility around 1-2 at% Zn. Al-fcc phase has binary solid solubility of 6.4 at% Zn. The experimental results indicate that no significant solid solubility of Al_6Mn. Binary homogeneity range of ε-phase is detected from 31 at% to 38 at% Mn. Okamoto and Tanner [74] reported that there were three separated phase fields in the ε-phase region. In the current experimental investigation, single phase has been found at 400℃ and nothing indicates the presence of phase separation.

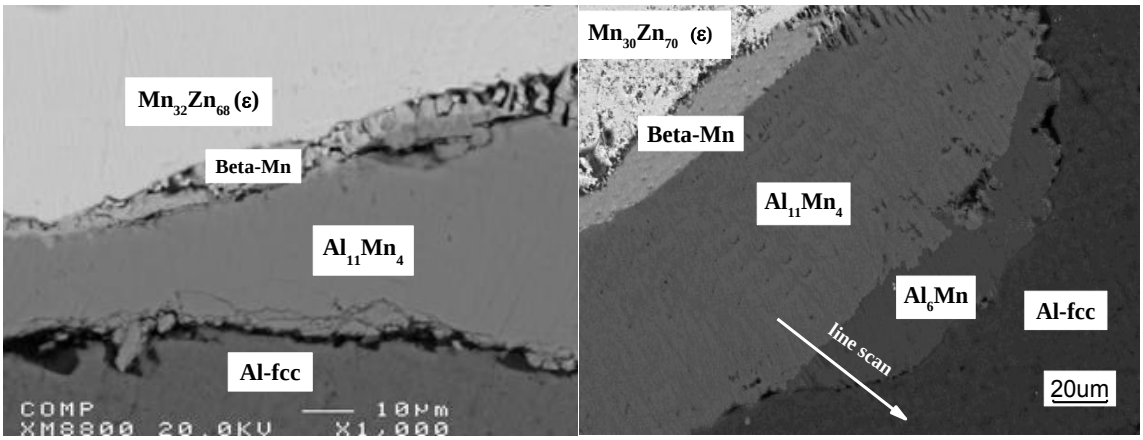

(a) (b)

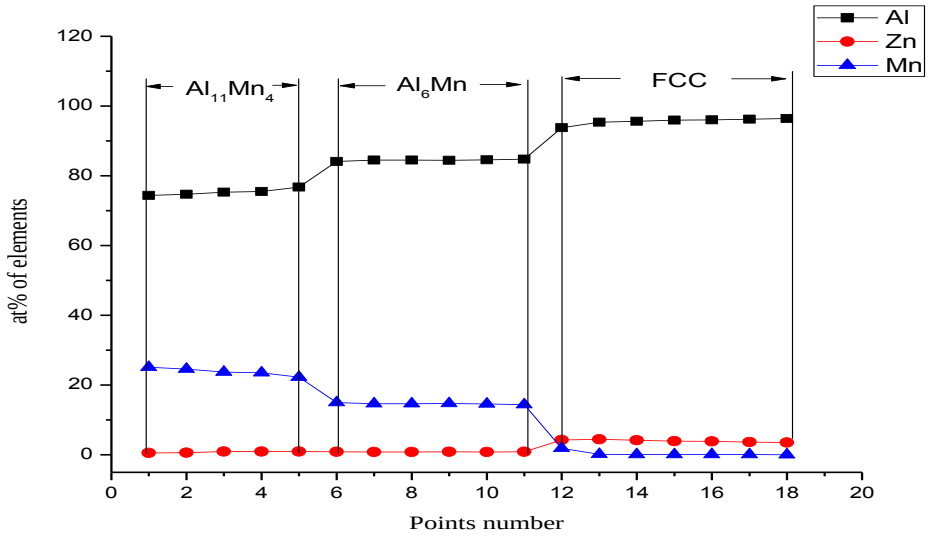

(c)

Figure 4.6: (a) BSE image of diffusion couple Al/$Mn_{32}Zn_{68}$; (b) BSE image of diffusion couple Al/$Mn_{30}Zn_{70}$; (c) composition profile of line scan in diffusion couple Al/$Mn_{30}Zn_{70}$.

Combining the EPMA results of 7 diffusion couples, a large amount of phase equilibrium information has been obtained. The triangulations of detected phases are summarized in Figure 4.7. Three new ternary intermetallic compounds have been found in this system. Diffusion couple results reveal that the ternary solid solubility of Al_8Mn_5 phase reaches 9 at% Zn. $Al_{11}Mn_4$ phase shows maximum ternary solid solubility of 5.1 at% Zn and the ternary solid solubility of β-Mn is determined as 5.89 at% Zn. Al_6Mn and $Al_{11}Mn_4$ phase also exhibit limited ternary solid solubility around 0.9 at% Zn and 1.5at% Zn respectively. Mn_5Zn_8 phase has ternary solid solubility of 4.5 at% Al.

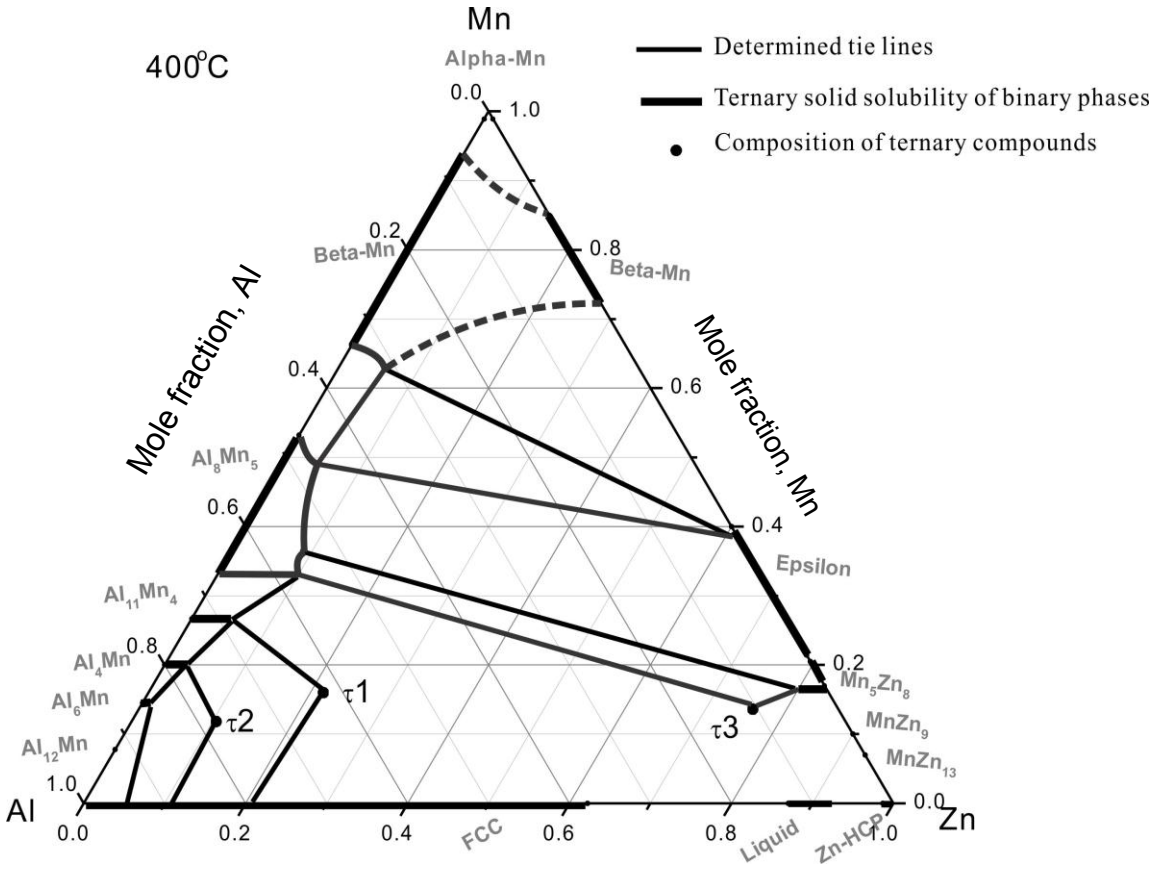

Figure 4.7: Determined phase relations of Al-Mn-Zn system obtained from diffusion couples annealed at 400℃ for 4 weeks.

4.2 Key alloys experimental results

4.2.1 Experimental study of Al_4Mn phase

In binary Al-Mn system, several types of phases will form with composition close to Al_4Mn. As solidification conditions change from very slow to extremely fast the following phases will form: hexagonal μ phase (a=1.995nm; c=2.452nm), hexagonal λ phase (a=2.841nm; c=1.238nm), decagonal quasicrystal, icosahedral quasicrystal and micro-quasicrystalline or amorphous phase [95]. The icosahedral quasicrystal phase forms in Al-Mn by rapid melt quenching and is metastable [96]. When the solidification conditions are slower, another metastable quasicrystal decagonal phase or crystalline phases can be formed icosahedral, decagonal and two other equilibrium hexagonal phases, μ and λ, all of them have a composition close to Al_4Mn [97, 98].

The decagonal quasicrystal has two well-known orthorhombic approximants called the Robinson, or the R approximant, the structure is based on $Al_{20}Mn_3Cu_2$ compound and the Taylor, or the T approximant. The T approximant is based on the structure of Al_3Mn first reported by Taylor [99]. These two decagonal approximants have been found to exist in a number of systems such as Al-Mn [100-102] and Al-Mn-Cu [103, 104].

In order to examine the relations between the formation of Al_4Mn phase and solidification conditions, five key samples have been studied. The composition of key samples and experimental results are presented in Table 4.1. The actual chemical compositions of the alloys are measured by ICP. Samples 1 to 3 have the same composition, but they are solidified at different rates. Post DSC sample often recognized as slow solidified sample because they are analyzed through DSC at relatively slow

cooling rate. As-cast and quenched samples have faster cooling rate due to the experimental process. These samples are always prepared by water cooling or quenching from high temperature.

Table 4.1: The actual composition of key samples and detected phases.

No.	Actual composition identified by ICP (at %)			Condition	Phases detected by XRD
	Al	Mn	Zn		
1	75	13	12	Post DSC	λ-Al_4Mn
2	75	13	12	As cast	Quasicrystal Al_4Mn (T approximant)
3	75	13	12	Quenched	Quasicrystal Al_4Mn (T approximant)
4	78	15	7	Quenched	Quasicrystal Al_4Mn (T approximant)
5	80	20	0	As cast	Quasicrystal Al_4Mn (T approximant)

Sample 1 is first analyzed by DSC under the 5℃/min scan rate. At this lower cooling rate, stable equilibrium Al_4Mn phase will form in the sample which is also mentioned in [65]. The XRD pattern of the post DSC sample 1 is shown in Figure 4.8. λ-Al_4Mn phase has been identified. This finding is also corresponding with Bendersky's suggestion [95] that the sample with compositions close to Al_4Mn will form the stable Al_4Mn phase at slow cooling rate.

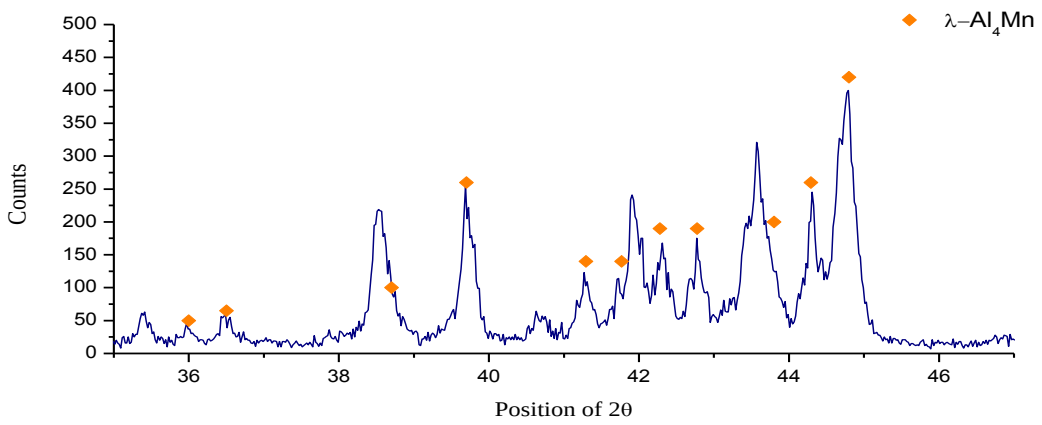

Figure 4.8: XRD pattern of post-DSC sample 1 (only Al_4Mn peaks are labeled to simplify the comparison).

XRD results of as-cast sample and quenched sample indicate that quasicrystal Al_4Mn could form at fast cooling rate. XRD patterns of investigated samples are illustrated in Figure 4.9. By using the crystallographic entry of Al_3Mn as the prototype to process XRD analysis for as cast samples 1 and 5, simulated Al_3Mn patterns could correspond to the XRD spectra of the key samples. Due to the fast cooling speed, quasicrystal Al_4Mn formed in samples 1 and 5.

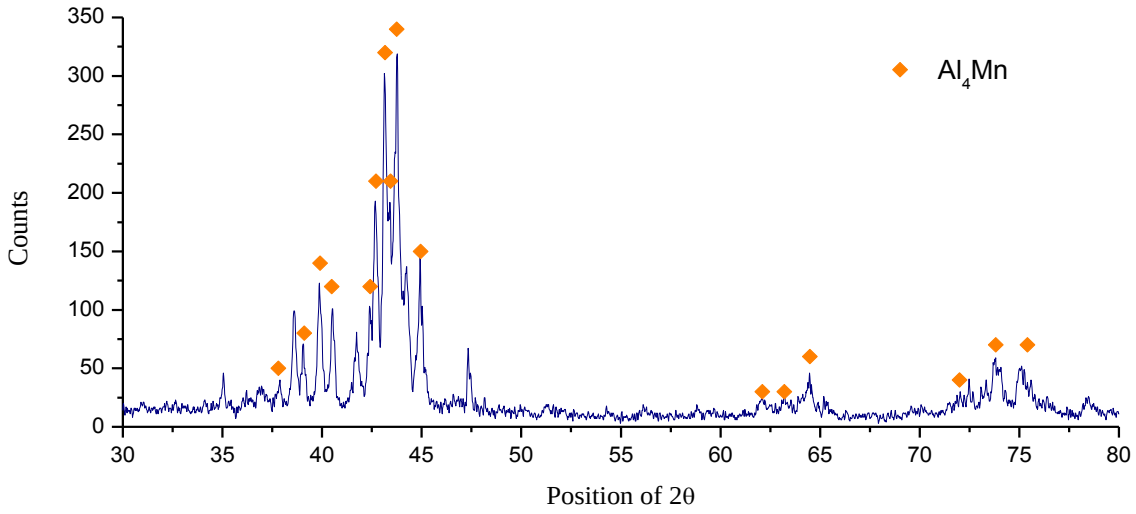

(a)

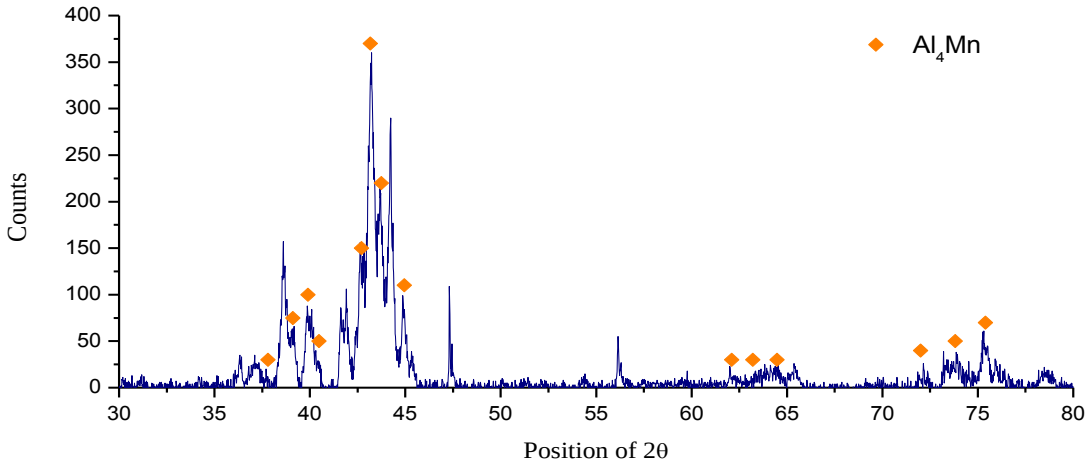

(b)

Figure 4.9: (a) XRD pattern of as-cast sample 5 (only Al_4Mn peaks are labeled); (b) XRD pattern of as-cast sample 1(only Al_4Mn peaks are labeled).

Another observation from experimental results is that the quasicrystal Al_4Mn still exists in the annealed sample at 400℃. As Singh et al. [86] mentioned in their research, Al_4Mn decagonal quasicrystal only can transform to a stable orthorhombic Al_4Mn phase at 500

and 600℃. These results also prove that at lower temperature 400℃, the Al_4Mn quasicrystal still exists in the annealed samples. Also, EPMA results show that the composition of Al_4Mn in quenched samples 3 and 4 varies in Mn range at 18-21 at%. This is because metastable quasicrystal compounds form in samples at this composition range which is also mentioned by Shechtman in his research [96]. He observed that composition of the metastable quasicrystals most likely lied in the 18-22.5 at% Mn range. This is close to the composition region of the stable μ-Al_4Mn phase. In Figure 4.10, the crystallographic entry of Al_4Mn quasicrystal corresponds to the peaks in XRD patterns of the annealed samples 1 and 2.

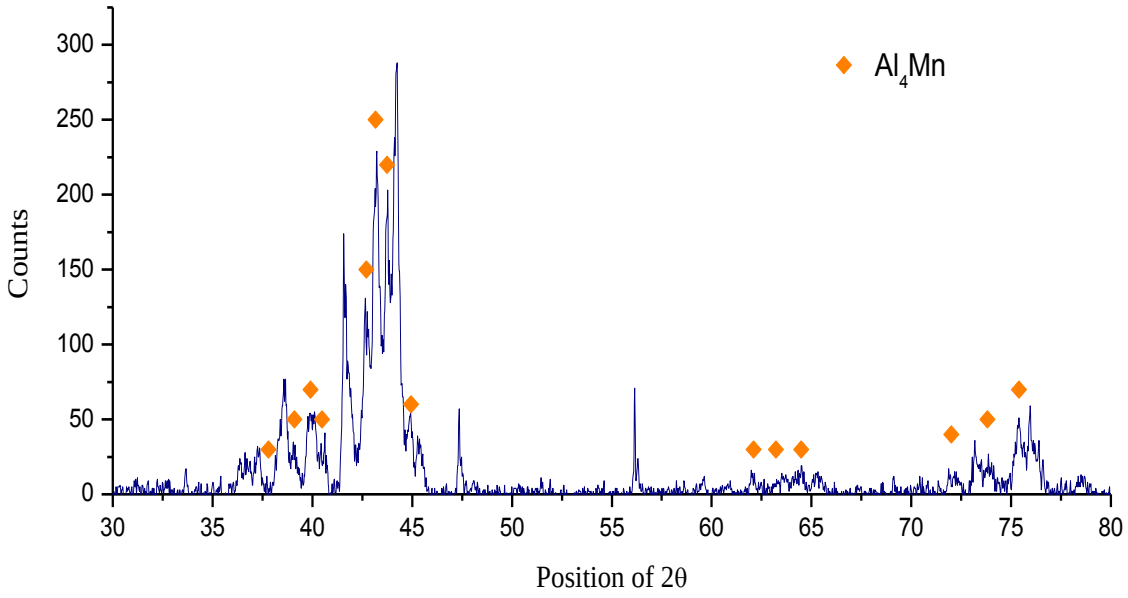

(a)

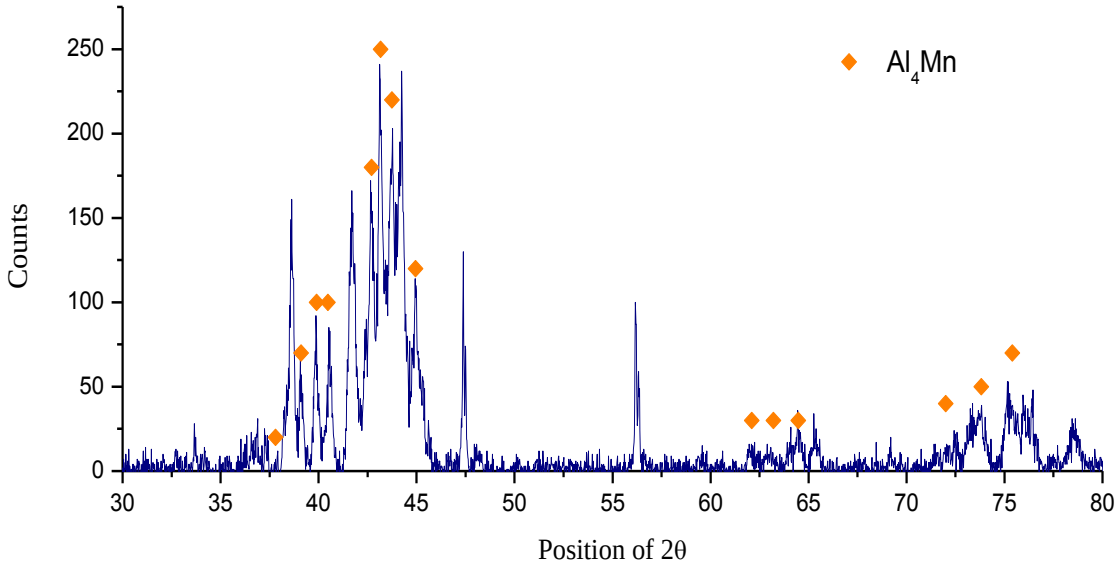

(b)

Figure 4.10: (a) XRD pattern of annealed sample 1(only Al_4Mn peaks are labeled); (b) XRD pattern of annealed sample 2 (only Al_4Mn peaks are labeled).

4.2.2 Phase relations in the Al-rich corner

Four key samples have been prepared to study the phase relations in the Al-rich corner. Three phases Al_4Mn, Al_6Mn and Al-fcc are observed in three key samples. The composition and phase identification of these samples are summarized in Table 4.2. The actual composition of key alloy is measured by ICP and the composition of the detected phases is determined by EPMA.

Table 4.2: The actual composition of key samples and detected phases.

Sample No.	Actual composition identified by ICP (at%)			Phase identification		Composition of identified phases by EPMA (at%)		
	Al	Mn	Zn	By EPMA	By XRD	Al	Mn	Zn
1	80	16	4	Al_6Mn	Al_6Mn	85	14	1
				Al_4Mn	Al_4Mn	76	21	3
				Al-fcc	Al-fcc	91	0.3	8.7
2	83	12	5	Al_6Mn	Al_6Mn	85	14	1
				Al_4Mn	Al_4Mn	75	22	3
				Al-fcc	Al-fcc	93	0.3	6.7
3	82	11	7	Al_6Mn	Al_6Mn	85.2	14	0.8
				Al_4Mn	Al_4Mn	75	20	5
				Al-fcc	Al-fcc	94.4	0.3	5.3
4	91	6	3	$Al_{12}Mn$		92	7.7	0.3
				Al-fcc		95.8	0.2	4
				Al_6Mn		82.9	15.8	1.3

Backscattered electron images of samples 1 and 2 are presented in Figure 4.11. There are some cracks or porosities in the samples. They are caused by the shrinkage of the Al_6Mn phase during the quenching process. EPMA point analysis is used to determine the composition of the detected phases. Based on EPMA results, Al_6Mn phase has ternary solid solubility close to 1 at% Zn. And, Al_4Mn has maximum ternary solid solubility up to 3 at% Zn. In order to confirm the phase relations obtained from EPMA, these samples are also studied by XRD. XRD analysis results show great consistency with those examined by EPMA. The XRD spectra of samples 1 and 2 are illustrated in Figure 4.12. The quasicrystal form of Al_4Mn is also found in these annealed samples. Phase relations among $Al_{12}Mn$, Al_6Mn and Al-fcc are also studied by sample 4 through EPMA. Ternary solid solubility of $Al_{12}Mn$ and Al_6Mn are also determined by EPMA point analysis.

$Al_{12}Mn$ has ternary solid solubility of 0.3 at% Zn and the ternary solid solubility of around Al_6Mn is found as 1.3 at% Zn.

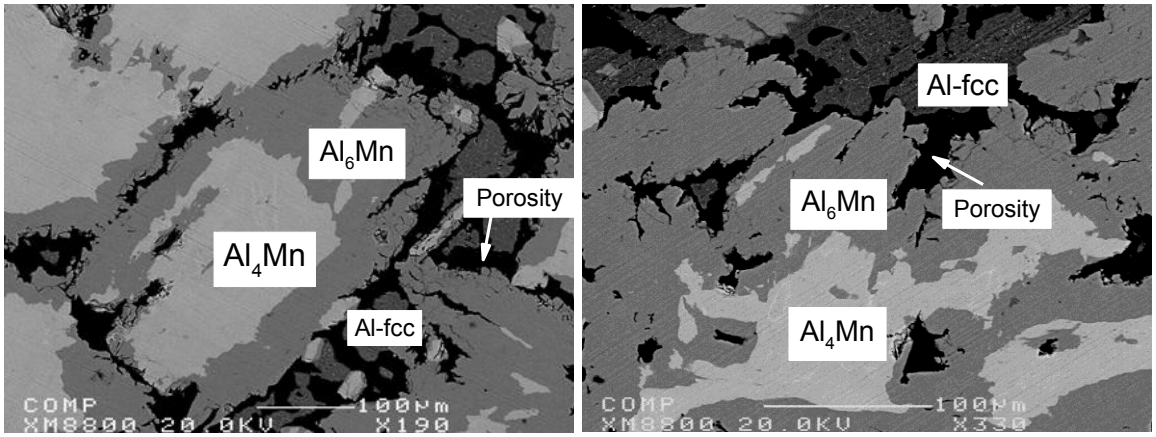

(a) (b)

Figure 4.11: (a) BSE image of sample 1; (b) BSE image of sample 2.

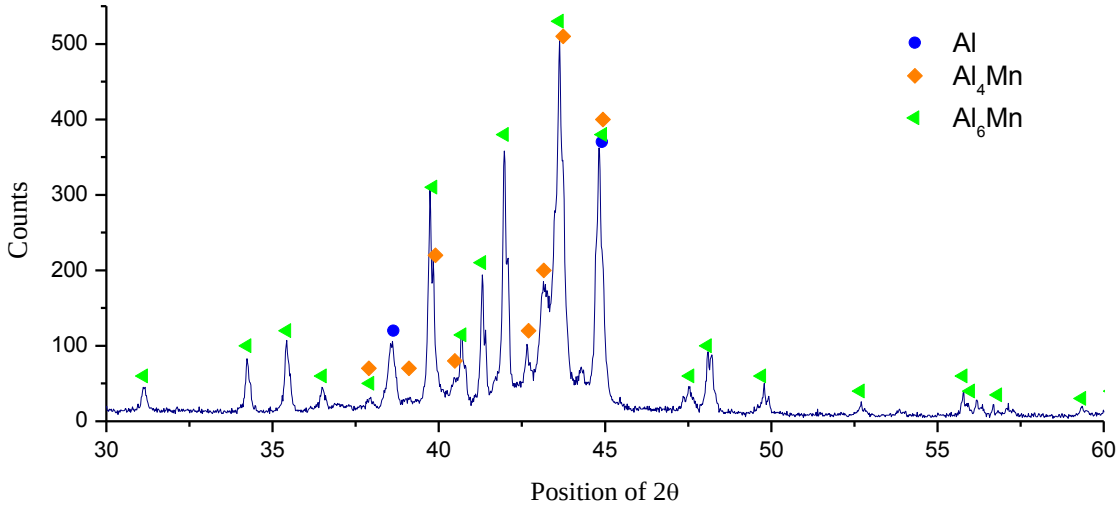

(a)

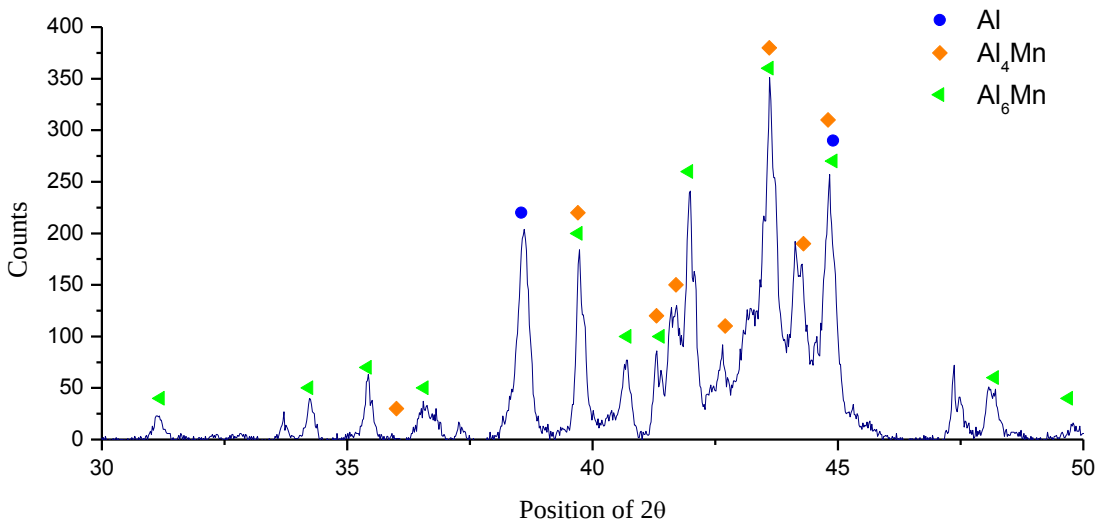

(b)

Figure 4.12: (a) XRD pattern of sample 1; (b) XRD pattern of sample 2.

4.2.3 Experimental study of ternary compounds τ_1 and τ_2

Ternary compounds τ_1 and τ_2 are first found in the diffusion couples which have been discussed in previous session. In order to confirm the existence of these two ternary intermetallic compounds and compare with the results of diffusion couples, several key samples have been prepared. The actual compositions of these annealed samples are measured by ICP and shown in Table 4.3. The compositions of the detected phases are also presented in Table 4.3 as well. Ternary compound τ_2 has been found in this system at 400℃ after analysis of 5 key samples. Same phase relations are observed from these samples through EPMA analysis. Backscattered electron images of samples 1 and 2 are shown in Figure 4.13. Three phases are found in these key samples: τ_2, Al-fcc and Al_4Mn. EPMA results indicate that the ternary compound τ_2 is approximately stoichiometric. The composition of τ_2 does not change too much in these samples and it has an average

composition of $Al_{76}Mn_{13}Zn_{11}$. Sample 6 also confirms the existence of another ternary intermetallic compound τ_1 which is found by diffusion couple $Al/Mn_{16}Zn_{84}$. τ_1 is also a new ternary stoichiometric compound with $Al_{64.2}Mn_{15.2}Zn_{20.6}$ composition.

Table 4.3: The actual composition of key samples and detected phases.

Sample No.	Actual composition identified by ICP (at%)			Phase identification		Composition of identified phases by EPMA (at%)		
	Al	Mn	Zn	By EPMA	By XRD	Al	Mn	Zn
1	75	13	12	τ_2		76	12	12
				Al_4Mn	Al_4Mn	74	20	6
				Al-fcc	Al-fcc	78	0.3	22
2	78	15	7	τ_2		76	13	11
				Al_4Mn	Al_4Mn	75.7	19.5	4.8
				Al-fcc	Al-fcc	88.5	0.5	11
3	79	10	11	τ_2		74	14	12
				Al_4Mn	Al_4Mn	76.8	19.6	3.6
				Al-fcc	Al-fcc	78.4	0.3	21.3
4	74	16	10	τ_2		75	13	12
				Al_4Mn	Al_4Mn	74	20.5	5.5
				Al-fcc	Al-fcc	75.4	0	4.6
5	74	15	11	τ_2		75	13	12
				Al_4Mn	Al_4Mn	74	20	6
				Al-fcc	Al-fcc	80	0	20
6	44	16	40	Al_4Mn	Al_4Mn	74	20	6
				τ_1		64.2	15.2	20.6
				Al-fcc	Al-fcc	55.5	0	44.5

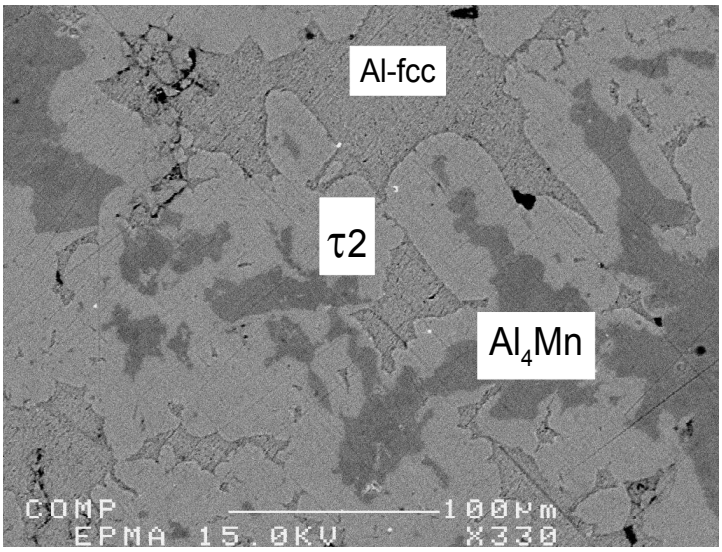

(a)

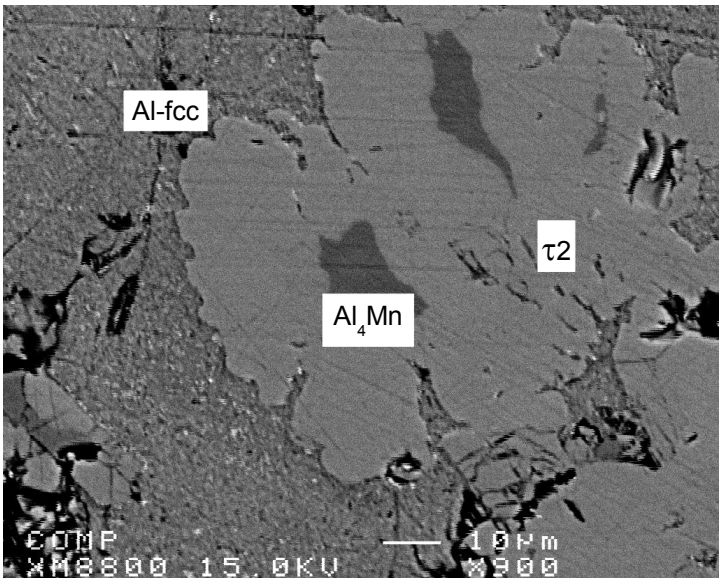

(b)

Figure 4.13: (a) Microstructure of sample 1; (b) Microstructure of sample 2.

In order to confirm the phase relations received from EPMA, these samples are also studied by XRD. The XRD patterns of samples 1, 2 and 6 are illustrated in Figure 4.14. Full pattern refinement has been carried out. The use of Si as an internal calibration standard enabled correcting the zero shift and specimen surface displacement. Al-fcc phase and Al_4Mn phase are identified from the XRD pattern. Also, there are several

unknown peaks which could correspond to the ternary compound τ_2. The 2θ positions and intensities of these peaks are shown in Table 4.4. τ_2 is a new stoichiometric compound and the prototype has not been reported yet. Thus, it is hard to determine the crystal structure of this ternary compound. The separated XRD pattern of ternary compound τ_2 is presented in the Figure 4.15. XRD spectrum of sample 6 is presented in Figure 4.14 (c). Al_4Mn and Al-fcc phases are identified. However, because of the lack of the crystallography information of ternary compound τ_1, this compound could not be identified in the current study. Thus, the peaks of τ_1 ternary phase are not labeled.

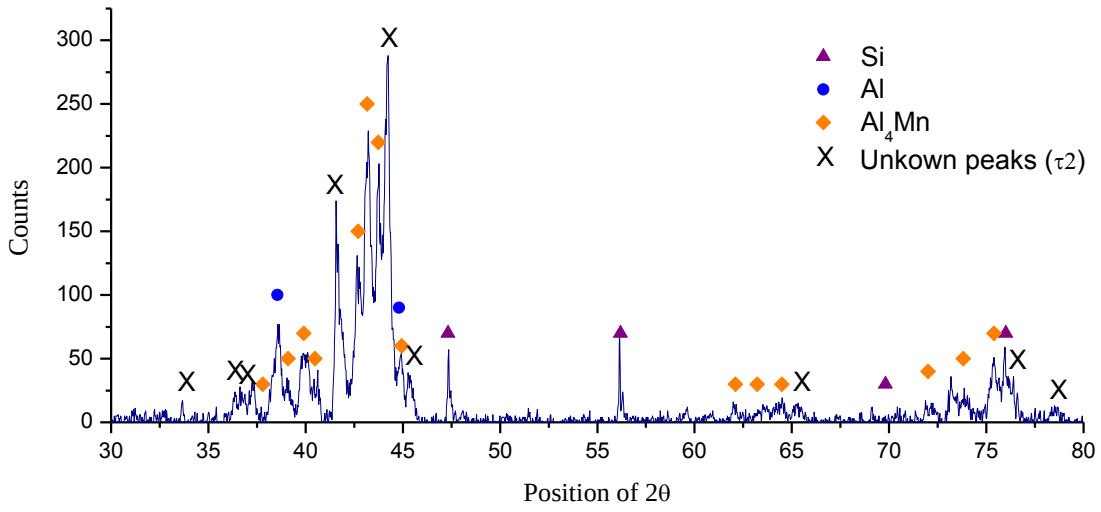

(a)

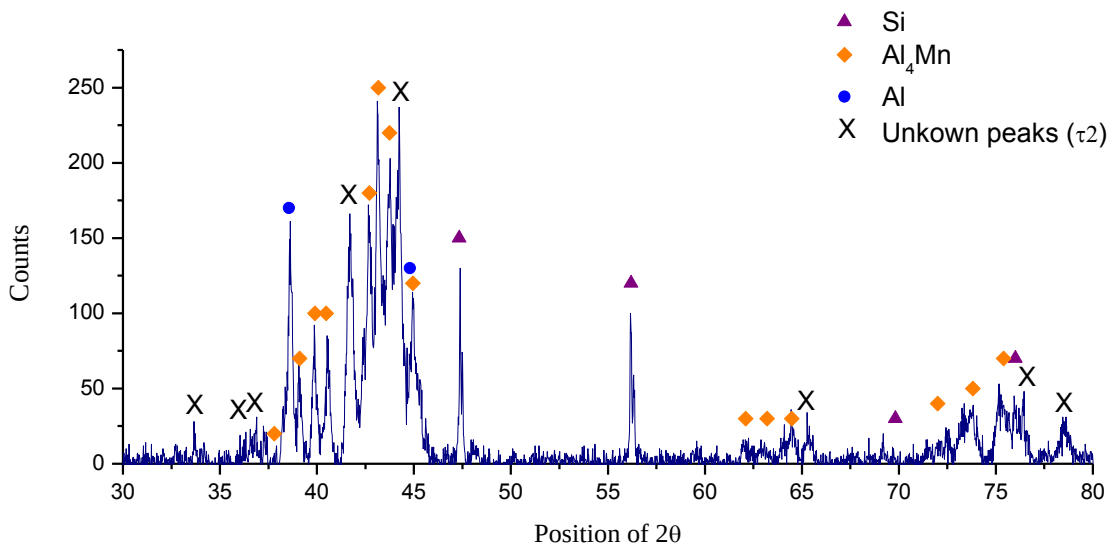

(b)

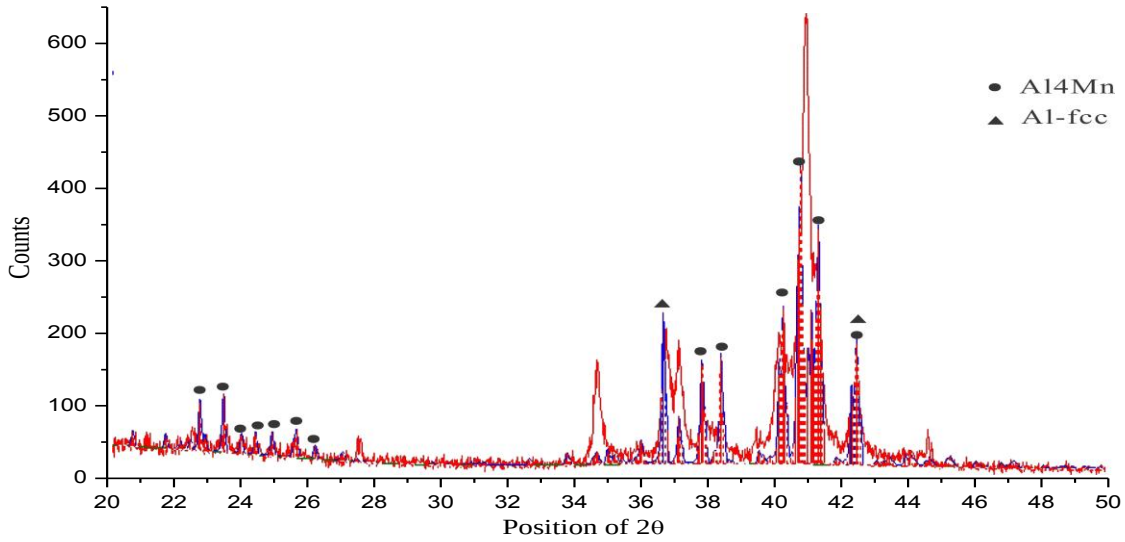

(c)

Figure 4.14: (a) XRD pattern of annealed sample 1; (b) XRD pattern of annealed sample 2; (c) XRD pattern of annealed sample 6.

Table 4.4: XRD pattern of ternary compound τ_2 acquired by XRD analysis.

Position of 2θ	21.654	27.379	31.26	33.718	36.597	36.823	37.276	41.674	44.133	65.279	67.446	75.956
Counts	75	31	26	43	51	54	51	216	273	30	22	85

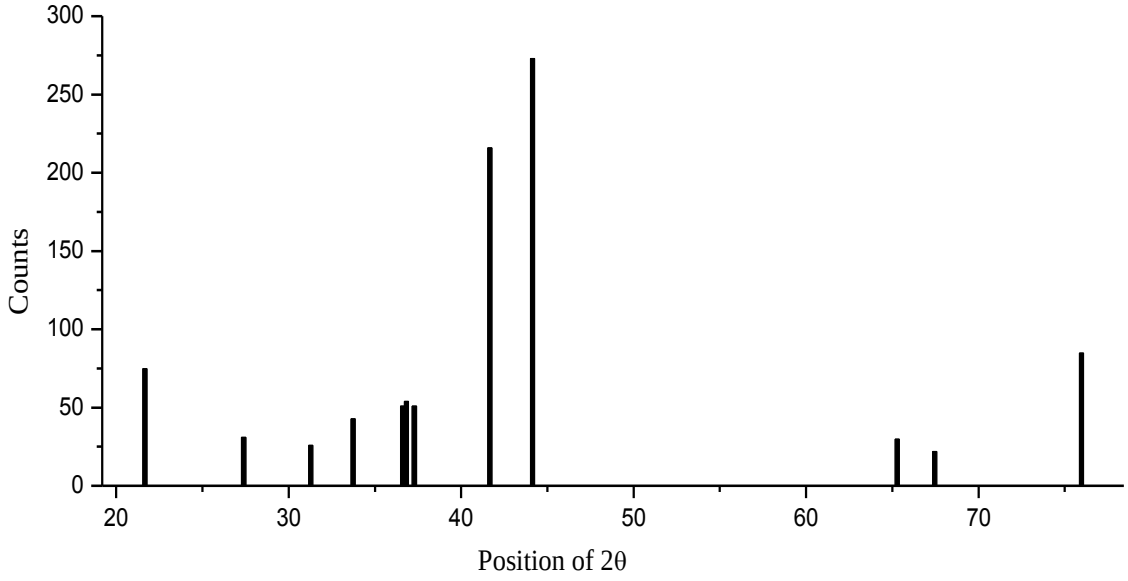

Figure 4.15: XRD pattern of ternary compound τ_2 obtained by XRD analysis.

4.2.4 Experimental study of ternary compound τ_3

Ternary compound τ_3 is first obtained from diffusion couple Al/$Mn_{13}Zn_{87}$ and the composition is primarily determined as 10 at% Al, 15 at% Mn and 75 at% Zn. Several key samples have been prepared to study this new ternary intermetallic compound τ_3. The actual compositions of key samples and the compositions of detected phases are listed in Table 4.5. Backscattered electron image of sample 1 is shown in Figure 4.16 (a). With magnified microstructure which is illustrated in Figure 4.16 (b), three phases have been found in this sample: Al_8Mn_5, $Al_{11}Mn_4$ and τ_3. Phase relationships and homogeneity range of these three phases are confirmed by both XRD and EPMA. Another ternary

phase τ_4 is found in sample 2 and 3 and microstructures of them show in Figure 4.16 (c) and (d). The composition of τ_4 is in the region around 23.3 at% Al, 15.5 at% Mn and 61.2 at% Zn. We suggested that τ_4 could be a metastable phase. There are the following reasons for it: samples 1 and 3 have similar actual composition but with the different annealing time. Sample 1 has been annealed for 40 days while sample 3 is annealed for 30 days. After 10 days prolong annealing, τ_4 phase disappeared in sample 1 and transforms into stable τ_3 phase. These three key samples have similar phase relations and the comparison is presented in Figure 4.17 (a). XRD spectra of both samples are quite similar as shown in Figure 4.17 (b) which also indicates the similar phase relations.

Table 4.5: The actual composition of key samples and detected phases.

Sample No.	Actual composition identified by ICP (at%)			Phase identification		Composition of identified phases by EPMA (at%)		
	Al	Mn	Zn	By EPMA	By XRD	Al	Mn	Zn
1	21	14	65	τ_3		12	11	77
				$Al_{11}Mn_4$	$Al_{11}Mn_4$	69	27.7	3.3
				Al_8Mn_5	Al_8Mn_5	56.3	36.7	7
2	16	14	70	τ_3		12.3	11	76.7
				τ_4		23.4	15.5	61.1
				$Al_{11}Mn_4$	$Al_{11}Mn_4$	71	25	4
3	23	16	61	τ_3		13	13	74
				τ_4		25	18	57
				$Al_{11}Mn_4$	$Al_{11}Mn_4$	68.6	27	4.3
				Al_8Mn_5	Al_8Mn_5	55	36	8.8
4	18.2	22	59.8	τ_3		10	15	75
				Al_8Mn_5		52-57	33-37	10-11

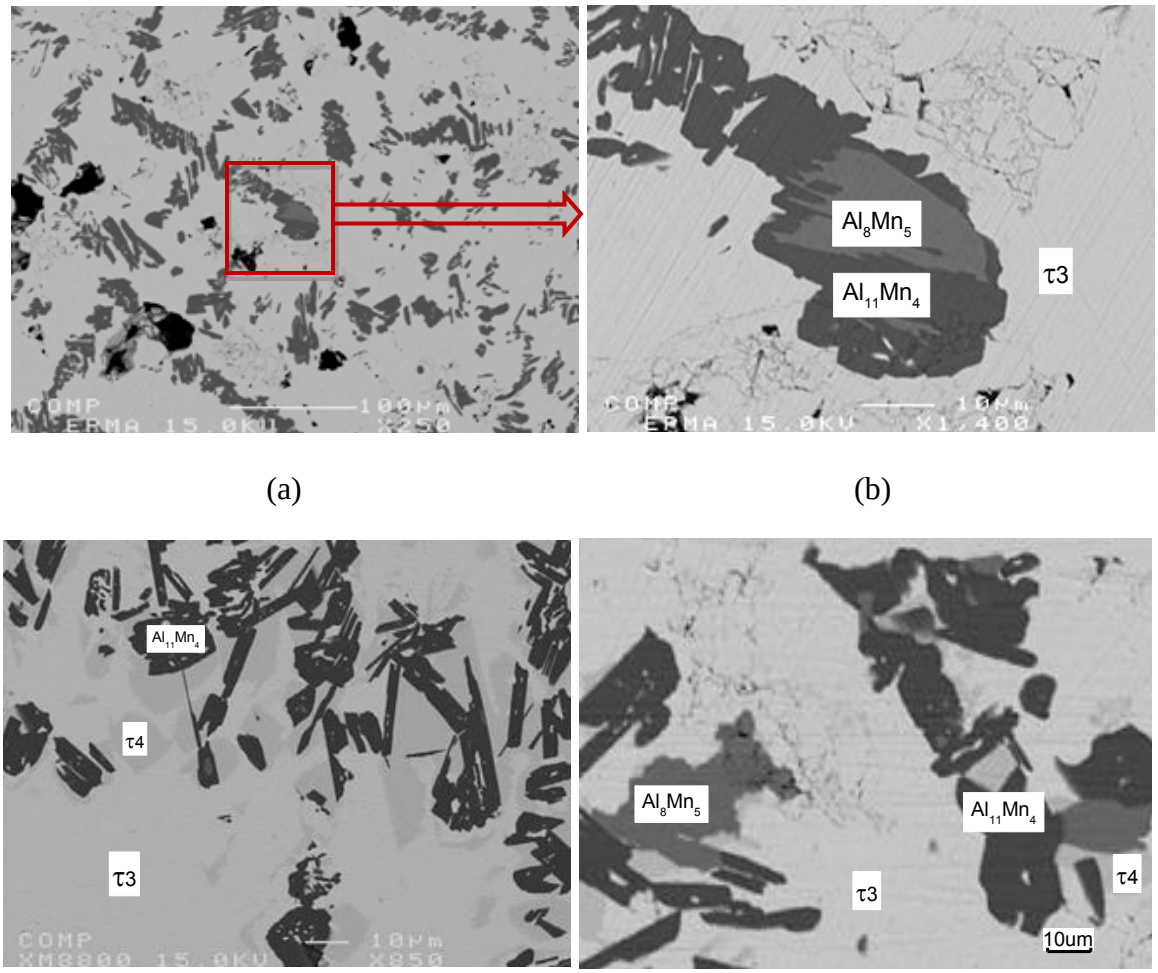

(a) (b)

(c) (d)

Figure 4.16: (a) Microstructure of sample 1; (b) Magnified area of sample 1; (c) Microstructure of sample 2; (d) Microstructure of sample 3.

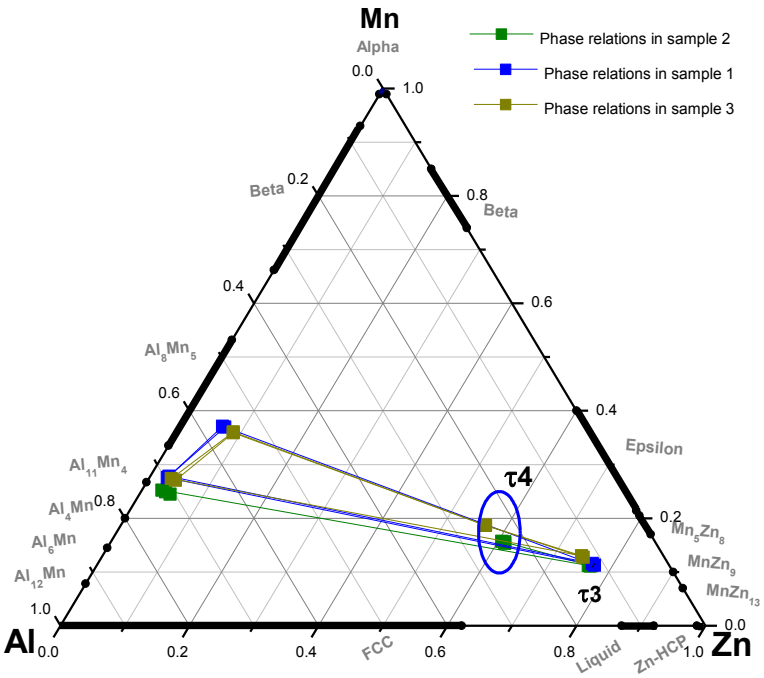

(a)

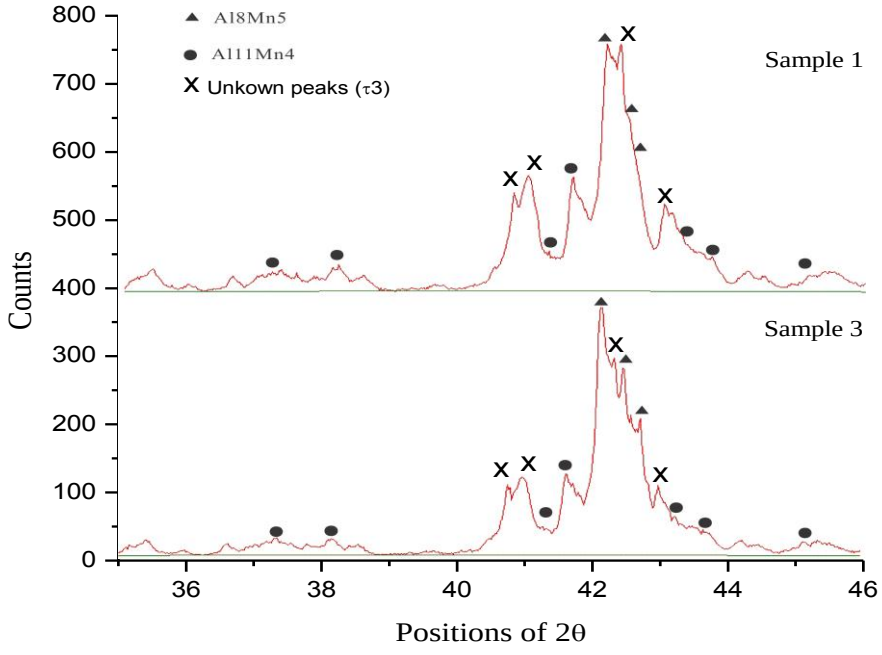

(b)

Figure 4.17: (a) Comparison of phase relations among three samples; (b) XRD comparison between samples 1 and 3.

Ternary compound τ_3 has a complex homogeneity range: 9.5-12.7 at% Al, 11-15 at% Mn, 74.6-77.2 at% Zn, which is determined by diffusion couple and key samples. τ_3 is also a new intermetallic compound which has not been reported before. Its prototype has not been determined. Hence this compound cannot be verified by XRD analysis. From the EPMA results, $Al_{11}Mn_4$ exhibits a ternary solid solubility reaching up to 5 at% Zn. Ternary homogeneity range of Al_8Mn_5 has been determined by EPMA method as 9 at% Zn. These observations also confirm the results, which are analyzed by previous diffusion couples.

4.2.5 Homogeneity range of $Al_{11}Mn_4$ and Al_8Mn_5

$Al_{11}Mn_4$ and Al_8Mn_5 show extended ternary solid solubility range in this system. Three samples have been prepared to study the ternary solubility limits of these two compounds. The composition and phase identification of these samples are summarized in Table 4.6. The actual chemical compositions of the alloys are measured by ICP and the compositions of $Al_{11}Mn_4$ and Al_8Mn_5 phases are determined by SEM/EDS. The phase relations are obtained from SEM and show great consistency with the XRD results. The backscattered electron image (BSE) of key sample 1 annealed at 400℃ for 4 weeks is shown in Figure 4.18 (a). Both $Al_{11}Mn_4$ and Al_8Mn_5 phases have been detected by SEM/EDS. From EDS point analysis, $Al_{11}Mn_4$ has a ternary solid solubility of about 4.23 at% Zn and Al_8Mn_5 has the maximum ternary solid solubility of 10.74 at% Zn. This finding also corresponds to the previous EPMA observation of key samples which are in the $Al_{11}Mn_4$+Al_8Mn_5+ τ_3 region. XRD results of sample 1, which are shown in Figure 4.18 (c) also confirm the same phase relations. Sample 3 has similar actual composition as sample 1, and SEM/EDS analysis also shows the same tie-line relations between

$Al_{11}Mn_4$ and Al_8Mn_5. These relations are also confirmed by XRD analysis which is shown in Figure 4.18 (e). In sample 2, Al_8Mn_5 shows ternary solid solubility of around 3.75 at% Zn. The presence of a single Al_8Mn_5 phase region is also confirmed by XRD which is illustrated in Figure 4.18 (d).

Table 4.6: The actual composition of key samples and detected phases.

Sample No.	Actual composition identified by ICP (at%)			Phase identification		Composition of phases identified by EPMA (at%)		
	Al	Mn	Zn	By EPMA	By XRD	Al	Mn	Zn
1	64	31	5	$Al_{11}Mn_4$	$Al_{11}Mn_4$	69.36	26.41	4.23
				Al_8Mn_5	Al_8Mn_5	55.08	34.18	10.74
2	56	37	7	Al_8Mn_5	Al_8Mn_5	57.35	38.9	3.75
3	55	35	10	$Al_{11}Mn_4$	$Al_{11}Mn_4$	69.7	27	3.3
				Al_8Mn_5	Al_8Mn_5	55.87	35	9.13

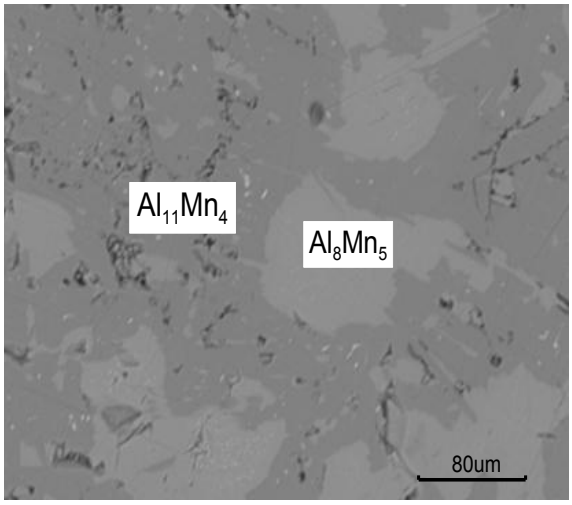

(a)

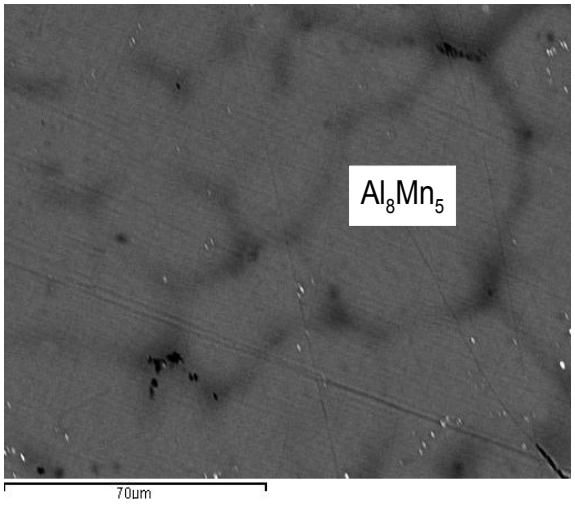

(b)

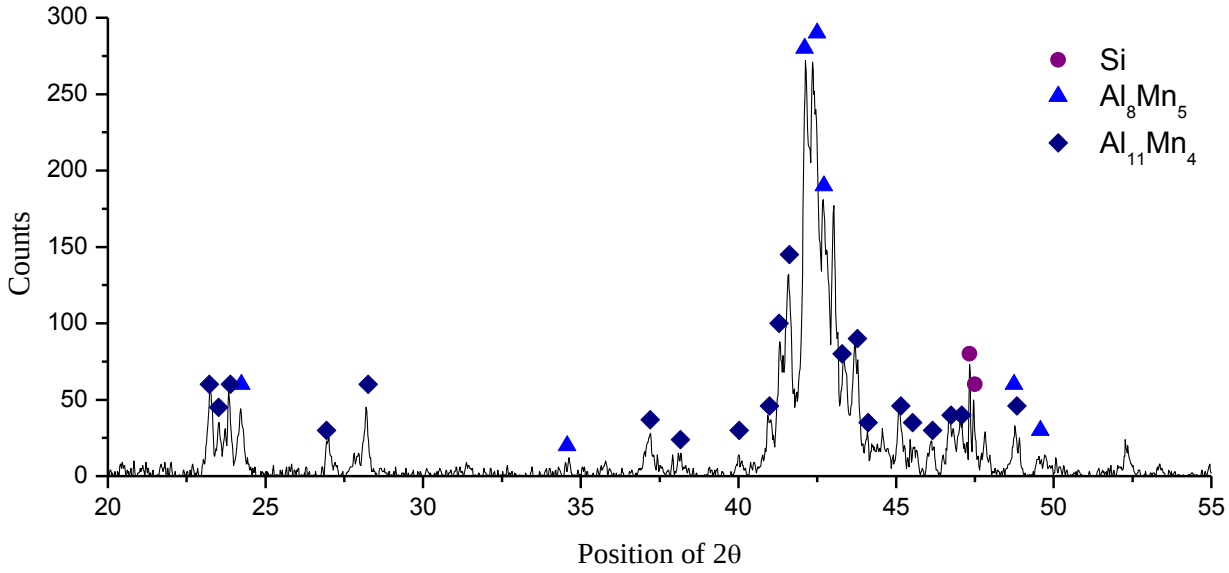
Counts
Position of 2θ
Si
Al8Mn5
Al11Mn4

(c)

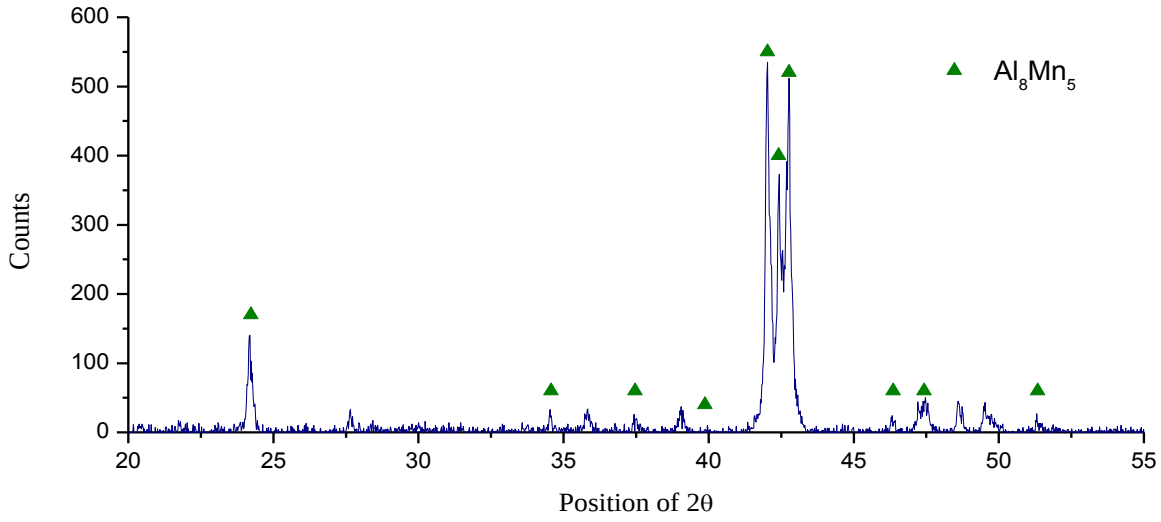
Counts
Position of 2θ
Al8Mn5

(d)

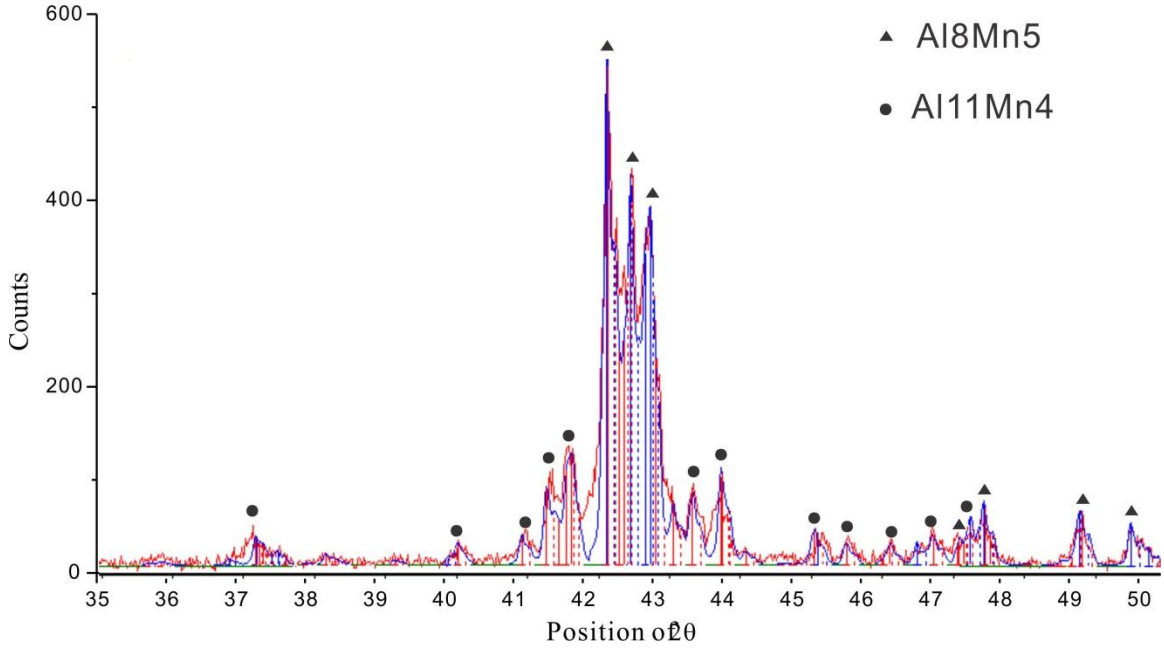

(e)

Figure 4.18: (a) BSE image of sample 1; (b) BSE image of sample 2; (c) XRD pattern of sample 1; (d) XRD pattern of sample 2; (e) XRD pattern of sample 3.

Al_8Mn_5 has a wide ternary solid solubility range in the Al-Mn-Zn system. Phase relations among Al_8Mn_5 and other phases such as $Al_{11}Mn_4$, ε, binary solid solution Mn_5Zn_8 and Beta-Mn are quite complex. The ternary homogeneity range of Al_8Mn_5 is plotted in Figure 4.19 which also illustrates its phase relations which are determined by key samples. Three ternary intermetallic compounds: $Al_{64.2}Mn_{15.2}Zn_{20.6}$, $Al_{76}Mn_{13}Zn_{11}$ and $Al_{9.5\text{-}12.7}Mn_{11\text{-}15}Zn_{74.6\text{-}77.2}$ are confirmed by key samples. The compositions of these compounds are compared with the results of diffusion couples. Al_4Mn has maximum ternary solid solubility of 6 at% Zn. $Al_{11}Mn_4$ reaches its maximum ternary solid solubility at 4.23 at% Zn. ε and Mn_5Zn_8 phases exhibit small ternary homogeneity ranges and have maximum ternary solid solubility of 3.69 at% and 4 at% Al respectively.

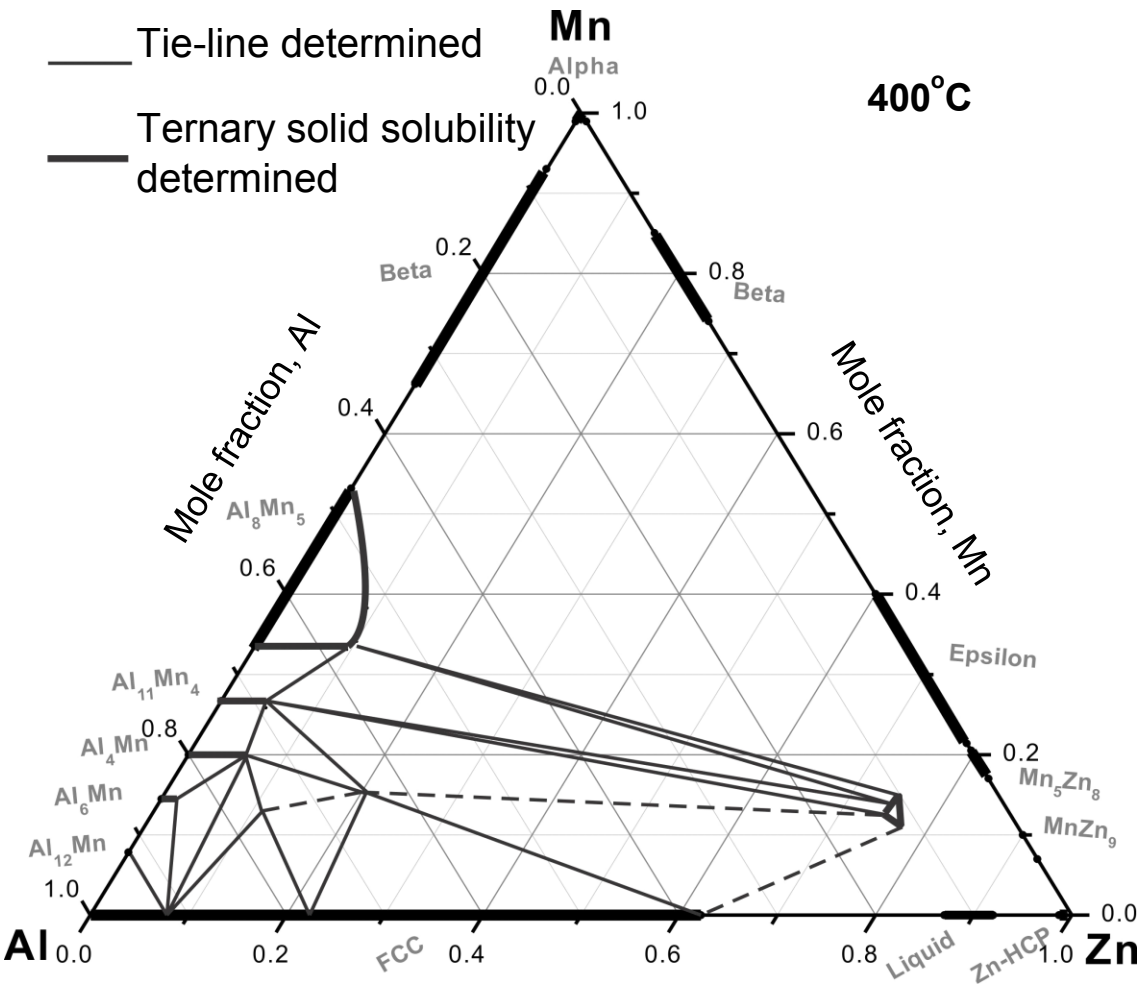

Figure 4.19: Tie lines determined by key samples technique.

4.3 Isothermal section of Al-Mn-Zn ternary system at 400℃

Combining the results which are obtained from diffusion couples and key samples, the isothermal section of the Al-Mn-Zn phase diagram at 400℃ has been constructed and presented in Figure 4.20. Solid lines represent the tie-line relations and solid solution which are determined from the current experimental results.

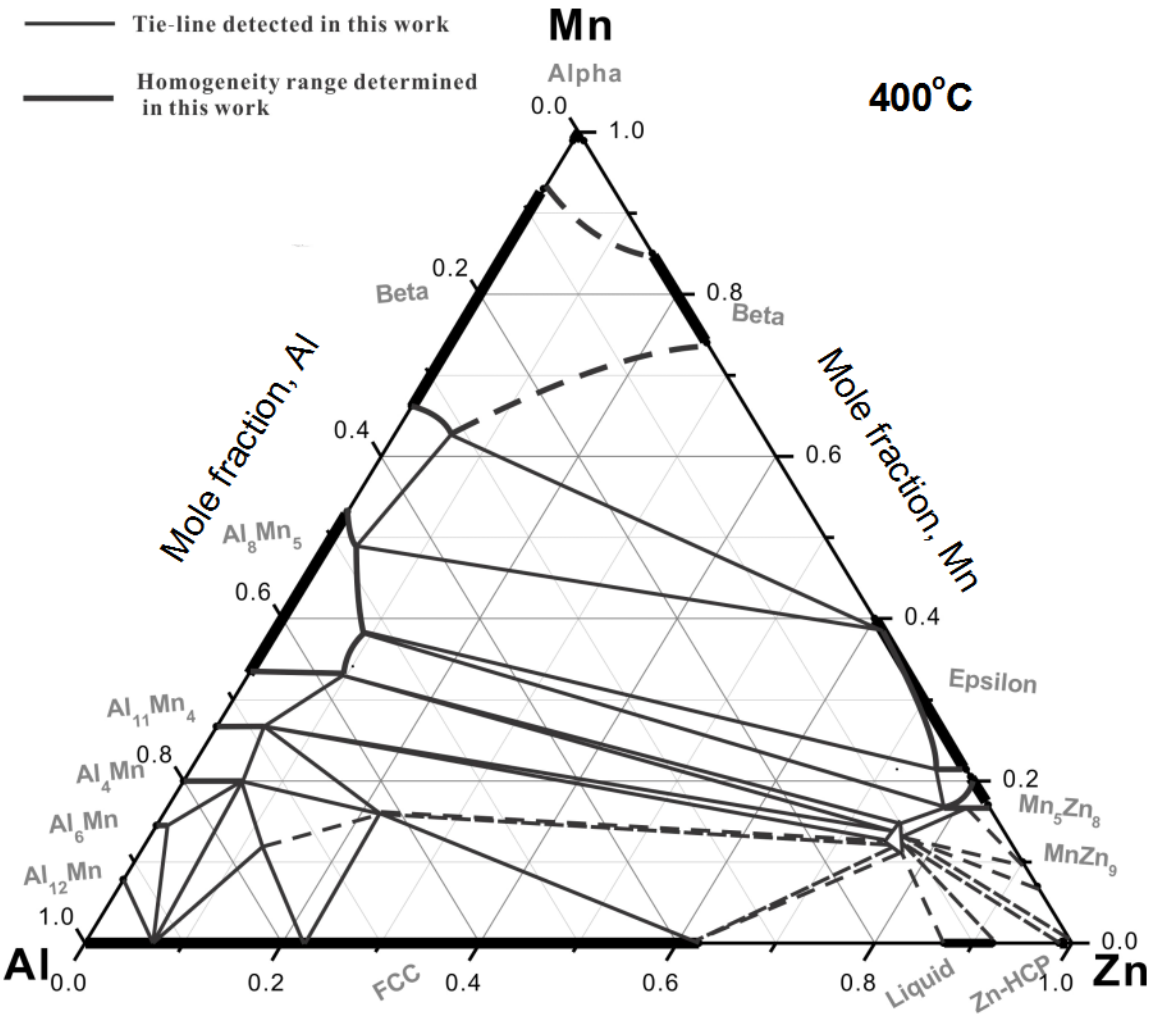

Figure 4.20: Isothermal section of Al-Mn-Zn ternary system at 400℃ constructed by diffusion couples and key samples.

4.4 Thermal analysis through DSC

12 samples have been prepared to study the liquidus of Al-Mn-Zn system by differential scanning calorimetry (DSC) technique. Vertical sections are calculated using the preliminary model, and it is compared with the experimental results. The preliminary thermodynamic model does not include the ternary phases. Thus, some discrepancies have been observed between the DSC results and the calculated vertical sections. In the current experimental investigation, the vertical sections close to 14 at% Mn are mainly studied here because it is important for industrial applications. It covers two ternary compounds and shows complex phase relations in the Al-rich corner. Samples are chosen in lower Zn content regions from 3 at% to 32 at% Zn in order to limit the influence of Zn evaporation. The actual compositions are measured by ICP and listed in Table 4.7. These DSC samples are categorized into 4 groups and plotted on the 400℃ isothermal section which is shown in Figure 4.21 for better illustration. The DSC results will be discussed in section 4.5.2.

Table 4.7: Actual compositions of selected DSC samples.

Group	Phase field	Sample No.	Al (at%)	Mn (at%)	Zn (at%)
1	Al-fcc, Al_4Mn and Al_6Mn	1	83	14	3
		2	80	14	6
2	Al-fcc, Al_4Mn and τ_2	3	76	14	10
		4	77	14	9
		5	77	15	8
3	Al_4Mn, τ_1 and τ_2	6	73	14	13
		7	76	13	11
4	Higher Zn content phase field	8	66	13	21
		9	56	14	30
		10	54	14	32
		11	57	14	29
		12	59	15	26

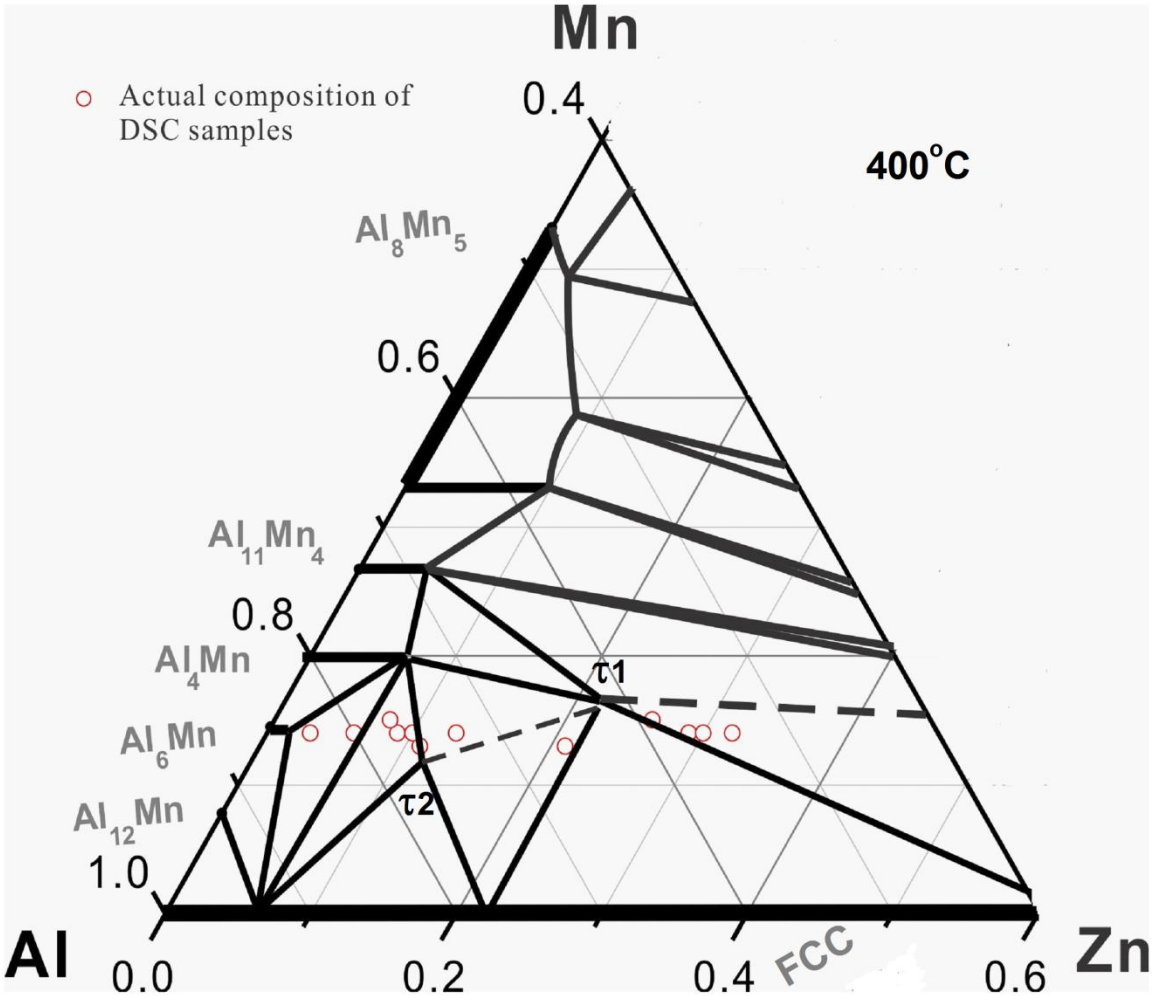

Figure 4.21: Composition of the samples used in the DSC experiments.

4.4.1 Supercooling effect

It is assumed that there is no barrier to nucleate during the cooling process. The solute diffusion is also sufficient to keep the phases uniformly distributed at each temperature in this process [105]. Thus, the cooling runs are taken into consideration here as due to this favorable kinetics. Also, the peak temperature of the last thermal event on heating should be considered as the liquidus temperature. If without supercooling effect, the first onset cooling temperature and the peak temperature of last heating peak should be very close.

During the current DSC study of the Al-Mn-Zn system, super cooling effect is a problem influencing the DSC analysis. Phases in the Al-corner are prone to super cooling effect [97, 98]. Thus, extrapolation method is introduced to use in order to obtain more accurate DSC results. The details of extrapolation are discussed in this section.

Supercooling effect is an effect is due to a failure of the solid phase to nucleate at the temperature given by the phase diagram. Because of the supercooling effect, corresponding exothermic peak is shifted to the lower temperature and overlapped with other peaks. The actual nucleation temperature is lower than the theoretical one. Supercooling effect is noticeable in the whole DSC analysis process. In order to decrease the influence of supercooling effect and enhance the accuracy of the results, lower scan rates are used to prolong the nucleation time. Three different scan rates are chosen: 15℃/min, 10℃/min and 5℃/min. The results show that the supercooling effect changes along with changing scan rates. Using sample 6 as an example to demonstrate the extrapolation process which is illustrated in Figure 4.22: at 15℃/min scan speed, two exothermic peaks overlapping with each other at the position of peak #4 and the onset cooling temperature of it is 652℃. By checking the enthalpy of the corresponding phase transformations of peaks #1 and #2, it is noticed that the enthalpy values are the same. Thus, because of supercooling effect, one exothermic peak shifts to the left and overlaps with another peak. At 10℃/min scan rate which is shown in Figure 4.22 (b), the overlapping peaks show some tendency to separate, the temperature of the onset peak changes from 652℃ to 664℃. At lower heating/cooling speed 5℃/min as presented in Figure 4.22 (c), peak #4 clearly separates into two peaks. The two onset cooling temperatures are 663℃ and 671℃, respectively. In order to diminish the supercooling

effect, it is better to extrapolate the scan rate to 0℃/min assuming that this is the rate guaranteeing equilibrium. The DSC results at different cooling rates and after extrapolation are summarized in Table 4.8.

Table 4.8: Extrapolated onset cooling signals of sample 6 along with the experimental values.

Scan rate / Onset cooling	15℃/min	10℃/min	5℃/min	0℃/min
1st	907℃	930℃	942℃	961℃
2nd	876℃	890℃	891℃	900℃
3rd	810℃	829℃	837℃	852℃
4th	652℃	664℃	671℃	681℃
5th	652℃	664℃	663℃	671℃

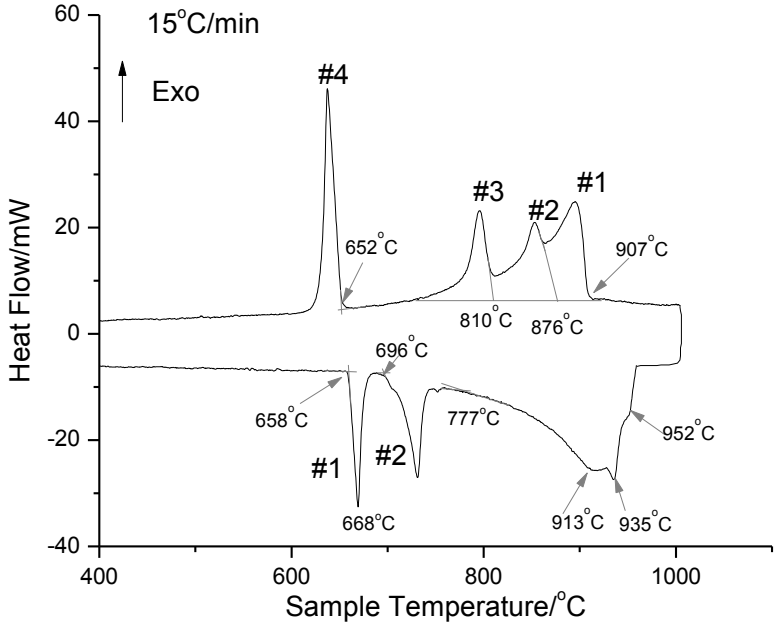

(a)

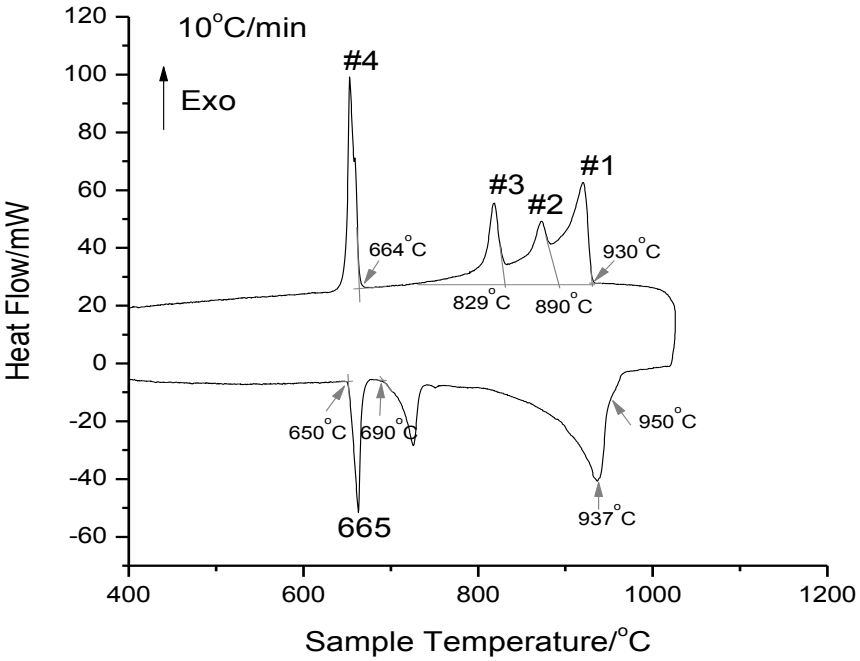

(b)

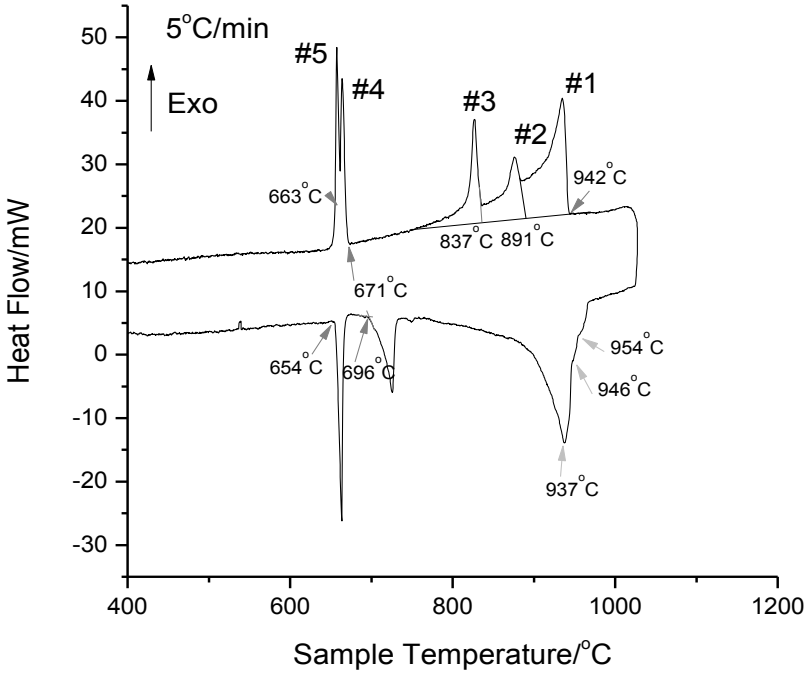

(c)

Figure 4.22: (a) DSC results of sample 6 under 15℃/min; (b) DSC results of sample 6 under 10℃/min; (c) DSC results of sample 6 under 5℃/min.

Extrapolation details are given in Figure 4.23. After extrapolation the overlapping peaks into 0℃/min scan rate, the onset cooling temperature of peak #4 shifts about 30℃ from 652℃ to 680℃. Without the supercooling effect, the temperature of phase transformation happens in peak #4 should register as 680℃. And the liquidus temperature is determined as 961℃ by extrapolated the first onset cooling temperatures. The extrapolated liquidus temperature is much closer to the maximum temperature of last heating event.

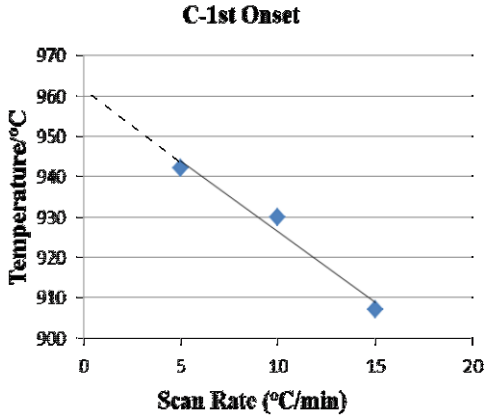

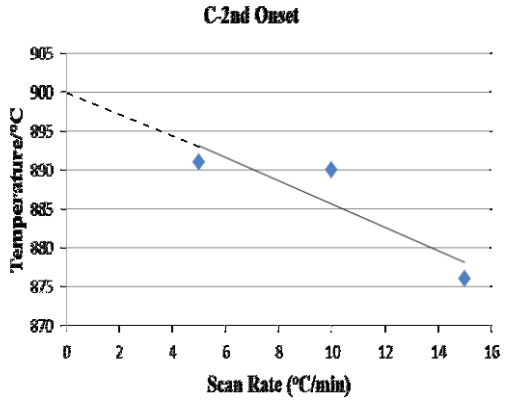

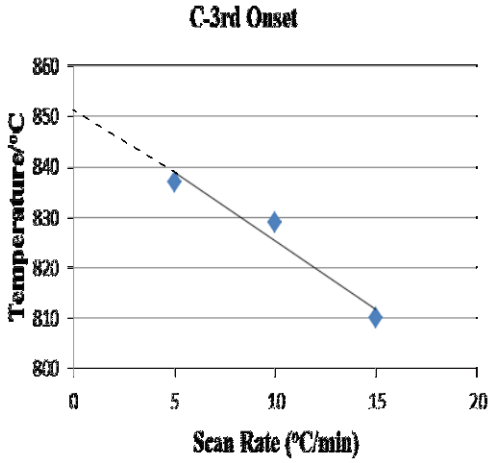

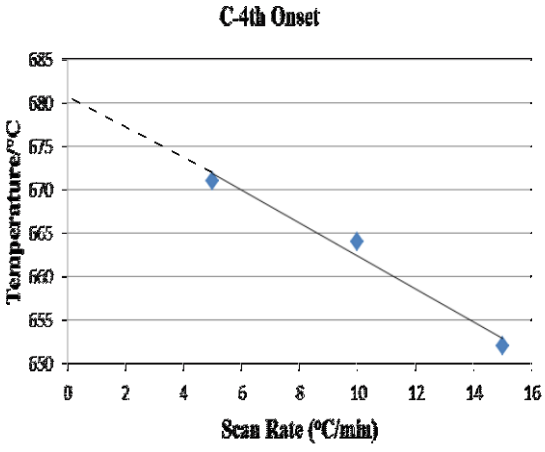

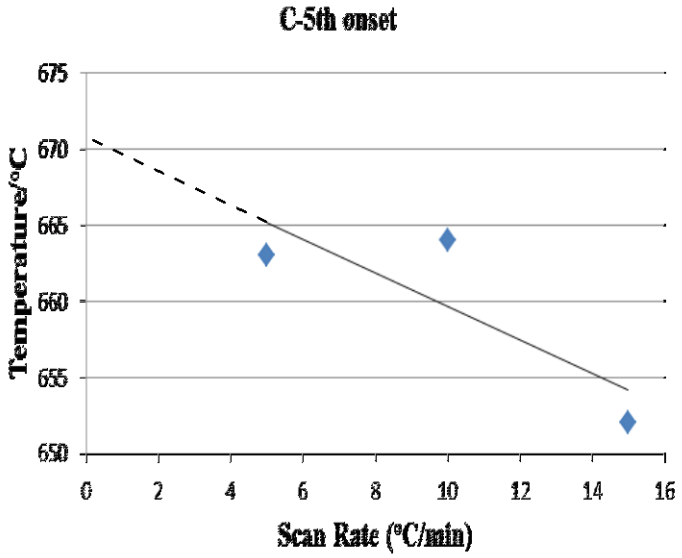

Figure 4.23: Extrapolation process of each onset cooling signal of sample 6.

4.4.2 DSC analysis results

DSC samples are grouped into 4 different phase regions based on the tie-line relations from the current study of the Al-Mn-Zn system at 400℃: (1) Al-fcc, Al_4Mn and Al_6Mn phase field; (2) Al_4Mn, Al-fcc and τ_2 phase field; (3) Al_4Mn, τ_1 and τ_2 phase field; (4) higher Zn content phase field.

4.4.2.1 Samples in the Al-fcc, Al_4Mn and Al_6Mn phase field

Samples 1 and 2 are in the same Al-fcc, Al_4Mn and Al_6Mn phase field. The DSC heating and cooling spectra of sample 1 at 15℃/min are shown in Figure 4.24. The large endothermic peak #6 in Figure 4.24 indicates two heating events are overlapping. The observation of the two overlapping peaks is confirmed during cooling. The onset temperature of exothermic peak #1 at 881℃ corresponds to the liquidus temperature. During the heating process, one sharp and high peak #4 is observed which denotes the peak of eutectic melting. The endothermic peak #5 at 709℃ which is lower and broader

indicates the univariant transition. The enthalpy of two overlapping exothermal peaks #1 and #2 is -84.47J/g and the enthalpy of the associated endothermic peak is 82.01J/g. By comparing enthalpy between the heating and cooling peaks, it is clear that two overlapping exothermal peaks #1 and #2 are corresponding to the big endothermic peak #6. Also at the transformation temperature around 653℃, the enthalpy of one signal eutectic peak #3 is equal to the area under peaks #4 and #5 endothermic peaks. This means two exothermic peaks are overlapping at 653℃ due to the supercooling effect.

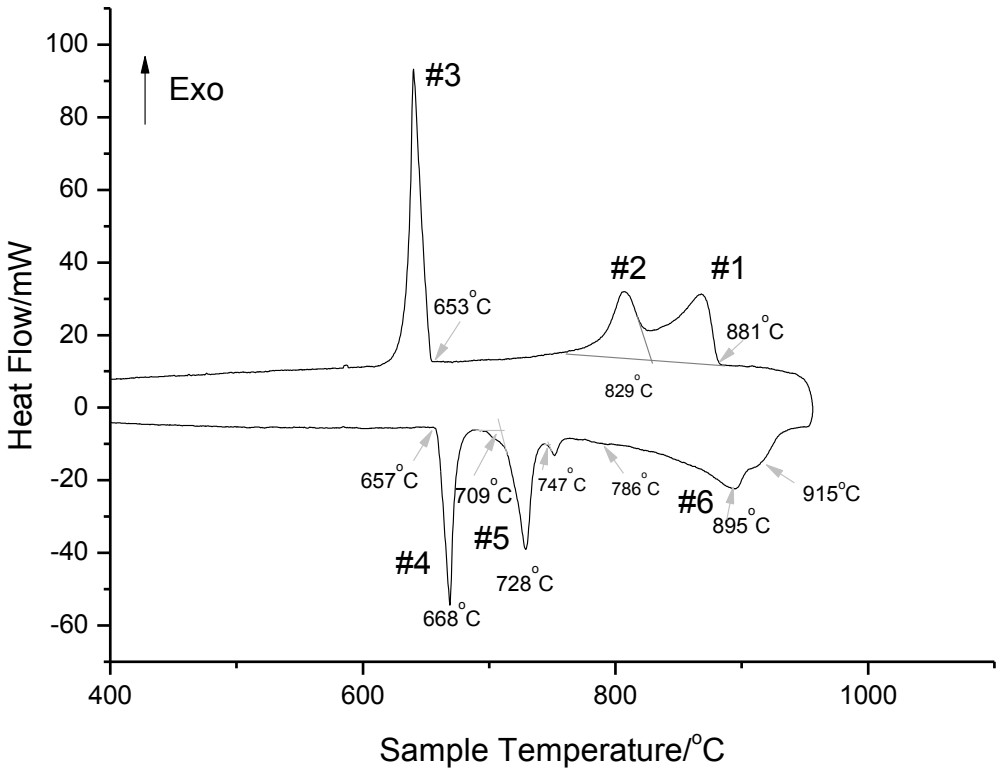

Figure 4.24: DSC spectra of sample 1.

The experimental results are compared with the preliminary thermodynamic calculations to confirm the transformation temperatures along with the associated reactions. Extrapolated transformation temperatures to 0 ℃/min cooling rate are listed in Table 4.9. Figure 4.25 shows the calculated vertical section of sample 1 ($Al_{83}Mn_{14}Zn_3$) and sample 2 ($Al_{80}Mn_{14}Zn_6$) with DSC signals from the cooling curve after extrapolation. Because there is no ternary phase in this phase field, it can be observed that the experimental values of DSC fairly correspond to the calculated vertical section. And, the extrapolated liquidus temperature is measured as 914℃ which matches very well with the peak temperature of the last heating peak at 915℃. However, the transformation temperature at 838℃ which is obtained from DSC analysis is not observed in the thermodynamic calculation. In sample 2, DSC signals show the phase transformation at 822℃. This temperature is lower than transformation temperature predicted by the thermodynamic calculations at 862℃. XRD is also used to identify the phases in the post DSC samples 1 and 2. XRD spectra of these samples are illustrated in Figure 4.26 and three phases (Al-fcc, Al_4Mn and Al_6Mn) have been identified. The results of XRD agree with the phase constitutions in the same region at 400℃.

Table 4.9: Transformation temperature at different scan rates.

No.	Composition (at%)	Scan rate (°C/min)	Transformation temperature at different scan rates (°C)				
1	$Al_{83}Mn_{14}Zn_3$	15	881	829	653	653	
		5	901	835	678	661	
		0	914	838	690	665	
2	$Al_{80}Mn_{14}Zn_6$	15	909	871	848	651	651
		10	925	873	846	655	655
		5	933	883	830	673	663
		0	946	891	823	681	668

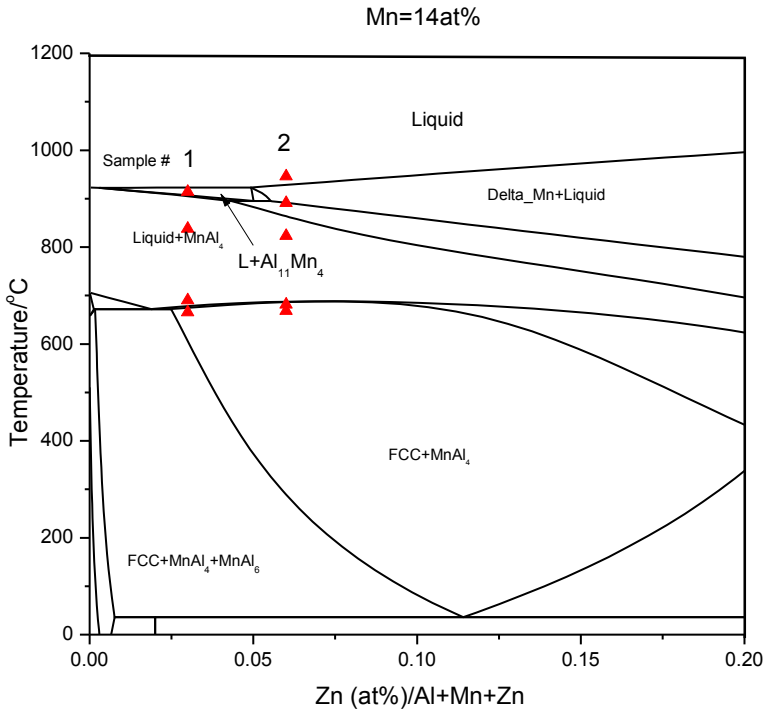

Figure 4.25: Calculated vertical section at 14 at% Mn with transformation temperature at 0°C/min cooling rate of samples 1 and 2.

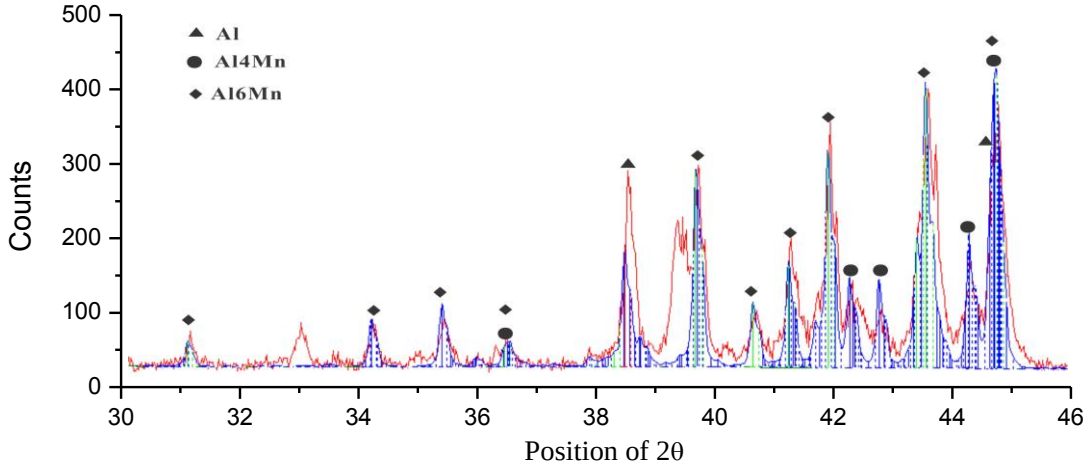

(a)

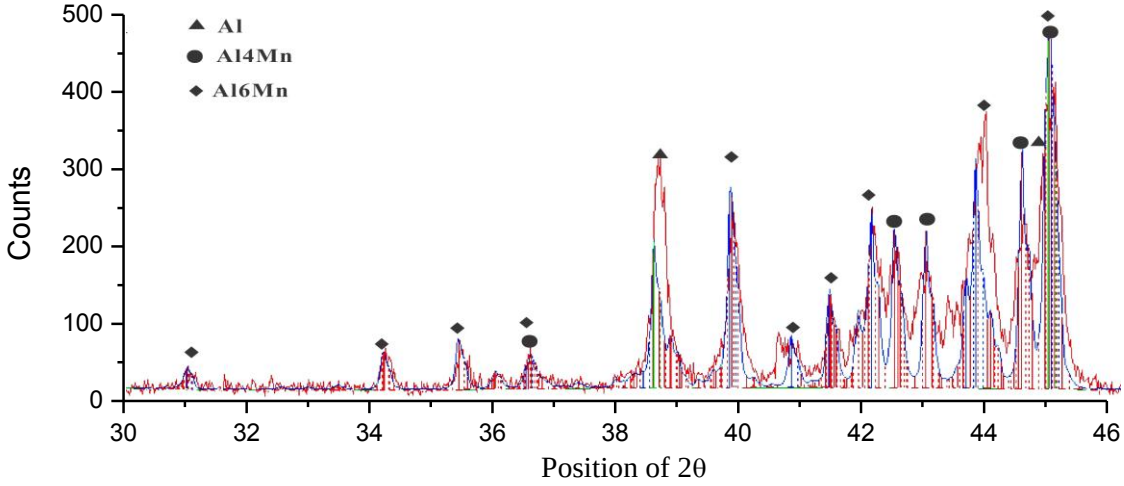

(b)

Figure 4.26: (a) XRD pattern of post DSC sample 1; (b) XRD pattern of post DSC sample 2.

4.4.2.2 Samples in the Al-fcc, Al_4Mn and τ_2 phase field

Three samples have been chosen in the Al-fcc. Al_4Mn and τ_2 phase field as shown in Figure 4.21. Extrapolated onset cooling temperatures to 0 ℃/min cooling rate are presented in Table 4.10 along with the actual compositions which are determined by ICP. The DSC spectra of samples 3 and 4 at 15℃/min are presented in Figure 4.27. Because of the supercooling, exothermal peaks are overlapping with each other in both samples. After extrapolating scan rate to 0℃/min, the liquidus temperature of sample 3 registers at 937℃ which fairly corresponds to the peak temperature of the last heating event. The liquidus temperature of sample 4 is found at 974℃. Moreover, the calculated vertical section does not include the information of these new found intermetallic compounds. Therefore, some controversies are observed from the DSC analysis. A comparison between the extrapolated DSC experimental results and the calculated vertical section at 14 at% Zn is demonstrated in Figure 4.28. Extrapolated cooling signals of another sample 5 in this phase field is also listed in Table 4.10 and plotted on the calculated vertical section at 15 at% Mn which is shown in Figure 4.29.

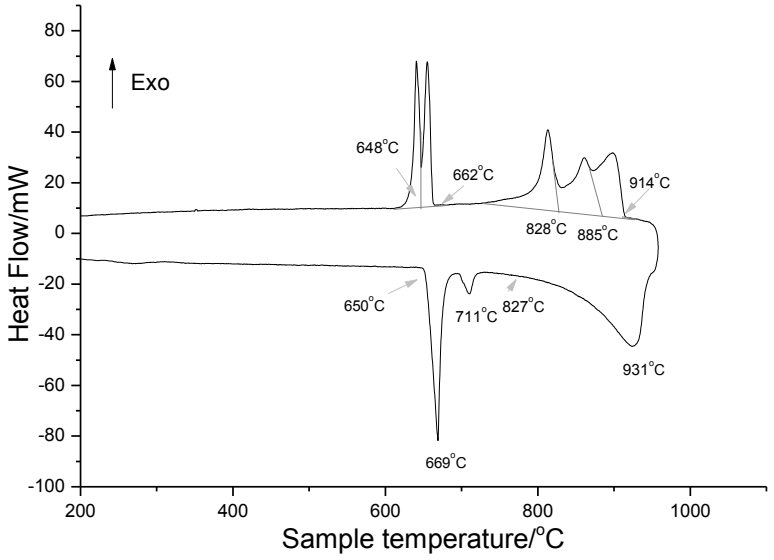

(a)

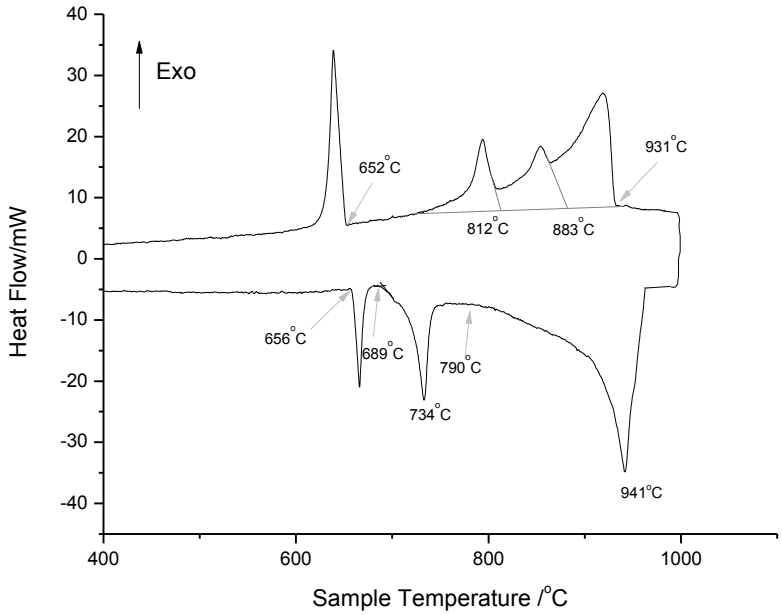

(b)

Figure 4.27: (a) DSC spectra of sample 3 at 15℃/min; (b) DSC spectra of sample 4 at 15℃/min.

Table 4.10: Transformation temperature at different scan rates.

No.	Composition (at%)	Scan rate (℃/min)	Transformation temperature at different scan rates (℃)				
3	$Al_{76}Mn_{14}Zn_{10}$	15	914	885	828	662	648
		5	929	877	840	664	659
		0	937	881	847	670	664
4	$Al_{77}Mn_{14}Zn_{9}$	15	931	883	812	653	653
		10	930	873	812	652	652
		5	950	895	830	671	662
		0	956	895	836	677	665
5	$Al_{77}Mn_{15}Zn_{8}$	15	931	876	812	651	651
		10	925	865	813	653	653
		5	926	868	815	655	652
		0	923	871	818	656	651

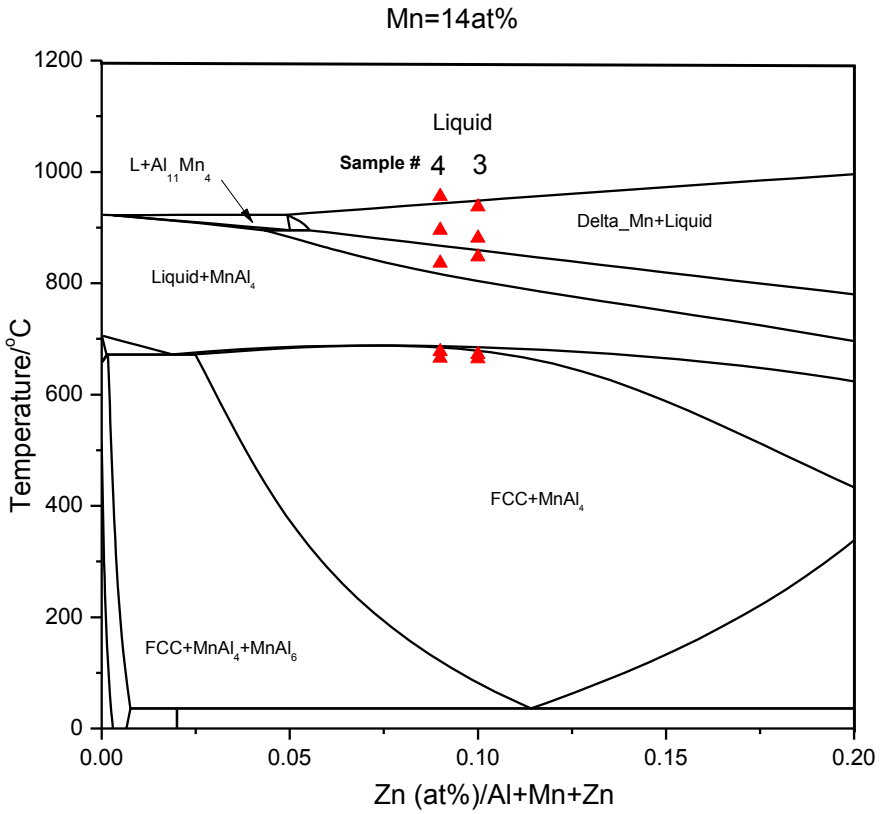

Figure 4.28: Calculated vertical section at 14 at% Mn with transformation temperature at 0℃/min cooling rate of samples 3 and 4.

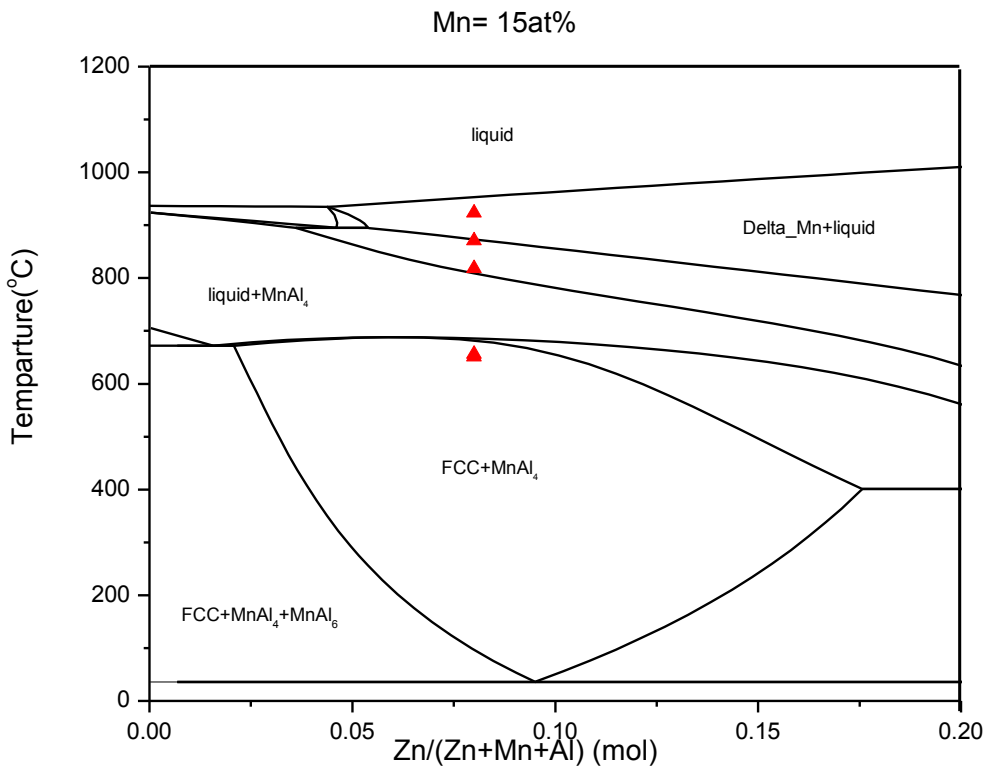

Figure 4.29: Calculated vertical section at 15 at% Mn with transformation temperature at 0℃/min cooling rate of sample 5.

4.4.2.3 Samples in the Al_4Mn, τ_1 and τ_2 phase field

In the Al_4Mn, τ_1 and τ_2 phase region, Figure 4.30 shows the DSC spectra of sample 6 during heating and cooling scans at 15℃/min rate. Mass loss has been observed for this sample. The large endothermic peak indicates a non-isothermal transition (univariant) starts at 777℃ and three heating peaks are overlapping. Upon cooling, three overlapping exothermic peaks were observed. The area under these three peaks is equal to that under the large endothermic peak. The onset temperature of exothermic peak #1 at 907℃ corresponds to the liquidus temperature which is determined by the intersection of tailing and the baseline as shown in Figure 4.30. One sharp and high peak #3 is observed

which denotes the peak of eutectic melting. The endothermic peak #4 at 696℃ which is lower and broader indicates the univariant transition. Also at the transformation temperature around 652℃, the enthalpy of peak #2 is equal to the enthalpy of #3 and #4 endothermic peaks. This means two exothermic peaks overlapping each other at the temperature of 652℃ due to the supercooling effect. The transformation temperatures after extrapolation to 0 ℃/min cooling rate are presented in Table 4.11. Figure 4.31 illustrates the calculated vertical section of sample 6 ($Al_{73}Mn_{14}Zn_{13}$) and 7 ($Al_{75}Mn_{14}Zn_{11}$) with DSC signals from extrapolated cooling curve. One DSC signal found in the Delta-Mn + Liquid region could be related to the ternary compounds transformation.

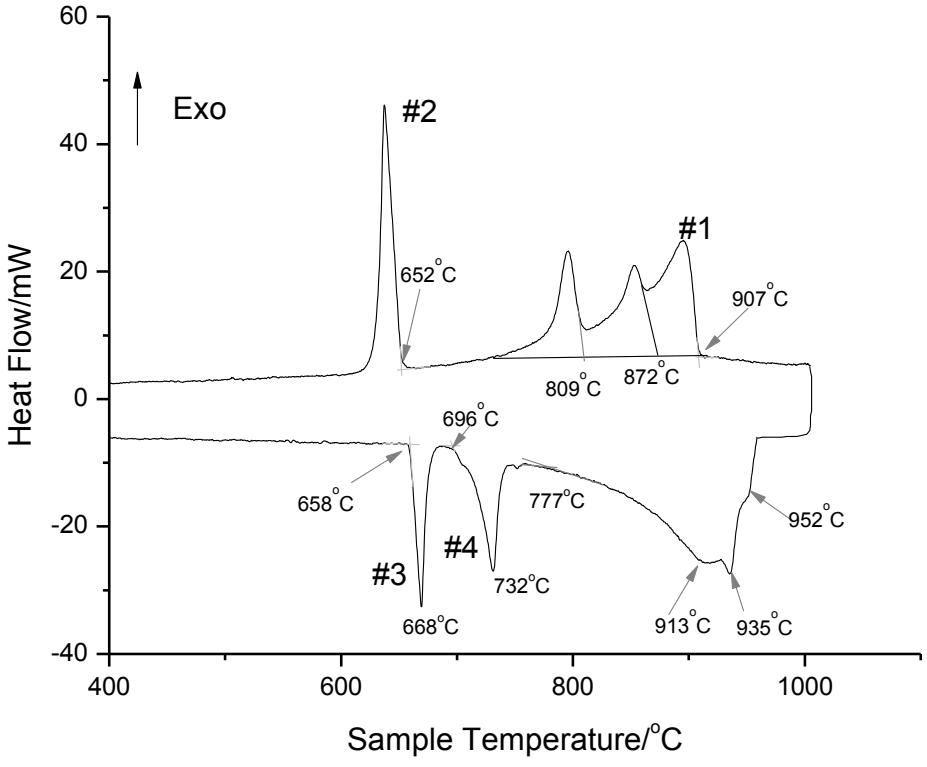

Figure 4.30: DSC spectra of sample 6 using 15℃/min scan rate.

Table 4.11: Transformation temperature at different scan rates.

No.	Composition (at%)	Scan rate (℃/min)	Transformation temperature at different scan rates (℃)				
6	$Al_{73}Mn_{14}Zn_{13}$	15	907	872	809	652	652
		10	930	880	829	664	664
		5	942	883	834	671	663
		0	961	898	852	681	671
7	$Al_{76}Mn_{13}Zn_{11}$	15	912	878	814	660	660
		10	921	898	837	662	662
		5	944	896	844	672	663
		0	958	908	862	679	666

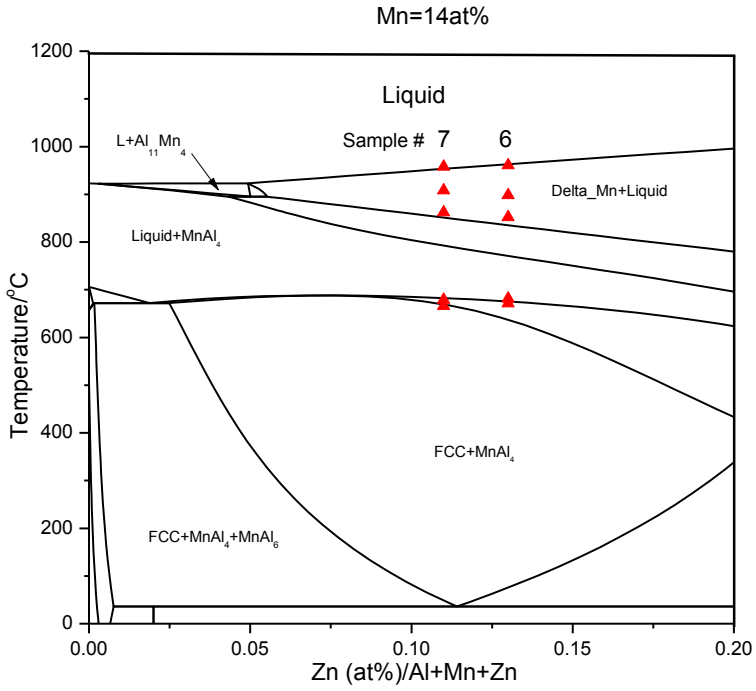

Figure 4.31: Calculated vertical section at 14 at% Mn with transformation temperature at 0℃/min cooling rate of sample 6 and 7.

4.4.2.4 Samples in higher Zn content phase field

Five samples have been studied by DSC to describe the phase field from 20 to 33 at% Zn. The actual compositions and extrapolated onset cooling temperatures of these samples are shown in Table 4.12. The extrapolated onset cooling temperatures are labeled on the vertical section in Figure 4.32 in relation to the thermodynamic calculation. Since the newly found ternary intermetallic compounds are not included in the thermodynamic model, there are some discrepancies between experimental and thermodynamic results. It is noticed that thermodynamic calculations cannot accurately predict all the phase transformation measured by DSC. Therefore, the Al-Mn-Zn system should be remodeled in light of the current experimental results.

Table 4.12: Transformation temperature at different scan rates.

No.	Composition (at%)	Scan rate (℃)	Transformation temperature at different scan rates (℃)				
8	$Al_{66}Mn_{13}Zn_{21}$	15	927	874	824	653	653
		5	944	894	834	675	663
		0	952	904	839	686	668
9	$Al_{56}Mn_{14}Zn_{30}$	15	947	877	807	659	648
		5	962	888	825	654	654
		0	969	887	834	657	651
10	$Al_{54}Mn_{14}Zn_{32}$	15	948	873	811	649	649
		5	963	885	825	670	659
		0	970	891	832	680	664
11	$Al_{57}Mn_{14}Zn_{29}$	15	951	877	804	654	654
		5	975	883	836	677	660
		0	987	886	852	688	663
12	$Al_{59}Mn_{15}Zn_{26}$	15	952	868	807	659	650
		5	963	888	820	759	686
		0	968	898	826	809	659

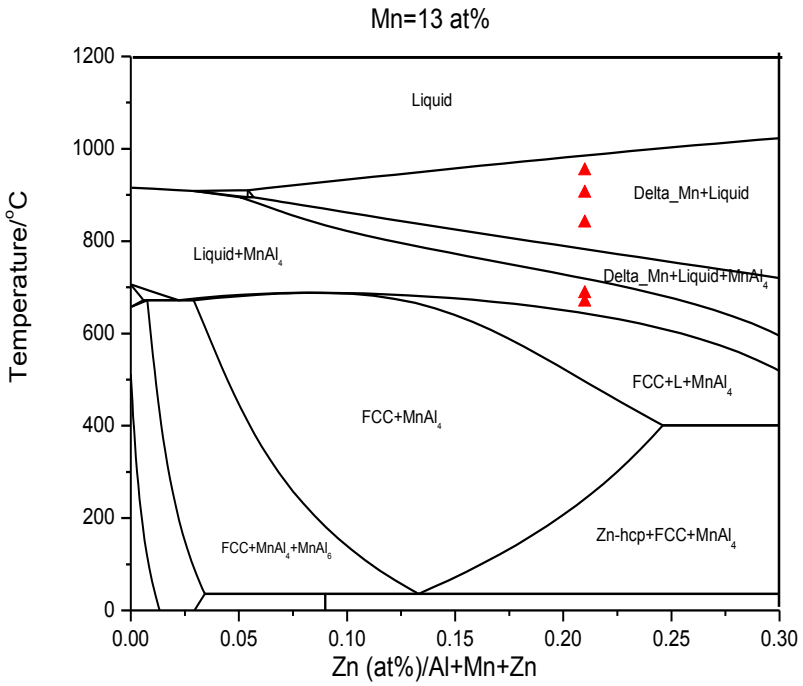
Mn=13 at%
Liquid
Delta_Mn+Liquid
Liquid+MnAl4
Delta_Mn+Liquid+MnAl4
FCC+L+MnAl4
FCC+MnAl4
FCC+MnAl4+MnAl6
Zn-hcp+FCC+MnAl4
Temperature/°C
Zn (at%)/Al+Mn+Zn
1200
1000
800
600
400
200
0
0.00
0.05
0.10
0.15
0.20
0.25
0.30

(a)

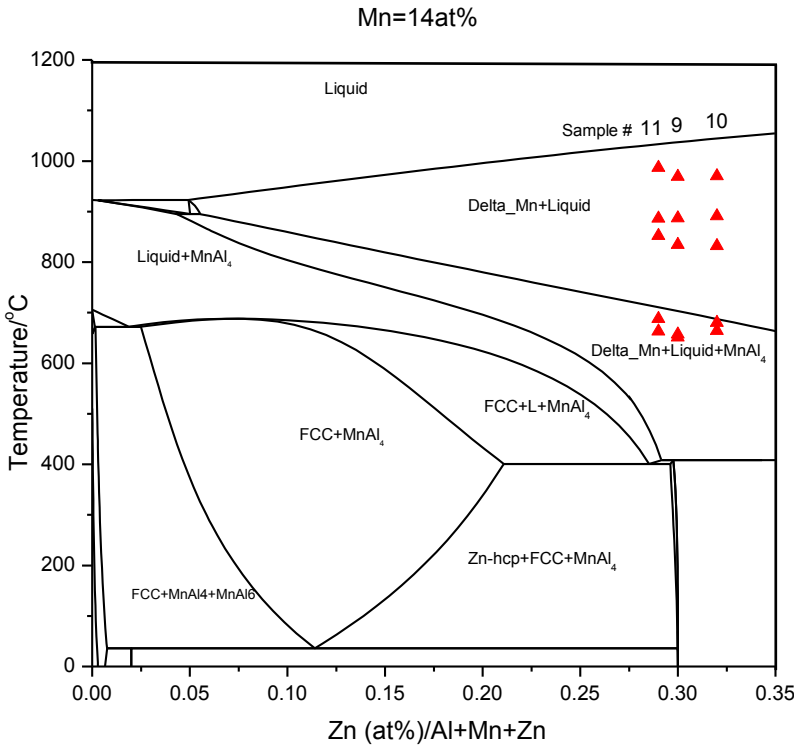
Mn=14at%
Liquid
Sample # 11 9 10
Delta_Mn+Liquid
Liquid+MnAl4
Delta_Mn+Liquid+MnAl4
FCC+L+MnAl4
FCC+MnAl4
Zn-hcp+FCC+MnAl4
FCC+MnAl4+MnAl6
Temperature/°C
Zn (at%)/Al+Mn+Zn
1200
1000
800
600
400
200
0
0.00
0.05
0.10
0.15
0.20
0.25
0.30
0.35

(b)

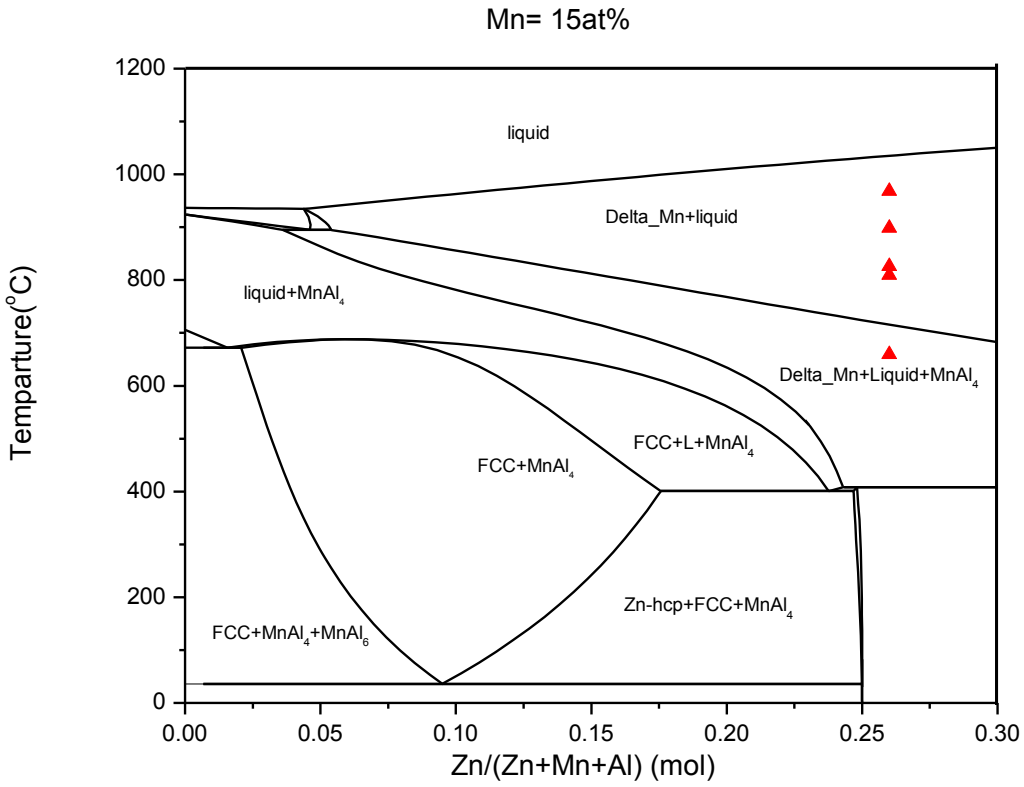

(c)

Figure 4.32: Calculated vertical sections at (a) 13 at% Mn; (b) 14 at% Mn; (c) 15 at% Mn; with transformation temperature at 0℃/min cooling rate of (a) sample 8; (b) sample 9, 10 and 11; and (c) sample 12.

CHAPTER 5

Concluding Remarks, Contributions and Recommendations

5.1 Concluding remarks

The Al-Mn-Zn ternary system has been experimentally studied through diffusion couple technique and selected equilibrated key alloys. Isothermal section of the Al-Mn-Zn system at 400℃ is constructed based on the current experimental investigation. Phase relations and solubility limits have been determined for the binary and ternary compounds using SEM/EDS, EPMA and XRD techniques. Three new ternary compounds have been found in this system, the compositions and homogeneity ranges of them have also been determined. These three ternary compounds have been reported for the first time. τ_1 and τ_2 are considered to be stoichiometric phases, and τ_3 is solid solution with small ternary solid solubility. The formulae of these ternary compounds are $Al_{62}Mn_{16}Zn_{22}$, $Al_{76}Mn_{13}Zn_{11}$, and $Al_xMn_yZn_z$ (x=9.5-12.7 at%; y=11-15 at%; z=74.6-77.2 at%) at 400℃. XRD pattern of τ_1 has been obtained. Because crystallographic information of these ternary compounds were not reported before, it is difficult to identify their crystal structure in the current study. Quasicrystal Al_4Mn phase which is reported before has been found and confirmed in the current study. Three binary compounds:

Al_4Mn, $Al_{11}Mn_4$ and Al_8Mn_5 have been found to have extended solid solubility into the ternary system.

Thermal analysis is also performed for the Al-Mn-Zn system using DSC technique. Vertical sections at 13at%, 14at% and 15at% Mn have been examined. Phase transformation and liquidus temperature have been reported in this work. Supercooling effect is observed during DSC analysis which is explained in details. The extrapolation method is used to minimize the supercooling effect and acquire the accurate thermal data.

A preliminary thermodynamic model was built by combining the three constituent binaries. This model was used as a road map for designing the experiments and for the selection of the compositions of key samples and diffusion couples. Also, the experimental results are compared with the thermodynamic calculations. Discrepancy is observed due to the absence of the ternary phases in the thermodynamic database. Therefore, the Al-Mn-Zn system should be thermodynamically remodeled in light of the current experimental results.

5.2 Contributions

The Al-Mn-Zn ternary system has been experimentally investigated combining diffusion couple technique and selected equilibrated key alloys. Isothermal section of Al-Mn-Zn at 400℃ has been constructed. Vertical section at 13at% Mn, 14at% Mn and 15at% Mn have been experimental investigated through DSC thermal analysis technique. In the present work, the following contributions have been achieved:

- Three new ternary intermetallic compounds τ_1, τ_2 and τ_3 have been discovered for the first time in the current study. The compositions of these three ternary intermetallic compounds have been studied by SEM, EPMA and XRD. XRD spectra of the three ternary compounds have been observed. XRD pattern of τ_1 has been extracted from the key samples by XRD analysis.
- Al_4Mn has been found to form quasicrystal in this system at 400℃. This finding is also confirmed and compared with the previous research works.
- The ternary solid solubility of Al_6Mn, Al_4Mn, $Al_{11}Mn_4$, Al_8Mn_5 and β-Mn binary phases have been determined for the first time using diffusion couples and key alloys.
- Three vertical sections at 13at% Mn, 14at% Mn and 15at% Mn have been studied for the first time via DSC thermal analysis method. Phase transformation and liquidus temperature of key samples have been reported in the present research.

5.3 Recommendations for future works

- Future experimental work is needed to identify the crystal structure of the ternary compounds in the Al-Mn-Zn system.
- The Al-Mn-Zn system should be optimized based on the current experimental results.

Reference

[1] H. J. McQueen, *J. Met.*, Vol. 32, No. 2, 1980, pp. 17–25.

[2] S. W. NAM and B. O. KONG, Development of weldable high strength Al alloy KOSEF technical report, 1993, pp.32.

[3] S. W. NAM and H. S. CHO, *J. Korean Inst. Met. Mater*. Vol.32, 1994, pp. 765.

[4] U. R. Kattner, The Thermodynamic Modeling of Multicomponent Phase Equilibria, *Journal of Metals*, Vol. 49, No. 12, 1997, pp. 14-19.

[5] Y. A. Chang, S. Chen, F. Zhang, X. Yan, F. Xie, R. Schmid-Fetzer and W. A. Oates, Phase Diagram Calculation: Past, Present and Future, *Progress in Materials Science*, Vol.49, 2004, pp.313-345.

[6] L. Kaufman and H. Bernstein, Computer calculation of phase diagrams with special reference to refractory metals, *Academic Press*, New York, 1970.

[7] K. C. Kumar, and P. Wollants, Some guidelines for thermodynamic optimization of phase diagrams, *Journal of Alloys and Compounds*, Vol. 320, 2001, pp. 189-198.

[8] "FactSage 6.0", Thermfact (Centre for research in computational thermochemistry), Montreal, QC, Canada, 2010.

[9] G. V. Raynor and W. Hume-Rothery, The constitution of Magnesium-Manganese-Zinc-Aluminum Alloys in the Range 0-5% Mg, 0-2% Mn, 0-8% Zn. Ⅱ - The composition of the $MnAl_6$ Phase, *J. Inst. Met.*, Vol.69, 1943, pp. 415-421.

[10] M. A. Taylor, Intermetallic Phases in the Aluminum-Manganese Binary system, *Acta Metall.,* Vol.8, 1960, pp.256-262.

[11] T. Godecke and W. Koster, A supplement to the constitution of the Aluminum-Manganese System, *Z. metallkd.*, Vol. 62, No.10, 1971, pp. 727-732.

[12] H. W. L. Phillips, The constitution of Alloys of Aluminum with Manganese, silicon, and Iron. I- The binary system: Aluminum-Manganese. Ⅱ- The ternary systems: Aluminum-manganese-Silicon and Aluminum-Manganese-Iron, *J. Inst. Met.,* Vol. 69, 1943, pp. 275-350.

[13] J. L. Murrary, A. J. McAlister, R. J. Schaefer, L. A. Bendersky, F. Biancaniello, and D. L. Moffat, Stable and Metastable. Phase Equilibria in the Al-Mn System, *Metall. Trans. A*, Vol. 18, 1987, pp. 385-392.

[14] E. H. Dix, W. L. Fink and L. A. Willey, Equilibrium relations in Aluminum-Manganese Alloys of high Purity, Ⅱ, *Trans, AIME*, Vol. 104, 1933, pp. 335-352.

[15] H. Kono, On the ferromagnetic Phase in Manganese-Aluminum System, *J. Phys. Soc. Jpn.,* Vol. 13, No.12, 1958, pp. 1444-145.

[16] G. M. Kuznetsov, A. D. barsukov, M. I. Abas, Solubility of Mn, Cr, Ti and Zr in Al in the Solid State, *Sov. Non-Ferrous Met. Res*., Vol. 11, 1983, pp. 47.

[17] C. Sigli, CALPHAD XXIV conference, Kyoto, Japan, 1995.

[18] M. Matuo, T. Muramatsu, A. Asanuma, S. Komatsu, K. Ikeda, Ketkinzoku, Vol. 47, 1997, pp.15.

[19] A. McAlister and J. Murray, The (Al-Mn) Aluminum-Manganese System, *Bull. Alloy Phase Diag.*, Vol. 8, No.5, 1987, pp. 438-447.

[20] M. Ellner, The Structure of the High-Temperature Phase MnAl(h) and the Displacive Transformation from MnAl(h) into Mn_5Al_8, *Metall. Trans. A*, Vol. 21, 1990, pp. 1669.

[21] A. Jansson, A Thermodynamic Evaluation of the Al-Mn System, *Metall. Trans. A*, Vol. 23, No. 11, 1991, pp. 2953-2962.

[22] X. Liu, R. Kainuma, H. Ohtani and K. Ishida, Phase Equilibria in the Mn-rich Portion of the Binary System Mn-Al, *J. Alloys Compd.*, Vol. 235, No.2, 1996, pp. 256-261.

[23] X. Liu, R. Kainuma and K. Ishida, Thermodynamic Assessment of the Aluminum-Manganese (Al-Mn) Binary Phase Diagram, *J. Phase Equilib.*, Vol. 20, No. 1, 1999, pp. 45-56.

[24] Mohammad Asgar-Khan and Mamoun Medraj, Thermodynamic Description of the Mg-Mn, Al-Mn and Mg-Al-Mn Systems Using the Modified Quasichemical Model for the Liquid Phases, *Materials Transctions* Vol. 50, No. 5, 2009, pp. 1113-1122.

[25] Y. Minamino, Y. Toshimi, H. Araki, N. Takeuchi, Y. Kang, Y. Miyamoto and T. Okamoto, Solid Solubilities of Manganese and titanium in Aluminum at 0.1 MPa and 2.1 GPa, *Metall. Mater. Trans. A*, Vol. 22A, No.3, 1991, pp. 783-786.

[26] H. Okamoto, Al-Mn (Aluminum-Manganese), *J. Phase Equilib.*, Vol. 18, No.4, 1997, pp. 398-399.

[27] C. Müller, H. Stadelmaier, B. Reinsch and G. Petzow, Merallurgy of the Magnetic τ-Phase in Mn-Al and Mn-Al-C, *Z. Metallkd.,* Vol. 87, No.7, 1996, pp. 594-597.

[28] A. Shukla and A. Pelton, Thermodynamic Assessment of the Al-Mn and Mg-Al-Mn Systems, J. Phase Equilib. Diffus.,:Section I: Basic and Applied Research, *J. Phase Equilibria and Diffusion,* Vol. 30, 2009, pp. 28-29.

[30] H. Kono, On the Ferromagnetic Phase in Manganese-Aluminum System, *J. Phys. Soc. Jpn.,* Vol. 13, No. 12, 1958, pp. 1444-1451.

[31] W. Koster and E. Wachtel, Constitution and Magnetic Properties of Aluminum-Manganese Alloys with More Than 25 At. % Mn, *Z. Metallkd.,* Vol. 51, 1960, pp. 271-280.

[32] A. Koch, P. Hokkeling, M. Steeg and K. Vos, New Material for Permanent Magnets on a Base of Mn and Al, *J. Appl. Phys.,* Vol. 31, No. 5, 1960, pp. 75-77.

[33] C. T. Heycock, F. H. Neville, The freezing points of alloys containing zinc and another metal, *Journal of the Chemical Society Transactions,* Vol.71, 1897, pp. 383-398.

[34] T. Isihara, On the equilibrium diagram of the aluminum-zinc system, *Science, Reports of the Tohoku Imperial University,* Vol. 13, 1924, pp. 18-21.

[35] T. Tanabe, Studies in the aluminum-zinc system, *Journal of the Institute of Metals,* Vol. 32, 1924, pp. 415-427.

[36] M. L. V. Gayler, M. Haughton, E. G. Sutherland, The constitution of aluminum-zinc alloys of high purity: The nature of the thermal change of 443^{o}C, *Journal of the Institute of Metals,* Vol. 63, 1938, pp.123-147.

[37] E. Pelzel, H. Schneider, Contribution to the understanding of Zn alloys, *Zeitschrift für Metallkunde*, Vol. 35, 1943, pp. 124-127.

[38] T. Morinaga, On the equilibrium diagram of the aluminum-zinc system, *Nippon Kinzoku Gakkaishi*, Vol. 3, 1939, pp. 216-221.

[39] Q. F. Peng, F. S. Chen, B. S. Qi, Y. S. Wang, Measurement of aluminum-zinc phase diagram by acoustic emission during solidification, *Transactions of the American Foundrymen's Society*, Vol. 99, 1991, pp. 199-202.

[40] W. L Fink, L. A. Willey, Equilibrium relations in aluminum-zinc alloys of high purity, II, *Transactions of the Metallurgical Society of AIME*, Vol. 12, 1936, pp. 244-260.

[41] M. Simerska, P. Bartuska, The X-ray diffraction and electron microscopic investigation of stable and metastable equilibria in Al-rich Al-Zn alloys, *Czech Journal of Physics*, Vol. B24, 1974, pp. 553-559.

[42] G. Borelius, L. E. Larsson, Kinetics of precipitation in aluminum-zinc alloys, *Arkiv för Matematik, Astronomi och Fysik*, Vol. 35A, No. 13, 1948, pp. 1-14.

[43] A. Münster, K. Sagel, Miscibility gap and critical point of the aluminum-zinc system, *Zeitschrift für Physikalische Chemie*, Vol. 7, 1956, pp. 267-295.

[44] H. Terauchi, N. Sakamoto, K. Osamura, Y. Murakami, Small angle X-ray critical scattering in an aluminum-zinc alloy with critical composition, *Transactions of the Japan Institute of Metals*, Vol. 16, No. 7, 1975, pp. 379-383.

[45] J. L. Murray, The Alumnum-Zinc System, *Bulletin of Alloy Phase Diagrams*, Vol. 4, No. 1, 1983, pp.55-73.

[46] S. A. Mey, Re-evaluation of the Aluminum-Zinc System, *Zeitschrift für Metallkunde*, Vol.84, No. 7, 1993, pp. 451-455.

[47] S. L. Chen and Y. A. Chang, A Thermodynamic Analysis of the Al-Zn System and Phase Diagram Calculation, *CALPHAD*, Vol.17, No. 2, 1993, pp.113-124.

[48] S. Wasiur-Rahman, Thermodynamic Modeling of the (Mg, Al)-Ca-Zn Systems, M.A.Sc Thesis in Mechanical and Industrial Engineering, 2009, Concordia University: Montreal, QC, Canada.

[49] C. T. Heycock, F.H. Neville, The freezing points of alloys containing zinc and another metal, *Journal of the Chemical Society Transactions*, Vol. 71, 1897, pp. 383-398.

[50] T. Isihara, On the equilibrium diagram of the aluminum-zinc system, *Science, Reports of the Tohoku Imperial University*, Vol. 13, 1924, pp. 18-21.

[51] T. Tanabe, Studies in the aluminum-zinc system, *Journal of the Institute of Metals*, Vol. 32, 1924, pp. 415-427.

[52] M. L. V. Gayler, M. Haughton, E. G. Sutherland, The constitution of aluminum-zinc alloys of high purity: The nature of the thermal change of 443^{o}C, *Journal of the Institute of Metals*, Vol. 63, 1938, pp.123-147.

[53] E. Pelzel, H. Schneider, Contribution to the understanding of Zn alloys, *Zeitschrift für Metallkunde*, Vol. 35, 1943, pp. 124-127.

[54] E. Butchers, W. Hume-Rothery, On the constitution of aluminum-magnesium-manganese-zinc alloys: The solidus, *Journal of the Institute of Metals*, Vol. 71, 1945, pp. 291-311.

[55] E. Pelzel, The positions of the liquidus and solidus curves in the Al-Zn system from 30 to 70 wt.% Al, *Zeitschrift für Metallkunde*, Vol. 40, 1949, pp. 134-136.

[56] I. S. Solet, H. W. S. Clair, Liquidus temperatures and liquid densities of zinc-aluminum alloys, *Bureau of Mines Report of Investigations 4553*, 1949, pp. 1-7.

[57] E. Gebhardt, Equilibrium experiments on the systems zinc-aluminum and zinc-aluminum-copper, *Zeitschrift für Metallkunde*, Vol. 40, 1949, pp. 136-140.

[58] E. C. Ellwood, The solid solutions of zinc in aluminum, *Journal of the Institute of Metals*, Vol. 80, 1951, pp. 217-224.

[59] W. L Fink, L. A. Willey, Equilibrium relations in aluminum-zinc alloys of high purity, II, *Transactions of the Metallurgical Society of AIME*, Vol. 12, 1936, pp. 244-260.

[60] M. Simerska, P. Bartuska, The X-ray diffraction and electron microscopic investigation of stable and metastable equilibria in Al-rich Al-Zn alloys, *Czech Journal of Physics*, Vol. B24, 1974, pp. 553-559.

[61] G. Borelius, L. E. Larsson, Kinetics of precipitation in aluminum-zinc alloys, *Arkiv för Matematik, Astronomi och Fysik*, Vol. 35A, No. 13, 1948, pp. 1-14.

[62] L. E. Larsson, Pre-precipitation and precipitation phenomena in the Al-Zn system, *Acta Metallurgica*, Vol. 15, 1967, pp. 35-44.

[63] W. M. Pierce, M. S. Palmerton, Studies on the constituent of binary zinc-based alloys, *Transactions of the Metallurgical Society of AIME*, Vol. 68, 1923, pp. 767-795.

[64] H. Auer, K. E. Mann, Magnetic investigation of the aluminum-zinc system, *Zeitschrift für Metallkunde*, Vol. 28, 1936, pp. 323-326.

[65] M. L. Fuller, R. L. Wilcox, Phase changes during aging of zinc-alloy die castings, II-Changes in the solid solution of aluminum in zinc and their relation to dimensional changes, *Transactions of the Metallurgical Society of AIME*, Vol. 122, 1936, pp. 231-246.

[66] A. Burkhardt, Zinc alloys as a substitute material, *Zeitschrift für Metallkunde*, Vol. 28, No. 10, 1936, pp. 299-308.

[67] K. Lohberg, X-ray determination of the solubility of aluminum and copper in zinc, *Zeitschrift für Metallkunde*, Vol. 32, 1940, pp. 86-90.

[68] W. Hoffman, G. Fahrenhost, Precipitation rates in high purity zinc-aluminum and zinc-copper alloys, *Zeitschrift für Metallkunde*, Vol. 42, 1950, pp. 460-463.

[69] A. Pasternak, The solid solubility of metals in lead and zinc, Bulletin International de l'Academie Polonaise des Sciences et des Lettres, Classe des Sciences Mathematiques et Naturelles, Serie A: Sciences Mathematiques Serial A, 1951, pp.177-192.

[70] A. Münster, K. Sagel, Miscibility gap and critical point of the aluminum-zinc system, *Zeitschrift für Physikalische Chemie*, Vol. 7, 1956, pp. 267-295.

[71] H. Terauchi, N. Sakamoto, K. Osamura, Y. Murakami, Small angle X-ray critical scattering in an aluminum-zinc alloy with critical composition, *Journal of the Japan Institute of Metals*, Vol. 16, No. 7, 1975, pp. 379-383.

[72] H. Araki, Y. Minamino, T. Yamane, K. Azuma, Y. S Kang and Y. Miyamoto, Partial phase diagrams of the aluminum-rich region of the aluminum-zinc system at 0.1 MPa and 2.1 GPa, *Journal of Materials Science Letters*, Vol. 11, No. 3, 1992, pp. 181-183.

[73] M. Hanson, Constitution of Binary Alloys, 2nd ed., McGraw-Hill, New York, 1958, pp. 962–963.

[74] H. Okamoto and L. Tanner, The Mn - Zn (Manganese-Zinc) System, *Bull. Alloy Phase Diag.* Vol. 11, No. 4, 1990, pp. 377-384.

[75] E. Wachtel and K. Tsiuplakis, Magnetic Properties of Zinc-rich Zinc-Manganese Alloys in the Liquid and Solid State, *Z. Metallkd.*, Vol. 58, No. 1, 1967, pp. 41-45.

[76] O. Romer and E. Wachtel, Constitution of the Zinc - Manganese and the Zinc - Manganese -Aluminum Systems, *Z. Metallkd.,* Vol. 62, No. 11, 1971, pp. 820-825.

[77] Y. Nakagawa and T. Hori, *Trans. Jpn. Inst. Met.,* Vol. 13, 1972, pp. 167–70.

[78] J. Miettinen, Thermodynamic Description of the Cu-Mn-Zn System in the Copper-rich Corner, *CALPHAD,* Vol. 28, No. 3, 2004, pp 313-320.

[79] H. H. Xu, X. Xiong, L. J. Zhang, Y. Du and P. S. Wang, *Metall. Mater. Trans. A*, Vol. 40, 2009, pp. 2042–2047.

[80] Jian lie Liang, Yong Du, Chang zhong Liao, Yi yuan Tang, Liang qin Nong, Feng Zheng and Hong hui Xu, Experimental investigation on the phase equilibria of the Mn–Ni–Zn system at 400^{o}C, *Journal of Alloys and Compounds*, Vol. 489, No. 2, 2010, pp. 362-368.

[81] Gebhardt, E, *Z. Metallk.* Vol. 34, 1942, pp. 259.

[82] G. V. Raynor and D. W. Wakeman, The Intermetallic Compound Phases of the System Aluminium-Manganese-Zinc, *Proceedings of the Royal Society of London. Series A, Mathematical and Physical Sciences*, Vol. 190, No. 1020, 1947, pp. 82-101.

[83] K. Robinson, The determination of the crystal structure, *Acta Cryst.*, Vol. 7, 1954, pp.494.

[84] A. Damjanovic, The Structure Analysis of the T_3 (A1MnZn) Compound, *Acta Crystallographica,* Vol. 14, 1961, pp. 982-987.

[85] Schaefer, R. J. and Bendersky, L., *Scripra Mecan*., Vol. 20, 1986, pp.745.

[86] A. Singh, S. Ranganathan and L. A. Bendersky, Quasicrystalline Phases and Their Approximants In Al-Mn-Zn Alloys, *Acta Materialia*, Vol. 45, No. 12, 1997, pp. 5327-5336.

[87] J. S. Kirkaldy and L. C. Brown, Diffusion Behaviour in the Ternary, Multiphase Systems, *Canadian Metallurgical Quarterly*, Vol. 2, No. 1, 1963, pp. 90-115.

[88] J. B. Clark, Conventions for Plotting the Diffusion Paths in Multiphase Ternary Diffusion Couples on the Isothermal Section of a Ternary Phase Diagram, *Transactions of the Metallurgical Society of AIME*, Vol. 227, 1963, pp. 1250-1251.

[89] A. A. Kodentsov, G. F. Bastin, and F. J. J. van Loo, The Diffusion Couple Technique in Phase Diagram Determination, *Journal of Alloys and Compounds*, Vol. 320, No. 2, 2001, pp. 207-217.

[90] J. C. Zhao, M. R. Jackson, and L. A. Peluso, Determination of the Nb-Cr-Si Phase Diagram Using Diffusion Multiples, *Acta Materialia*, Vol. 51, No. 20, 2003, pp. 6395-6405.

[91] YiNan Zhang, Experimental investigation of the Ca-Mg-Zn system via diffusion couples and key experiments, MASc thesis, Concordia University, Montreal (Canada) 2010.

[92] H. H. Xu, Y. Du, Y. C. Zhou, and Z. P. Jin, Determination of Phase Diagram Using the Diffusion Couple Technique, *Rare Metals*, Vol. 25, No. 5, 2006, pp.427-430.

[93] H. Putz, K, Brandenburg, Pearson's Crystal Data, Crystal Structure Database for Inorganic Compounds, CD-ROM software version 1.3.

[94] MD Anwar Parvez, Experimental Investigation of the Ternary Mg-Al-Sr System, MASc thesis, Concordia University, Montreal (Canada) 2004.

[95] L. A. Bendersky, Quasicrystals and quasicrystal-related phases in Al-Mn system, *Materials science and engineering*, Vol. 99, 1988, pp. 331-334.

[96] D. Shechtman, I. Blech, D. Gratias and J. W. Cahn, Metallic Phase with Long-Range Orientational Order and No Translational Symmetry, *Phys. Rev. Lett.*, Vol. 53, 1984 1951-1953.

[97] L. Bendersky, Quasicrystal with one-dimensional translational symmetry and a tenfold rotation axis, *Phys. Rev. Lett.*, Vol. 55, 1985, pp. 1461-1463.

[98] R. J. Schaefer, L. A. Bendersky, D. Shechtman, W. J. Boettinger and F. S. Biancaniello, *Metall. Trans.A*, Vol. 17, 1986, pp. 2117.

[99] M. A. Taylor, Intermetallic phases in the aluminium-manganese binary system, *Acta Metall.*, Vol. 8, No. 4, 1960, pp. 256-262.

[100] J. D. Fitz Gerald, R. L. Withers, A. M. Stewart, and A. Calka, The Al-Mn decagonal phase 1. A re-evaluation of some diffraction effects; 2. Relationship to crystalline phases, *Phil. Mag. B*, Vol. 58, No. 1,1988, pp. 15-33.

[101] T. L. Daulton, K. F. Kelton and P. C. Gibbons, Decagonal and Related Phases in Al-Mn Alloys: Electron Diffraction and Microstructure, *Phil. Mag. B*, Vol. 63, 1991, pp. 687-715.

[102] X. Z. Li, and K. H. Kuo, Orthorhombic crystalline approximants of the Al-Mn-Cu decagonal quasicrystal, *Philos. Mag. B*, Vol. 66, 1992, pp. 525-533.

[103] Van Tendeloo, G., Singh, Alok and Ranganathan, S, Quasicrystals and their crystalline homologues in the Al- Mn-Cu ternary alloys, *Philos. Mag. A*, Vol. 64, No. 2, 1991, pp. 413-427.

[104] X. Z. Li and K. H. Kuo, Orthorhombic crystalline approximants of the Al-Mn-Cu decagonal quasicrystal, *Philos. Mag. B*, Vol. 66, 1992, pp.117-124.

[105] W. J. Boettinger, U. R. Kattner, K.-W. Moon and J. H. Perepezko, *DTA and Heat-flux DSC Measurements of Alloy Melting and Freezing*, U.S. Government printing office, Washington, 2001.